# Liquid-solid contacting in trickle-bed reactors

by

**Arjan van Houwelingen**

A dissertation submitted in partial fulfillment
of the requirements for the degree

**Philosophiae Doctor in Chemical Engineering**

in the

Department of Chemical Engineering
Faculty of Engineering, the Built Environment and Information Technology

University of Pretoria
Pretoria

**October 30, 2009**

UNIVERSITEIT VAN PRETORIA
UNIVERSITY OF PRETORIA
YUNIBESITHI YA PRETORIA

# Liquid-solid contacting in trickle-bed reactors


| | |
|---|---|
| Author: | Arjan van Houwelingen |
| Supervisor: | W. Nicol |
| Department: | Department of Chemical Engineering<br>University of Pretoria |
| Degree: | Philosophae Doctor (Chemical Engineering) |


## Abstract


Several types of reactors are encountered in industry where reagents in a gas and a liquid phase need to be catalysed by a solid catalyst. Common reactors that are used to this end, are trickle-bed reactors, where gas and liquid flow cocurrently down a packed bed of catalyst. Apart from the catalytic process itself, several mass transfer steps can influence the rate and/or selectivity of a solid catalysed gas-liquid reaction. In trickle-bed reactors, flow morphology can have a major effect on these mass transfer steps.

This study investigates the interaction between liquid flow morphology and mass transfer in trickle-bed reactors from three different angles. The primary focus is on liquid-solid mass transfer and internal diffusion as affected by the contacting between the liquid and the catalyst. First, the contacting between the liquid and the solid in trickle-flow, or wetting efficiency, is characterised using colorimetry. Though this investigation is limited to the flow of nitrogen and water over a packed bed at ambient conditions, it provides useful information regarding liquid flow multplicity behaviour and its influence on the distribution of fractional wetting on a particle scale. The colorimetric study also provides descriptions of the geometry of the liquid-solid contacting on partially wetted particles.

These are used in a second investigation, for the numerical simulation of reaction and diffusion in partially wetted catalysts. This second investigation uses numerical simulations to evaluate and develop simple theoretical decriptions of liquid-solid contacting effects on catalyst particle efficiency. Special attention is given to the case where external and intraparticle mass transfer rates of both a volatile and non-volatile reagent affect the overall rate of reaction. Also, since these are not often considered in theoretical studies, some suggestions are made for the evaluation of the particle efficiency of eggshell catalyst.

Finally, liquid-solid contacting is investigated in a high-pressure pilot reactor. Wetting efficiency is measured with a useful technique that does not rely on descriptions of particle kinetics or liquid-solid mass transfer rates. Liquid-solid mass transfer coefficients are also measured and results agree well with the colorimetric investigation, suggesting the existence of different types of flow within in the hydrodynamic multiplicity envelope of trickle-flow.

Since it consists of different investigations of liquid-solid contacting from different

angles, the study highlights several aspects of liquid-solid contacting and how it can be expected to influence trickle-bed reactor performance.

KEYWORDS: trickle-bed reactor, trickle flow, wetting efficiency, liquid-solid mass transfer, colorimetry, pellet efficiency factor, finite element method, hydrodynamics, multiplicity

# Acknowledgements

Many people have contributed to making this work possible. Thank you all. My supervisor, Prof. Willie Nicol for continued support and guidance. Sasol Technology Research and Development for financial support, as well as the important assistance in the design and construction of the high-pressure experimental set-up described in Chapter 5. In this regards, I particularly want to acknowledge the efforts of Johann Rademan and Randall Hopley. The construction of this set-up was not trivial and would not be possible without their expertise. Also for financial support, the National Research Foundation of South-Africa. The programming skills of Carl Sandrock and the training in finite element methods by Schalk Kok were of extreme importance for the work presented in Chapters 3 and 4. Lastly, to all family and friends as well as the colleague students at the University of Pretoria for guarding my sanity, or insanity, where necessary.

# CONTENTS

# LIST OF FIGURES

# LIST OF TABLES

# CHAPTER 1

# INTRODUCTION

Packed bed reactors that process gas and liquid reagants are extensively utilised in industry, most notably in the petrochemical industry for hydroprocessing (Satterfield, 1975; Gianetto and Specchia, 1992). Other typical examples of the industrial applications of these reactors include the production of fine chemicals via a catalysed gas-liquid reaction step and the catalytic oxidation of wastewater.

For the succesful commercialisation of a specific reaction process, it is necessary to develop and/or select a suitable catalyst, to design and develop a viable reactor with appropriate surrounding unit operations and finally to operate the resulting plant well enough to meet production specifications. Historically, these steps would be performed completely seperately: For example, a catalysis group develops or identifies a suitable catalyst with primary focus on the chemistry of the reaction. A preliminary design of a commercial process for this reaction is then verified with pilot studies, after which commercialisation can be initiated. Finally, the process is operated on a commercial plant. In all these steps, different aspects of the final process are emphasised so that it is quite possible that catalyst design teams may have little or no knowledge of reactor scale effects such as heat and mass transfer or flow characteristics, and that pilot scale studies are interpreted with little regard to the effect of scale. However, reactor operation and optimisation are often performed without proper knowledge of the underlying catalysis process. It is clear that such an approach, though successful to some extent, probably would not lead to optimal processes.

It is for this reason that a more integrated approach is advocated, where both the chemistry (catalysis) and engineering (reactor design and operation) are of importance throughout the development of the process (Dudukovic et al., 2002; Larachi, 2005). To achieve such integration, a good understanding of both particle-scale (e.g. catalysis and particle efficiency) and reactor-scale behaviour (e.g. hydrodynamics and transfer pro-

cesses) is important.

In packed bed gas-liquid reactors, it is well known that flow configuration and characteristics have an important effect on the behaviour of a reactor. These reactors can be operated in gas-liquid cocurrent downflow, cocurrent upflow, or countercurrent flow. Due to flexibility in terms of throughput, gas-liquid downflow reactors, commonly known as trickle-bed reactors (TBRs), are often preferred when large process streams are involved (Sie and Krishna, 1998; Dudukovic et al., 2002). The hydrodynamic behaviour of these reactors and its effect on reactor performance are especially intricate, due to the possible existence of incomplete catalyst wetting, multiple flow morphologies and hydrodynamic hysteresis.

Though not only studies regarding the solid catalysis of gas-liquid reaction systems, but also studies regarding trickle-bed reactor hydrodynamics are abundant, the development of the relevant theories is mostly driven separately. For example, a large part of the literature data and theoretical developments regarding trickle-bed hydrodynamics is based on cold mock-ups (involving for example air and water without any reaction). Such studies are of great importance to the understanding of trickle-bed reactors, but can ultimately only speculate about that which is of final importance, i.e. the influence on reactor performance. By contrast, many pilot studies exist with a predominantly practical focus, for example to prove the concept of a new process. Reactor hydrodynamics is then only loosely touched upon.

Proper reactor studies will always be needed to verify and guide theoretical development (including cold data), and highlight which knowledge of hydrodynamics is of primary importance. However, it is very difficult and even unlikely to understand a reactor correctly without the knowledge resulting from studies that focus exclusively on reactor hydrodynamics and relevant theories, or studies that focus entirely on the catalytic process on particle scale. One will never reach the goal of integrated reactor development without integrated research.

This work follows an integrated approach to studying the role of liquid-solid contacting in a trickle-bed reactor. The study focuses on two aspects of liquid-solid contacting: partial wetting and liquid-solid mass transfer rates. Firstly, fractional wetting in a TBR is characterised on a bed and particle scale in a non-reactive air-water experimental study, making use of colorimetry. Results regarding particle-scale wetting topology form the basis for numerical modelling of reaction within monodispersed and eggshell catalysts under different reaction conditions (i.e. rate, kinetic expression, internal and external mass transfer resistances), which is in turn used in the verification of existing pellet efficiency models and the development of new ones. The knowledge obtained from the visualisation of wetting efficiency and subsequent particle efficiency modelling is then used for the interpretation of conversion data and the development of a novel method of wetting efficiency/liquid-solid mass transfer measurement in a large-scale high-pressure

pilot reactor. This reactor study is based on a reaction for which the rate is limited by the rate of liquid reagent supply to the catalyst.

It is clear that liquid-solid contacting is strongly affected by flow morphology and local liquid velocity profiles. Previous studies have established that these are subject to hydrodynamic multiplicity when operating in the partial wetting (trickle) flow regime: Flow patterns and behaviour are strong functions of the history of flow (Kan and Greenfield, 1978; Lutran et al., 1991). Multiplicity behaviour should therefore be included in the study of solid-liquid contacting. It is possible to operate along the boundaries of hydrodynamic multiplicity by utilising predefined pre-wetting procedures (Loudon et al., 2006; van der Merwe and Nicol, 2009). This strategy is followed for all the presented experimental studies in order to explore the boundaries of hydrodynamic multiplicity.

Wetting efficiency and liquid-solid mass transfer measurements, partially wetted pellet efficiency modelling and reactor conversion data interpretation are not new. Even the integration of hydrodynamic theory with reactor conversion data measurements is, though less abundant than studies that focus almost exclusively on either reactor perfomance or hydrodynamics, quite common. The literature review in the next chapter serves to identify and illustrate where contributions can be made to the study of liquid-solid contacting and its effect on reactor performance, and motivates the experimental and theoretical developments in the subsequent chapters. The literature study is a broad review of studies relevant to the overall contribution of this work. More specific literature is discussed in each chapter, if necessary.

# CHAPTER 2

# LITERATURE

Apart from the catalytic process itself, several mass transfer steps can influence the rate and/or selectivity of a solid catalysed gas-liquid reaction as illustrated in Figure 2.1. In packed bed gas-liquid reactors, it is well known that flow configuration and characteristics have an important effect on these transfer processes. Especially for trickle-bed reactors operating in the trickle flow regime, these processes can have an intricate interaction. Trickle flow is characterised by gravity-driven liquid flow over a packed bed with gas continuous flow. The liquid trickles down the packing, giving rise to (possibly) incomplete wetting, liquid velocity profiles and liquid maldistribution. This morphology of liquid flow directly influences the mass transfer steps depicted in Figure 2.1:

- The area available for liquid-solid mass transfer is directly affected by the fraction of external particle area contacted by the flowing liquid.
- The area available for gas-solid mass transfer is directly affected by the fraction of external particle area contacted by the flowing liquid. Gas-solid mass transfer is generally regarded as being fast enough not to be rate-determining.
- Liquid velocity and liquid velocity profiles will affect gas-liquid and liquid-solid mass transfer coefficients.
- The geometry and the extent of fractional wetting affect intraparticle diffusion (Yentekakis and Vayenas, 1987).
- Maldistribution of the liquid can cause parts of the catalyst bed to be almost completely dry or almost completely flooded. The former gives rise to bed-scale incomplete catalyst utilisation if the liquid reagent is non-volatile, or the formation of hot spots if reaction can occur in the gas-phase (Sedriks and Kenney, 1972). The

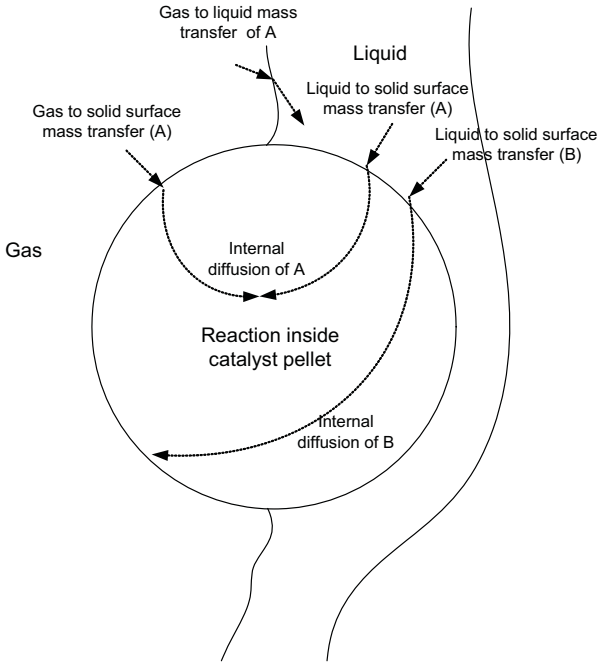


**Figure 2.1:** Mass transfer steps in a trickle-bed reactor.

latter can result in part of the bed becoming completely deprived of the gaseous reagent (Ravindra et al., 1997b).

In this thesis, the interaction between liquid flow morphology and the different mass transfer steps is collectively termed liquid-solid contacting. The primary focus is on liquid-solid mass transfer and internal diffusion as affected by liquid flow morphology. Since the study of partial wetting is integral to all work, the study focuses mainly on trickle flow, where partial wetting occurs and mass transfer effects are of major importance. Several other flow regimes are possible for gas-liquid downflow in trickle-bed reactors. Flow maps (Satterfield, 1975; Gianetto and Specchia, 1992; Sie and Krishna, 1998) and correlations (Fukushima and Kusaka, 1977; Larachi et al., 1999) can be used to determine the flow regime applicable to a specific reactor. In terms of pilot and industrial trickle-bed reactors, the trickle and pulsing flow regimes are the most important (Gianetto and Specchia, 1992). An excellent hydrodynamic description of pulse flow as a hybrid between trickle flow (at the high interaction boundary) and dispersed bubble flow is provided by Boelhouwer et al. (2002).

## 2.1 Liquid-solid contacting: A short historical overview

The simplest way of modelling a trickle-bed reactor is by assuming first-order kinetics, plug flow behaviour and no resistances to mass transfer of the reagents to the catalyst surface, so that the general design equation can be used:

$$\begin{aligned} -\ln(1-X) &= k_r \cdot \tau \\ \tau &= \frac{V_R}{Q_L} \end{aligned} \tag{2.1}$$

where $k_r$ is based on the active catalyst volume. This basis for $k_r$ is not standard, but will be used throughout this chapter to link with the notation used in Chapter 4. Early work on trickle-bed reactors showed that such ideal behaviour cannot be assumed even if dispersion is not expected to play a role (Mears, 1971), and is summarised by Satterfield (1975). An interesting early study that gives evidence of hydrodynamic effects on reaction rates in trickle-bed reactors was performed by Henry and Gilbert (1973) who studied pilot reactor conversion data to find the following approximate proportionality:

$$-\ln(1-X) \propto Z^{1/3}\tau^{2/3}d_p^{-2/3} \tag{2.2}$$

This translates to an effective rate constant proportional to $v_{SL}^{1/3}d_p^{-2/3}$. According to a laminar film flow model developed by Satterfield et al. (1969), the liquid holdup in a trickle-bed reactor is proportional to $v_{SL}^{1/3}d_p^{-2/3}$. The authors therefore proposed that the efficiency of a trickle-bed reactor is directly determined by the liquid holdup. Though Satterfield (1975) disputed this proposal soon afterwards, the observations are clear evidence of hydrodynamic effects. Satterfield (1975) suggested that the observed proportionality may be a result of decreased particle size leading to higher catalyst efficiency factors; and/or increased velocities and bed lengths leading to less dispersion. Mears (1974) stated that the effect of incomplete catalyst wetting was observed, supported by the correlation of Puranik and Vogelpohl (1974) that states that wetting efficiency is proportional to $v_{SL}^{0.31}$.

By proposing a direct proportionality between reaction rates in a trickle-bed reactor and wetting efficiency, one of the following is indirectly suggested:

- Particles in a trickle-bed reactor are either completely dry or completely wetted; or
- catalyst efficiency for a partially wetted pellet is directly proportional to the fractional coverage of its surface with the flowing liquid; or
- external liquid-solid mass transfer is proportional to wetting efficiency and determines the rate of reaction.

Dudukovic (1977) argued that the effect of incomplete wetting should be considered on a particle scale, rather than a reactor scale and, based on the work of Aris (1957), arrived at the following expression:

$$-ln\,(1-X) = \eta \cdot k_r \cdot \tau \tag{2.3}$$

$$\eta = f \cdot \frac{\tanh\left(\frac{\phi_G}{f}\right)}{\phi_G} \tag{2.4}$$

More details of the derivation appear in Chapter 4. The original work also incorporated incomplete pore filling of the catalyst. This is not shown here, since complete pore fill-up is generally assumed, ever since the residence time distribution study of Schwartz et al. (1976)[1]. The effects of external liquid-solid mass transfer were not considered, due to the notion of Satterfield et al. (1969) that external liquid-solid mass transfer probably does not play a role in a trickle-bed reactor. This was later incorporated in the usual way that external mass transfer resistances are treated:

$$\begin{aligned} -ln\,(1-X) &= \eta_0 \cdot k_r \cdot \tau \\ \eta_0 &= \eta \cdot \frac{C_s}{C_{bulk}} \\ k_{LS}S_p.f\,(C_{bulk}-C_s) &= \eta \cdot k_r V_R C_s \\ \therefore \eta_0 &= \eta\frac{C_s}{C_{bulk}} = \eta\left(1+\frac{\phi_G^2}{Bi'.f}\eta\right)^{-1} \end{aligned} \tag{2.5}$$

All the work discussed so far was about reactions for which the reagent(s) in the liquid determine the overall rate of reaction inside a trickle-bed reactor and are non-volatile. Early evidence of wetting efficiency effects on reactions involving volatile or gaseous reagents was provided by Sedriks and Kenney (1972) for the hydrogenation of crotonaldehyde. Reactor conversions for the dry startup and pre-wetted startup of a trickle-bed reactor were compared. It was visually observed that the wetting efficiency for dry startup was considerably lower than when the bed was pre-wetted, but conversions were considerably higher for dry startup, especially at low liquid flow rates. As for the approach of Mears (1974), the effect of wetting efficiency was modelled as a bed-scale effect:

$$r = (1-f) \times r_d + f \times r_w \tag{2.6}$$

At atmospheric pressure, where the reaction was performed, both reagents were present

[1] An exception is the case of highly exothermic reactions. These are not considered in this work, but for more information on this work, read for example Kirillov and Koptyug (2005).

in the gas phase. Due to the smaller resistances to external and internal mass transfer for dry pellets, $r_d \gg r_w$, resulting in higher reaction rates for lower wetting efficiencies. It is debateable whether this bed-scale decription is entirely correct, but a pellet scale model for a reaction that is limited by a volatile reagent on a partially wetted catalyst, derived by Ramachandran and Smith (1979) suggest more or less the same form. The only difference is that the particle is internally wetted, so that partial wetting only affects the overall particle effectiveness through enhanced external mass transfer over the dry pellet surface and not through enhanced internal diffusion. Nevertheless, the rate enhancement effect of partial wetting for volatile limiting reagents was observed several times, with the data of Mata and Smith (1981) giving a fine illustration of the combined effect of wetting efficiency and liquid-solid mass transfer for such a reaction. The pellet scale model of Ramachandran and Smith (1979) is discussed in more detail in Chapter 4, where it forms an integral part of the work. Apparently there are no suggestions in the literature for the simple treatment of reactions for which both the liquid and gas reagents play a role.

As for most hydrodynamic parameters in trickle-bed reactors, early estimations of wetting efficiency were based on packed column data, but not long after it was shown that wettig efficiency could be of importance in trickle-bed reactors, methods for the measurement of this hydrodynamic parameter were suggested (Schwartz et al., 1976; Colombo et al., 1976) and more and more data became available. This is discussed in section 2.2.1. Possibly due to the early general consensus that liquid-solid mass transfer is of lesser importance, liquid-solid mass transfer measurements remained mostly based on dissolution techniques for larger size, non-porous particles. The first reactor-derived data were published by Morita and Smith (1978) for the hydrogenation of $\alpha$-methylstyrene to cumene. The importance of liquid-solid mass transfer had however been illustrated several times before for the oxidation of components in an aqueous solution (Klassen and Kirk, 1955; Hartman and Couglin, 1972; Goto et al., 1975). Based on mass transfer correlations and typical reaction rates, Sie and Krishna (1998) estimate that liquid-solid mass transfer can play an important role in hydrotreaters. Measurement of and correlations for liquid-solid mass transfer are discussed in section 2.2.2.

## 2.2 Measurement and correlations for solid-liquid contacting

### 2.2.1 Wetting efficiency

The first wetting efficiency correlation that was used in TBR studies/modelling is based on packed column data (Puranik and Vogelpohl, 1974). Most wetting efficiency data are derived from a tracer response measurement technique, based on the effect that

intraparticle diffusion has on a tracer response curve. The technique was first proposed by Colombo et al. (1976) and later streamlined by Mills and Dudukovic (1981). Based on a Thiele modulus argument related to the work of Dudukovic (1977), the wetting efficiency is taken as the square root of the apparent effective diffusivities measured for trickle- and single-phase liquid flow.

$$f = \sqrt{\frac{D_{TBR}}{D_{LF}}} \tag{2.7}$$

A more complete theoretical development of the effect of partial wetting on a tracer response curve was given by Ramachandran et al. (1986), but was never used for the measurement of wetting efficiency. The work was however used by Julcour-Lebigue et al. (2007), for a theoretical validation of the usual tracer technique. The major disadvantage of the tracer wetting efficiency measurement method is that it is model-based.

For the purpose of correlating wetting efficiency with liquid and gas properties and operating conditions, the tracer technique has always been the most important tool for data generation. Other important wetting efficiency measurement methods are the dissolution method (Specchia et al., 1978; Lakota and Levec, 1990; Gonzalez-Mendizabal et al., 1998), colorimetry and reaction methods. Pironti et al. (1999) proposed a wetting efficiency measurement method based on pressure drop, which was later shown to be inaccurate by Baussaron et al. (2007).

The dissolution method compares dissolution rates for trickle flow with dissolution rates in liquid-full operation at the same interstitial velocities. The disadvantage of this method is that liquid-full operation measurements are required over the whole flow range and that a good estimate is needed for liquid holdup (interstitial velocity). Also, it is not completely certain whether or not single-phase liquid flow and trickle flow has the same mass transfer characteristics at the same interstitial velocities. A second disadvantage is that non-porous or slightly porous soluble packing material is used, contrary to the porous catalysts encountered in trickle-bed reactors.

Colorimetry makes use of colourant in the liquid to colour particles in the bed where they were in contact with the liquid. The bed is dismantled, and the particles are then examined through optic methods such as photography and subsequent image processing. The major advantage of colorimetry is that it is direct and no model or assumptions are needed. Also, more information can be extracted about catalyst wetting other than the average wetting efficiency. The liquid flow pattern should however be stable so that the wetting efficiency is not overestimated. The major disadvantage is that the method is destructive and requires bed re-packing after each experimental run. Other aspects of and the possible pitfalls in the colorimetric evaluation of wetting efficiency is discussed in Chapter 3, which reports a colorimetric study to obtain the distribution of particle wetting. Until recently, very little colorimetric wetting efficiency data were available in the

literature, with the first data for trickle-bed reactors reported by Lazzaroni et al. (1988). Thereafter, Ravindra et al. (1997a) performed a colorimetric study to describe trickle-flow morphology rather than to measure wetting efficiencies. Recently, Baussaron et al. (2007) generated an extensive amount of colorimetric wetting efficiency data for several fluids, expanded by Julcour-Lebique et al. (2009) to propose a colorimetry-based wetting efficiency correlation.

In terms of direct applicability, wetting efficiency measurements from reactor studies are arguably the most important. After all, an important reason for the study of wetting efficiency or any hydrodynamic parameter is to understand the possible effects it has on reactor performance. The biggest disadvantage for reaction methods as a tool for parametric studies of wetting efficiency, is that most reaction studies are specific to a certain system with specific reagents and catalyst combined under specific operating conditions. Also, the existing reaction methods are based on some reactor model that require estimates for either external mass transfer or particle kinetics or both. Specific reaction-based wetting efficiency studies are discussed in more detail in section 2.3.

Figure 2.2 shows wetting efficiency correlations developed from data that were obtained with different measurement methods. Predicted wetting efficiencies are applicable to the reaction system that is employed in the study that is reported in Chapter 5. Also included is the prediction of the artificial neural network (ANN) of Larachi et al. (2001). It is based on almost all the known wetting efficiency data published before the correlation was developed, and can therefore be recommended for trickle-bed reactors where there are no experimental studies at the exact reactor conditions. However, empirical correlations can fail to extrapolate accurately, and it is often recommended that correlations that were developed from data generated at conditions close to the conditions of interest should be used (Dudukovic et al., 2002). To reduce sensitivity to extrapolation, Iliuta and Larachi (1999) developed a semi-theoretical model which integrates liquid holdup, pressure drop and wetting efficiency.

In Figure 2.2, only $v_{SL}$ is shown as independent variable which determines wetting efficiency. Generally, the liquid flow rate increases wetting efficiency and incomplete wetting can be expected for liquid velocities less than $4\,^{\mathrm{mm}}/_{\mathrm{s}}$. Though important, $v_{SL}$ is of course not the only parameter that affects wetting efficiency. The effect of gas flow rate and pressure is rather disputed in the literature. The most widely accepted theory is that increased gas mass velocity helps with spreading the liquid over the particles, thus increasing the wetting efficiency (Al-Dahhan and Dudukovic, 1995; Dudukovic et al., 2002), but some studies suggest the opposite (Burghardt et al., 1995; Herskowitz and Mosseri, 1983) whereas yet others did not find any noteworhty effects of the gas flow rate(Lazzaroni et al., 1988). Decreased particle size and porosity improve wetting due to cappilary forces (Lappalainen et al., 2008), but porosity variations can adversely affect the overall liquid distribution (Sie and Krishna, 1998). The contact angle between the liquid and the

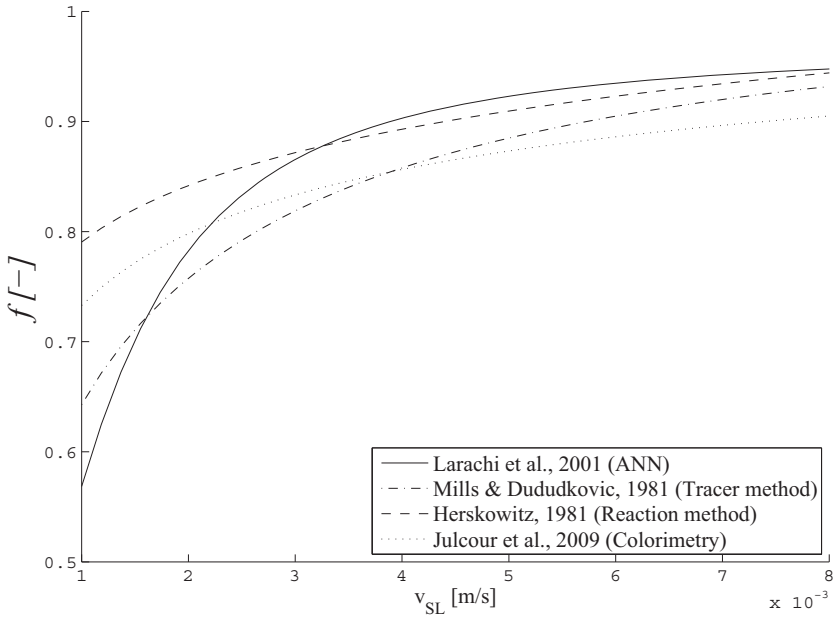


**Figure 2.2:** Literature correlations for wetting efficiency as measured with different methods.

solid affects spreading of the liquid, and also has a major effect on liquid distribution or multiplicity behaviour (van der Merwe and Nicol, 2009).

### 2.2.2 Mass transfer

The overwhelming majority of liquid-solid mass transfer measurements were obtained using either a dissolution or an electrochemical technique. The dissolution technique makes use of packing material which is coated with a soluble solid, and the amount of solute in the effluent can be used to determine the rate of liquid-solid mass transfer. The effluent concentrations should be far from equilibrium to ensure that the process is controlled the rate of liquid-solid mass transfer. The solute is usually sparingly soluble in the liquid to prevent excessive change in packing characteristics. Typical coating materials for the dissolution in water (which is generally used in this technique) are bezoic acid and naphthalene (Specchia et al., 1978; Lakota and Levec, 1990). In the electrochemical technique, an electrolyte solution is used as the process liquid, and undergoes an eloctrochemical reaction with a cathode in the bed. The cathode is usually a single pellet with the same geometry as the packing, and the method is therefore especially suited to the measurement of local mass transfer rates at a specific position in the bed. An example of this is the characterisation of liquid-rich and gas-rich pulses in the pulsing flow regime (Chou et al., 1979). Since it has to be an electrolyte, the choice of process liquids is limited (Latifi et al., 1988), which make it unsuitable for liquid-solid mass transfer measurement for typical trickle-bed reactor systems such as hydroprocessing reactors.

Most trickle-bed reactor studies make use of a correlation based on one of the above

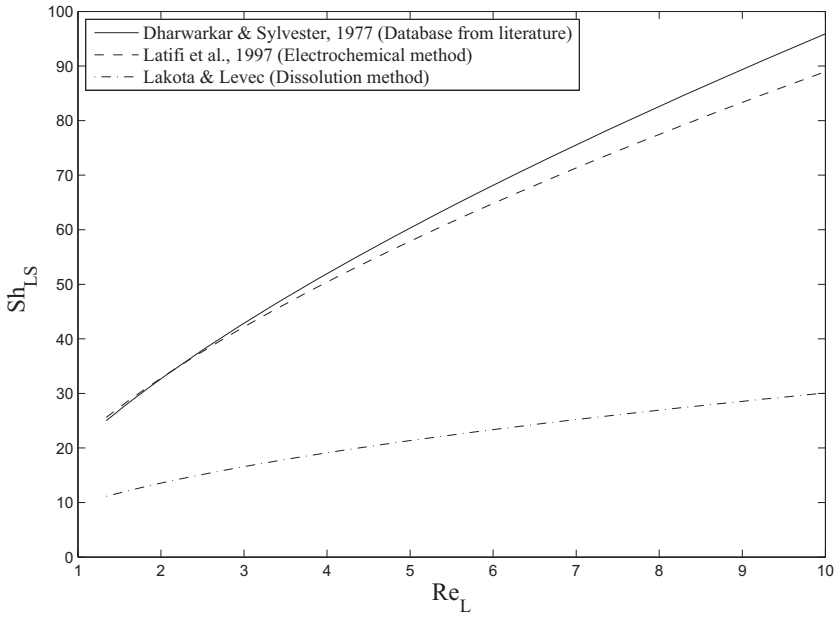


**Figure 2.3:** Literature correlations for liquid-solid mass transfer as measured with different methods.

techniques to estimate liquid-solid mass transfer, if necessary. Exceptions are those of Morita and Smith (1978) and Goto et al. (1975). The latter measured liquid-solid mass transfer with the dissolution technique, after which it was applied to the catalytic oxidation of formic acid in a trickle-bed reactor. Banchero et al. (2004) measured overall gas-to-particle mass transfer rates and concluded that currently, mass transfer resistances are overpredicted for high-pressure trickle-bed reactors[2]. There is a large deficiency of reactor-based measurements, especially under high pressures (Highfill and Al-Dahhan, 2001; Dudukovic et al., 2002). Most correlations of liquid-solid mass transfer are of the form

$$Sh = A \cdot Re_L^n Sc_L^{1/3} \tag{2.8}$$

Some liquid-solid mass transfer correlations for different measurement methods are shown in Figure 2.3. Again the figure is based on the reaction system in Chapter 5 ($Sc_L \approx 2000$).

Gas-liquid mass transfer is usually measured through the physical absorption or desorption of a gaseous component in the liquid or through chemical absorption using of a fast (uncatalysed) reaction between a gas and liquid component (Marquez et al., 1994). The overall resistance to gas-liquid mass transfer is constructed of a gas-side and a liquid-side mass transfer resistance (see Figure 2.1). The gas-side mass transfer coefficient is usually much faster and therefore less important than the liquid-side coefficient, but may have an effect when the gas density is high (Dudukovic et al., 2002). At atmospheric pressures,

[2]The authors did not take into account any partial wetting enhancement effect, which may be an explanation. Still, operation was at typical near-complete wetting conditions.

where most experimental studies are performed, only the liquid-side mass transfer coefficients are usually measured. Based on literature correlations, overall gas-liquid mass transfer coefficients appear to be of the same order of magnitude as liquid-solid mass transfer, though possibly slightly lower[3]. Gas-solid mass transfer is generally considered to be instantaneous for all practical purposes.

### 2.2.3 Liquid flow morphology and multiplicity

Insights into liquid flow morphology are usually obtained by "visual" studies such as tomography (Lutran et al., 1991; Sederman and Gladden, 2001; van der Merwe et al., 2007) or colorimetry (Ravindra et al., 1997a). In the trickle-flow regime the liquid is suggested to be present in the form of film-type flow or rivulet-type flow (Zimmerman and Ng, 1986; Lutran et al., 1991). For poor inlet distribution, channelling of the liquid can also be expected (Ravindra et al., 1997a). The different flow structure types have been used to explain the phenomenon of hysteresis in trickle flow, where the hydrodynamic behaviour of the bed is a function of flow history (Kan and Greenfield, 1979; Christensen et al., 1986). A more theoretical account of the mechanism underlying hysteresis behaviour was given by van der Merwe and Nicol (2009) in terms of pore cappilary forces and liquid-solid contact angles. It has been shown that the boundaries of hydrodynamic multiplicity can be defined by the behaviour of the bed after it has been subjected to specific pre-wetting procedures (Loudon et al., 2006; van der Merwe and Nicol, 2009). The most important amongst these are Levec pre-wetting, which represents the lower boundary in pre-wetted beds for most hydrodynamic parameters, and Kan-liquid or Super pre-wetting representing the upper boundary. In the former case, the bed is pre-wetted and drained prior to operation whereas the Kan-liquid boundary is obtained by operating the bed in the pulsing regime before steady state operation. Super pre-wetting refers to a startup where the bed is flooded, but not drained before the liquid is introduced at the operational flow rate. It was shown that Kan-liquid and Super pre-wetted beds have similar behaviour (van der Merwe, 2008), and these pre-wetting methods are collectively referred to as "extensive pre-wetting" in the rest of this thesis. In most investigations, some form of pre-wetting is employed in order to be able to generate repeatable results. The precise pre-wetting procedure is often not reported.

Almost all morphological and hysteresis studies are performed for atmospheric air-water systems, though Kuzeljevic et al. (2008) recently quantified pressure-drop hysteresis for a high-pressure system and van der Merwe et al. (2008) investigated the hysteretic behaviour of a pilot trickle-bed reactor. Most hysteresis studies report pressure-drop and liquid holdup data. Little work on the multiplicity behaviour of wetting efficiency

[3]Unlike liquid-solid mass transfer, gas-liquid mass transfer is depends strongly on the gas flow rate. A direct comparison is therefore not possible.

(van der Merwe and Nicol, 2009) and liquid-solid mass transfer (Sims et al., 1993) has been performed so far.

## 2.3 Reactor studies and liquid-solid contacting

Though countless trickle-bed reaction studies are avaiable in literature, only those that integrate knowledge of hydrodynamics with trickle-bed reactor results will be discussed here. Generally, two approaches are taken to the integration of reactor studies with trickle-flow hydrodynamics: Either, hydrodynamic theory is used to predict reactor performance such as conversion, which is then compared to experimental reaction data (predictive approach); or reaction data are used to make hydrodynamic measurements (diagnostic approach).

In the latter category, several studies were done to obtain estimations of wetting efficiency under trickle-flow conditions, sometimes coupled with measurements for liquid-solid or gas-liquid mass transfer coefficients. In most of the studies the limiting reagent was present in the gas and the liquid, or only in the gas. The effect of wetting efficiency and mass transfer resistances is then described according to the additive model stated in Equation (2.6), first used by Hartman and Couglin (1972) to find agreement between experimental data and a model based on literature estimation of gas-liquid and liquid-solid resistances.

Though most of these studies employ the additive model, they do so in different ways and are sometimes interpreted differently. As shown previously, Sedriks and Kenney (1972) used Equation (2.6) as a description of bed-scale wetting, estimating wetting efficiencies from overall rate estimations for completely wetted and completely dry particles, to illustrate the importance of pre-wetting. Ruecker and Ackgerman (1987) took a similar approach, determining the reaction rates in a vapour-phase packed bed reactor to determine $r_d$ and then in an (almost exclusively) liquid-phase packed bed reactor to determine $r_w$. It was possible to operate the bed in the vapour phase employing a very high $H_2$-to-liquid feed ratio. Realising that the methods of Sedriks and Kenney (1972) and Ruecker and Ackgerman (1987) violate the (probable) condition of internal pore filling, Llano et al. (1997) studied the hydrogenation of anthracene for different vapour-to-liquid feed ratios of the limiting reagent. The data were extrapolated to zero liquid feed to obtain an estimation of the overall rate of reaction for an externally dry, internally wetted pellet. This was used in the additive model for the estimation of wetting efficiency. The method implicitly assumes that the average surface concentration of the limiting reagent is a function of wetting efficiency only, so that no external mass transfer data were reported.

Goto and Mabuchi (1984) employed an estimate of $\eta k_r$ for the oxidation of ethanol (first-order with respect to oxygen) by measuring conversions of an upflow reactor at high

liquid flow rates. Literature correlations were used to estimate gas-liquid and liquid-solid mass transfer in trickle-flow operation so that $r_w$ and $r_d$ could be determined for each experimental condition, in order to estimate wetting efficiency. The disadvantage of this method is that mass transfer rates are estimated with correlations, and not determined independently. The study focuses mainly on how fractional wetting affects conversions as compared to the complete wetting obtained during upflow operation. In another gas-limited reaction study, Mata and Smith (1981) varied liquid feed inlet saturation levels in order to be able to approximate particle kinetics and fractional wetting independently without the need for further kinetic studies. They had to rely however, on correlations for external mass transfer.

Morita and Smith (1978) managed to measure mass transfer and wetting efficiency indepently by conducting experiments at the same feed flow rates with catalysts of different activity. This work has the considerable advantage that the measurements are not affected by the accuracy of correlations, although an estimation of particle kinetics is needed, as well as a gas-liquid mass transfer correlation in order to decouple gas-liquid and liquid-solid mass transfer. A very similar method was used by Herskowitz et al. (1979) for a more complete set of wetting efficiency and liquid-solid mass transfer measurements.

Whereas all previous diagnostic studies of trickle-bed reactors are based on linear kinetics, Mogalicherla et al. (2009) developed a method for wetting efficiency estimation in a reactor where Langmuir-Hinshelwood kinetics are applicable. Using internal diffusion theory for nonlinear kinetics[4], it was possible to relate overall trickle-bed efficiency to average surface concentration of the rate-limiting (volatile) reagent, and hence to $f$.

All diagnostic studies seem to be on a reaction where the rate is determined by a volatile reagent, though especially in the refining industry, the performance of many reactors can be expected to be determined by a non-volatile reagent (Dudukovic, 1977; Sie and Krishna, 1998). Several integrated predictive reactor studies deal with these, for example the studies of Wu et al. (1996) and Khadilkar et al. (1996). The latter study was used for the development of a criterion to identify whether the reaction rate is controlled by the gas or (non-volatile) liquid component. Based on this criterion and experimental results, recommendations could be made for the mode of operation of a three-phase packed bed reactor (upflow vs. downflow).

The predictive approach is well suited to the investigation and verfication of existing hydrodynamic theories and correlations. Whereas diagnostic studies have to be simple to enable one to correctly identify and quantify certain hydrodynamic aspects, the predictive approach can incorporate complex reaction kinetics (Khadilkar et al., 1999; Chaudhari et al., 2002) or hydrodynamic modelling at different levels (Ravindra et al., 1997b; Gunjal and Ranade, 2007). Yet, it seems that the behaviour of a trickle-bed still leads to surprising (not modeled) results: Levec and Smith (1976) had to con-

[4]Similar to the Bischoff modulus discussed in Chapter 4.

clude that channelling occured inside the reactor, Ravindra et al. (1997b) found that liquid distribution, multiplicity and packing orientation led to unmodelled results and Gunjal and Ranade (2007) illustrated how sensitive a reactor can be to its hydrodynamics. Clearly, there is much to learn about liquid flow morphology and how it affects the performance of a reactor.

## 2.4 Conclusions

While trickle-bed reactors are widely used in industry and subject to numerous studies in laboratories, the research in this field are too often restricted to either reactor performance studies, hydrodynamic studies or theoretical studies. A more integrated approach coupling reaction phenomena, mass transfer and hydrodynamic characteristics with special emphasis on wetting efficiency can be highly recommended. Research opportunities that may aid in this cause include a more complete physical description of liquid-solid contacting, integration and validation of theoretical modeling with this description; and a reactor study on liquid-solid contacting that does not rely on correlations.

# Nomenclature

| | |
|---|---|
| $Bi'$ | modified Biot number, $Bi' = \frac{k_{LS}V_R}{S_p D}$ |
| $C$ | concentration, $^{mol}/_{m^3}$ |
| $D$ | reagent effective diffusivity, $^{m^2}/_{s}$ |
| $D_m$ | molecular diffusivity, $^{m^2}/_{s}$ |
| $d_p$ | catalyst pellet diameter, m |
| $f$ | wetting efficiency, dimenionless |
| $k_r$ | first-order reaction rate constant based on $V_R$, $s^{-1}$ |
| $k_{LS}$ | liquid-solid mass transfer coefficient, $^{m}/_{s}$ |
| $Q_L$ | liquid volumetric flowrate, $^{m^3}/_{s}$ |
| $r$ | reaction rate based on active catalyst volume, $^{mol}/_{m^3 s}$ |
| $Re_i$ | Reynolds number of $i$-phase, $Re_i = \frac{\rho_i v_{Si} d_p}{\mu_i}$ |
| $Sc_i$ | Schmidt number of reagent in the $i$-phase, $Sc_i = \frac{\mu_i}{\rho_i D_m}$ |
| $Sh_{LS}$ | Sherwood number for liquid-solid mass transfer, $Sh_{LS} = \frac{k_{LS} d_p}{D_m}$ |
| $S_p$ | pellet external area, $m^2$ |
| $V_R$ | catalyst pellet volume or shell volume for an egghell catalyst, $m^3$ |
| $v_{SL}$ | superficial liquid velocity $v_{SL} = \frac{Q_L}{A_c}$, $^{m}/_{s}$ |
| $X$ | conversion, dimensionless |
| $Z$ | reactor length, m |

*Greek letters*

| | |
|---|---|
| $\phi_G$ | Generalised (Aris) modulus, $\phi_G = \frac{V_R}{S_p}\sqrt{\frac{k_r}{D}}$ |
| $\eta$ | pellet efficiency factor, dimensionless |
| $\eta_0$ | overall efficiency factor, dimensionless |
| $\tau$ | reactor residence time, s |

*Subscripts*

| | |
|---|---|
| bulk | refers to bulk liquid |
| d | refers to (externally) completely dry pellet |
| L | refers to liquid phase |
| LF | refers to liquid-filled operation |
| s | refers to catalyst surface |
| TBR | refers to downflow (trickle flow) operation |
| w | refers to completely wetted pellet |

# CHAPTER 3

# VISUALISATION OF WETTING MORPHOLOGY

Colorimetric measurements of wetting effiency that will form the basis for pellet internal diffusion modelling in Chapter 4 are presented in this chapter. This work is an extract from work published in two papers (van Houwelingen et al., 2006, 2007).

Though usually well rationalised, most work on the measurement of wetting efficiency and modelling of its effect on reactor performance is based on theoretical "visualisations" of partial wetting under trickle-flow conditions: the vast majority of wetting efficiency data is inferred from tracer response curves and the influence of fractional wetting on trickle-bed efficiency is mostly modeled based on theoretical geometries and simplifying assumptions. The distribution of particle wetting efficiency is, although it was shown to potentially affect reactor performance (Beaudry et al., 1987), generally disregarded. Until recently, the literature of fractional wetting in trickle-flow suffered a definite shortage on direct wetting efficiency measurements.

This shortage was supplemented by colorimetric measurements (which is arguably the most direct measurement technique) by Baussaron et al. (2007). Also, through theoretically constructing tracer response curves based on the mass balance equations for bulk liquid dispersion and internal pellet diffusion proposed by Ramachandran et al. (1986), Julcour-Lebigue et al. (2007) have shown that the generally accepted but previously intuitive tracer method has good theoretical grounds. Baussaron et al. (2007) satisfactorily compared wetting efficiency data derived from tracer experiments and data obtained from the direct colorimetric method.

The focus of this work is therefore not predominantly on extending the existing database on direct wetting efficiency, but on obtaining insight into the morphology of wetting efficiency for a better understanding of the role that wetting efficiency can play

in a trickle-bed reactor. To this end, colorimetric experiments were conducted to obtain photos of particles that contain information about the global variation in, and the geometry of, partial wetting. Both boundaries of the hydrodynamic multiplicity of pre-wetted trickle flow as explained in Chapter 2 were explored.

## 3.1 Experimental

The principle behind the colorimetric evaluation of wetting efficiency/trickle flow patterns is simple: a suitable colourant is selected, which can be used to colour the particles in a packed bed as liquid flows over it. The packed bed then contains an immense amount of data on where and how the liquid contacted the solid. Not all of these data can directly be extracted and quantified and different aspects of wetting efficiency were previously reported using colorimetry, such as average wetting efficiency (Onda et al., 1967; Lazzaroni et al., 1988; Baussaron et al., 2007) or trickle-flow patterns, (Ravindra et al., 1997a)). As said, the focus in this work is on the global variation in particle scale wetting and on particle scale wetting geometry.

### 3.1.1 Trickle-flow setup and experimental procedure

The experimental setup is shown in Figure 3.1 and consists of a 1.0 m long, 63 mm I.D. glass column packed with 2.5 mm porous $\gamma$-alumina spheres, a low pressure $N_2$ feed system and two separate liquid feed systems, one for a clear water feed and one for water doped with a water-soluble colourant, Chrome-Azurol S. This colourant was previously used successfully by Lazzaroni et al. (1988) for the determination of wetting efficiency and has the advantage that it adsorbs irreversibly onto the external surface of the porous $\gamma$-alumina spheres without diffusing through the particles, thereby colouring only the surfaces that were contacted by the liquid. The clear water feed is used during start-up and for pre-wetting the packing, and is fed to the column until steady state is reached. This steady state is verified with liquid holdup and pressure-drop measurements, and visual observations through the glass column wall. Liquid holdup is measured with a weighing technique using a load cell, and pressure drop is measured with a differential pressure transmitter. Though the relative measurement of these parameters are considered good enough for the validation of steady state, absolute measurements are not considered accurate enough to be reported as experimental results.

After steady flow has been obtained, the feed is switched to the tank that contains a 0.2 g/L solution of the colourant Chrome-Azurol S. Liquid recycle lines with needle valves are installed around both feed tanks, which can be used to minimise disturbances during feed switchover. For a constant Chrome-Azurol S concentration of 0.2 g/L, 20 minutes of contacting time is required before the colour intensity of the colourant on the particles

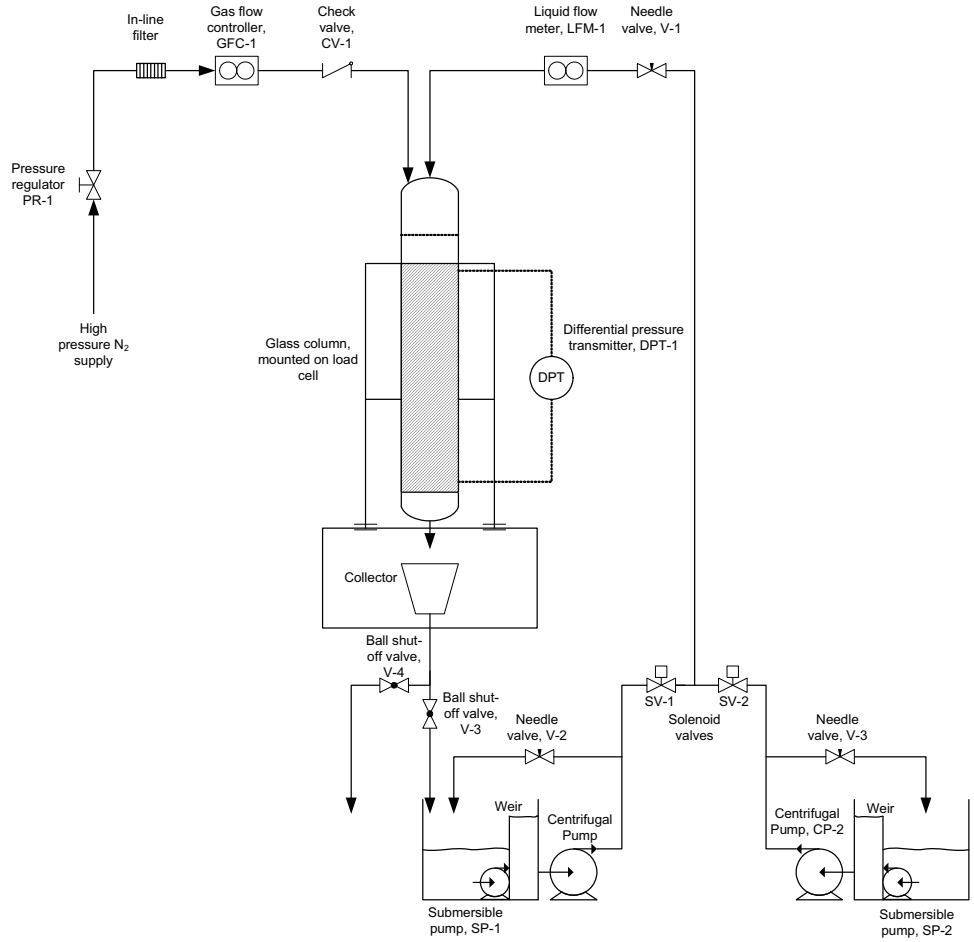


**Figure 3.1:** Trickle-bed experimental setup for colorimetric evaluation of wetting efficiency.

remains constant (Lazzaroni et al., 1988). After switchover, the colourant is initially stripped from the solution, and 40 minutes of steady-state colourant flow was required to avoid an axial colour intensity profile through the bed. Inherent in colorimetric methods is the assumption that trickle-flow is stable during steady state: flow fluctuations will lead to an overestimation of wetting efficiency. This assumption is supported by data from van der Merwe and Nicol (2005) and van der Merwe et al. (2007). It is also likely that flow instabilities will show in colour intensity variations of the particle surfaces that were contacted with the colourant. No significant variations were observed.

When exploring the effect of pre-wetting, startup procedures for flow experiments have to be well defined and carefully maintained. The boundaries of pre-wetted multiplicity were obtained through the following procedures:

- *Levec pre-wetting.* Prior to liquid irrigation, the bed is kept completely submersed in water for at least 3 hours to ensure complete internal saturation, and the complete external wetting of all particles. The bed is then drained under experimental gas-flow conditions until only the residual liquid holdup remains, after which liquid irrigation at the required rate is introduced.

- *Extensive pre-wetting.* After the packing has been internally saturated, the bed is drained and gas flow is set to the required rate. Liquid flow is increased until the pulsing regime is encountered and is then gradually set back to the required rate.

In both cases, coulourant is introduced only after steady state was achieved. These two pre-wetting methods represent the lower (Levec) and higher (extensively pre-wetted) hydrodynamic multiplicity cases for pre-wetting (Loudon et al., 2006). The flow conditions investigated in this work are listed in Table 3.1.

| Pre-wetting procedure | L ($kg/m^2s$) | G ($kg/m^2s$) |
|---|---|---|
| Levec | 1.6 | 0.152 |
| - | 5.35 | - |
| Extensive | 1.6 | 0.152 |
| - | 5.35 | - |

**Table 3.1:** Experimental flow conditions.

### 3.1.2 Data capturing and processing

After the bed is dry, the particles in the bed are unloaded and the whole population of particles is mixed, so that the sample particles are representative of the particles in the bed. These sample particles are captured in a plate in which a $17 \times 17$ grid of 2.7 mm holes have been drilled. Particles in the grid are retained by two clear PVC plates fastened on both sides of the grid and these are then photographed in a light box as shown in Figure 3.2 to obtain consistent images. The grid is photographed from two sides, resulting in two photos for each particle, so that the largest possible area can be evaluated. Fifteen samples of $17 \times 17$ particles were used to characterise each bed that was subjected to colorimetric flow experiments. Using software from Matlab's® Image Processing toolbox, half-particles are identified and extracted from the image and the wetted fraction of each half-particle is calculated. The imaging was designed to exploit the fact that Matlab® handles an image as a three-dimensional matrix containing the red, green and blue colour intensity for each pixel. The grid colour was blue, resulting in a good contrast between the grid and the particles when applying a red filter to the images; whereas the background colour was green for easy realignment of the image if the photographed grid was skew. Each half-particle is extracted as a separate $70 \times 70$ pixel image, and each pixel on each image is classified as wetted or non-wetted based on its colour.

The fractional wetting of an imaged half-particle was then calculated by weighting each pixel on an image according to the surface area it represented on the 3-D praticle for the given position of its 2-D projection on the image. Half particles in the two photos

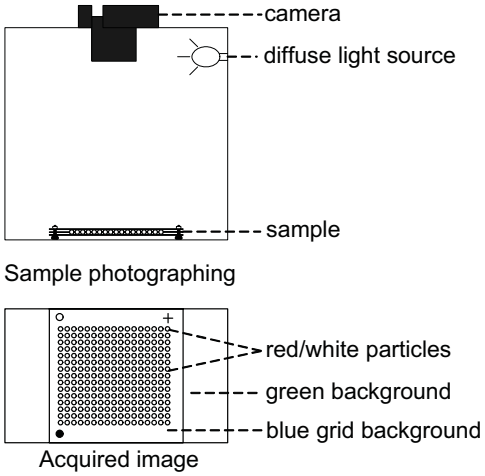


**Figure 3.2:** Particle imaging.

for the same grid were then matched to give the wetting efficiency of each (complete) particle. Reference points for the matching of half-particles were supplied by markings on the grid as is shown in Figure 3.2. An example of the extracted half-particle images is shown in Figure 3.3.

For information on wetting geometry, 14 particles were hand-picked for an as-large-as-possible wetting efficiency range and each of them was captured in 2 high-resolution photographs of opposite hemispheres. These results are utilised in Chapter 4.

### Data accuracy

Though the image analysis is rather straightforward, some important analysis steps are necessary to ensure that results are accurate and statistically significant. One of the major sources of possible error in wetting efficiency estimation is the fact that it is almost impossible to classify the pixels on the outer perimeter of a half-particle image due to blurriness, imperfect cropping of, and shadows on the image. Since the pixels near the outer perimeter of a 2-D projection of a 3-D sphere represent a large fraction of the spherical area, incorrect classification of these pixels can lead to large errors in wetting efficiency estimation and have to be discarded. This "boundary effect" is illustrated in Figure 3.4. Based on several images of fully wetted and completely dry half-particles, it was found that all pixels further away than $r/r_p = 0.91$ from the centre point of the image had to be discarded due to the boundary effect (the outer three rings of pixels in the $70 \times 70$ pixels image exhibit boundary errors). This means that only 60% of the total particle area can be taken into account.

The fact that only 60% of a particle's surface could be evaluated, give rise to an important question: is 60% of the surface area enough for the data on the global variation in particle scale wetting efficiency to be meaningful? For example, if only one pixel could be evaluated, a conclusion of the study would be that all particles in a TBR are

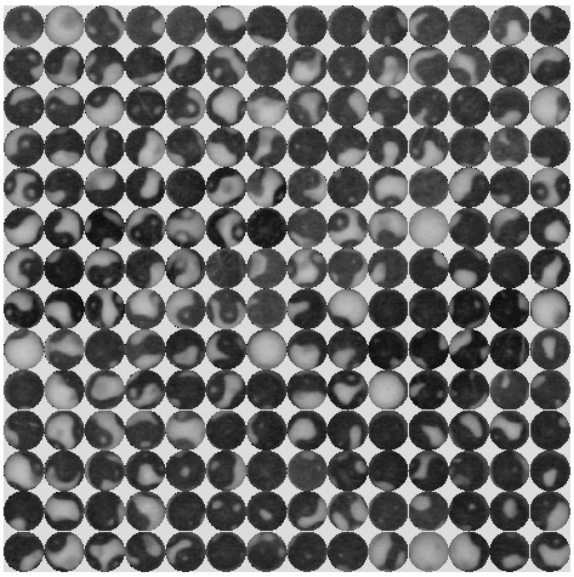

**Figure 3.3:** An example of extracted half-particle images.

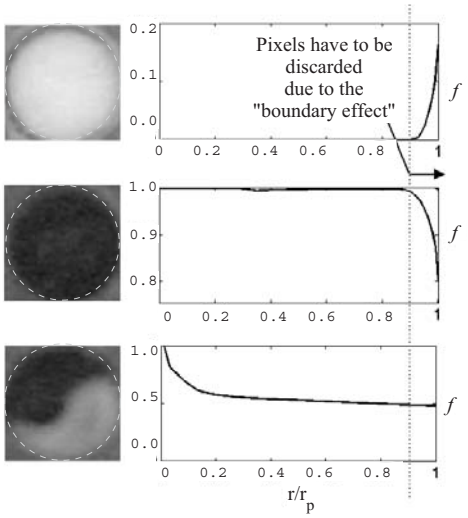


**Figure 3.4:** The boundary effect as a source of possible experimental error.

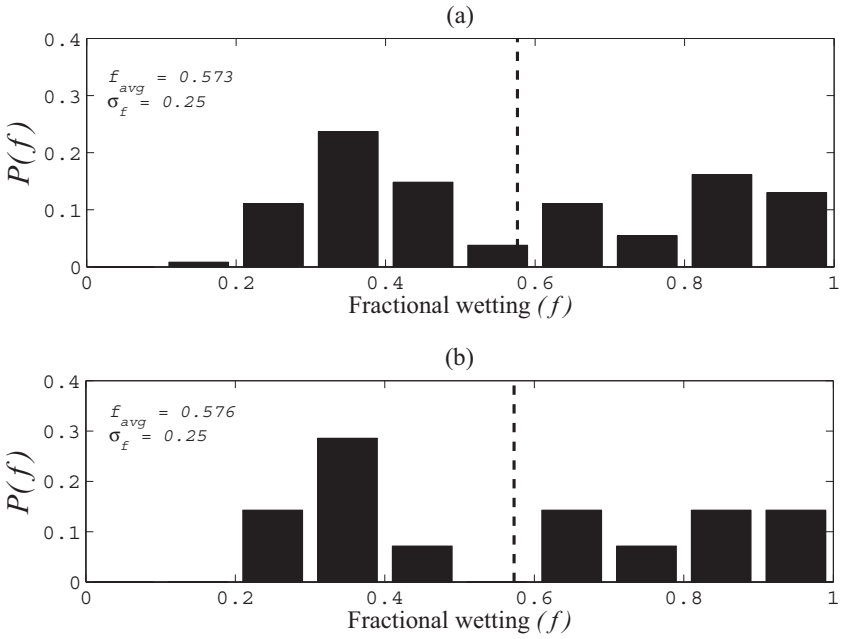


**Figure 3.5:** Simulated (a) 60% PWD for (b) a well characterised PWD consisting of 14 particles.

either completely wet or completely dry. The data in Figure 3.5 was generated to ensure that 60% of the total surface area is indeed enough. Shown in the figure are particle wetting distributions (PWDs), histograms of the distribution of particle scale wetting efficiency. The difference between the two PWDs in the subfigures is an estimate of how representative the PWDs are if only 60% of each particles surface can be evaluated: the 14 fractionally wetted particles that were photographed in high resolution ($>$ 90% of the surface can be evaluated) were characterised in detail so that wetting geometry and extent are known for each particle. This information was built into a computer model and each particle was then "viewed" from 500 random viewing angles. Two caps on opposite sides of the particle (together constituting of 60% of the particle area) were then used to estimate the wetting efficiency for each particle viewed at each angle. This simulated image capturing is very similar to the physical method of random sampling and photographing the opposite half-particles, and one can predict the (60%) PWD that would be obtained for this single well-known PWD with the current photographing and image analyis method. Since Figure 3.5(a) and (b) agree closely, the 60% PWDs are good representations of the true PWDs.

It is also important to ensure that enough particles are photographed to be representative of the bed population. In this investigation, a packed bed contained between 300 000 and 400 000 particles, whereas a maximum of 289 particles could be photographed and analysed in one grid. For each experiment, 15 grids were photographed and analysed. Figure 3.6 shows the average wetting efficiencies for 15 different samples from the same bed. It is clear that even only one sample is quite representative of the bed in terms of

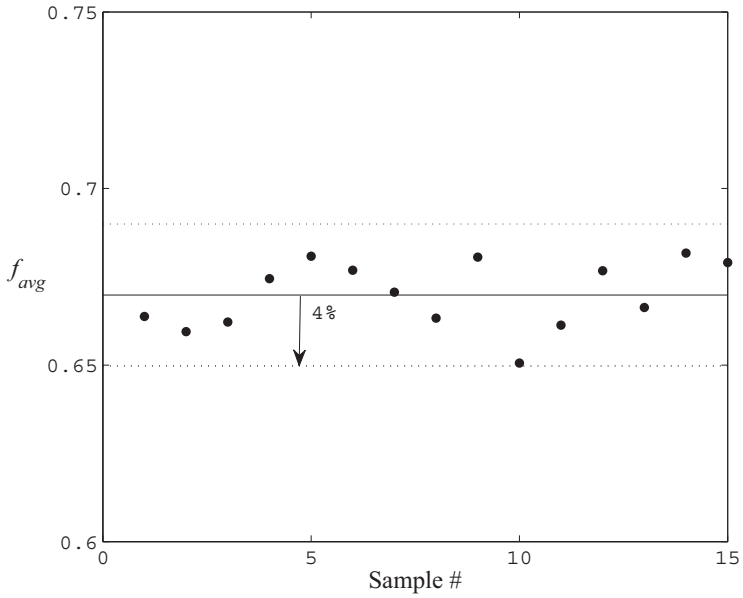


**Figure 3.6:** Average wetting efficiencies for different samples from the same bed population. One sample consists of $\leq$ 289 particles, photographed in the 17 $\times$ 17 capturing grid

the average wetting efficiency: all values are within 4% of the mean.

This is not the case for the standard deviation of the distribution, which varied by up to 10% for different samples consisting of about 17 $\times$ 17 particles taken from the same bed population as is shown in Figure 3.7a. One sample is clearly not representative of the bed in terms of the standard deviation of the particle wetting efficiency distribution. For the PWDs to be statistically representative, the value of the total population standard deviation should converge within the fifteen samples that were taken from the bed. That this is indeed the case, is shown in Figure 3.7b: A total sampled population of more than 2000 particles is enough for representative distributions in terms of the standard deviation, and for all experiments $\pm 3000 - 4000$ particle were sampled.

## 3.2 Results and discussion

Particle wetting distributions for the two investigated pre-wetting methods are shown in Figures 3.8 (low liquid flow rate, L = 1.60 $^{kg}/_{m^2s}$) and 3.9 (high liquid flow rate, L = 5.35 $^{kg}/_{m^2s}$). The effect of pre-wetting is striking. The extensively pre-wetted beds have a fractional wetting of most particles close to the average wetting, whereas the PWD's Levec pre-wetted beds clearly show the existence two populations of particles - a significant fraction of particles is very poorly wetted or even completely dry, so that parts of a Levec pre-wetted bed may not be utilised whatsoever. This effect is more pronounced at the lower liquid flow rate (figure 3.8). Apart from the differences in PWDs, average

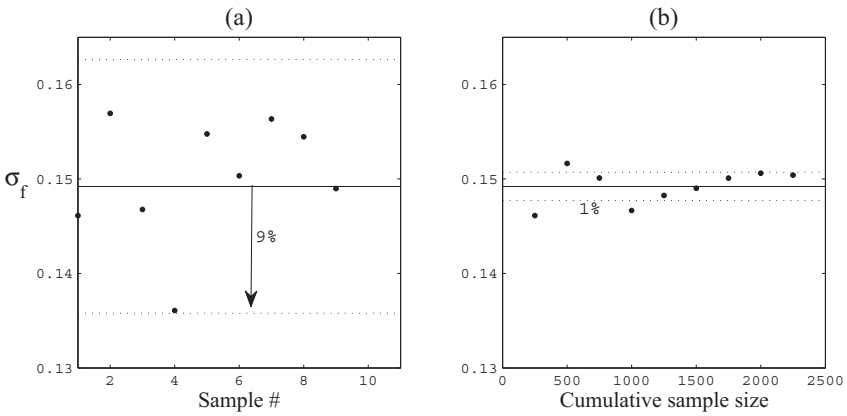


**Figure 3.7:** Standard deviation for (a) different samples from the same bed, and (b) as a function of the sampled population size sampled from the same bed.

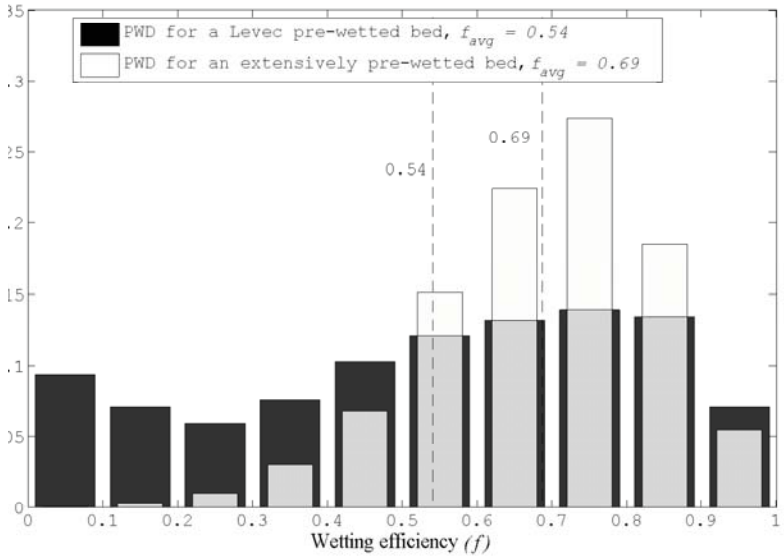


**Figure 3.8:** Particle wetting distributions for Levec- and extensively pre-wetted beds at L = 1.60 $^{kg}/_{m^2s}$. Gas flow rate was G = 0.15 $^{kg}/_{m^2s}$

wetting efficiencies are far lower for the Levec pre-wetted beds than for the Kan pre-wetted beds at corresponding liquid and gas flow rates.

One might argue that the only difference between the Levec and extensively pre-wetted beds is only in average wetting efficiency and that the PWD is only determined by the average wetting efficiency. That this is not the case, becomes clear when one compares the PWD for the extensively pre-wetted bed at L = 1.60 $^{kg}/_{m^2s}$ (Figure 3.8) with that for the Levec pre-wetted bed at L = 5.35 $^{kg}/_{m^2s}$: Though both beds had more or less the same average wetting efficiency, the PWDs are completely different. Where the PWD of the extensively pre-wetted bed shows a Gaussian distribution around the average wetting efficiency, the bimodal distributions in the Levec pre-wetted beds suggest two types of flow, or at least channelling/bypassing of the liquid. The average wetting is

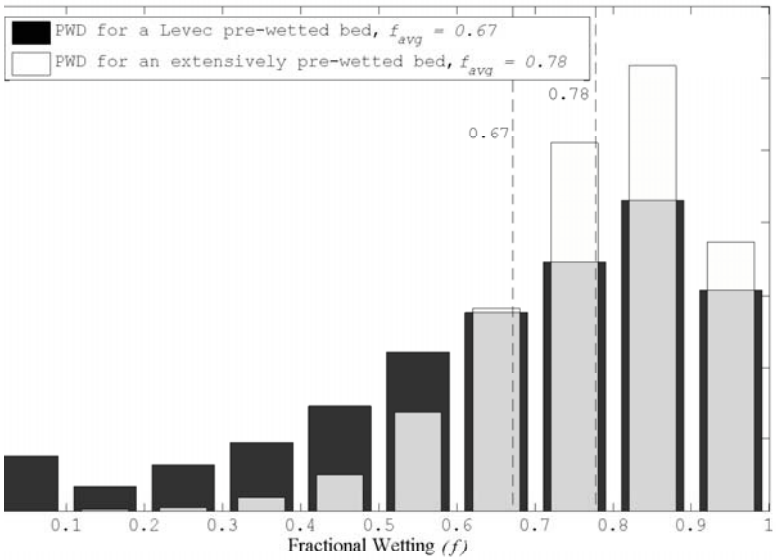


**Figure 3.9:** Particle wetting distributions for Levec- and extensively pre-wetted beds at L = 5.35 $^{kg}/_{m^2s}$. Gas flow rate was G = 0.15 $^{kg}/_{m^2s}$

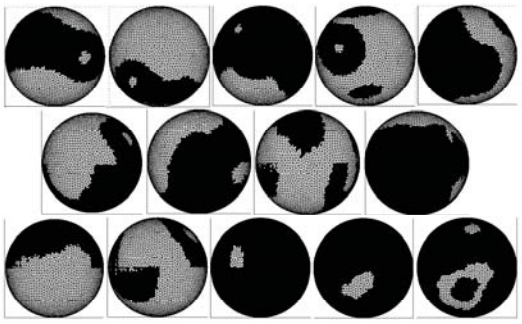

**Figure 3.10:** Graphic representation of obtained wetting geometry data

therefore not necessarily a good description of the PWD's.

A secondary result from the colorimetry experiments is a complete three-dimensional description of wetting geometries. A graphic representation of the 14 well-characterised particles is shown in Figure 3.10. A white colour represents dry zones, and black the wetted zones. Fractional wetting of these particles varies between $f = 0.26$ and $f = 0.97$. An interesting feature of the wetting geometry present on most particles are dry spots where the particles were in contact with one another. These can also be seen in Figure 3.3.

## 3.3 Summary

The work presented in this chapter suggests that different types of flow can prevail in trickle-bed reactors, depending on the hydrodynamic state and operating conditions.

The PWDs can be summarised as follows: for the extensively pre-wetted beds, all of the particles were in some fashion contacted by the flowing liquid. The shapes of the PWDs are consistent, suggesting that flow in extensively pre-wetted beds was stable and very similar for all experimental flow conditions. The Levec pre-wetted beds contain a large amount of dry and poorly wetted particles, especially at the lower liquid flow rate. The shapes of the distributions are very different from those of the extensively pre-wetted beds, and two local maxima suggest two different types of flow, or at least channelling/bypassing of the liquid flow. Visually, wetting geometries look very similar to those reported by Baussaron et al. (2007). In the next chapter, these geometries will be used for modeling of intraparticle diffusion.

# Nomenclature

| | |
|---|---|
| $f$ | fractional wetting of particle, dimensionless |
| $G$ | gas mass flux, $^{kg}/_{m^2s}$ |
| $L$ | liquid mass flux, $^{kg}/_{m^2s}$ |
| $P(f)$ | fraction of particles with fractional wetting within histogram bin, dimensionless |
| $r$ | distance from centrepoint of half-particle image, pixels |
| $r_p$ | half-particle radius on image, pixels |

# CHAPTER 4

# EFFECTIVENESS FACTORS FOR PARTIALLY WETTED CATALYSTS

In this chapter, experimental wetting geometries are used to investigate reaction and diffusion in partially wetted catalysts. Models that describe these have been in existence for some time, and have been used with some success (Wu et al., 1996; Llano et al., 1997). The theorectical verification of existing models is usually based on easily definable theoretical wetting geometries such as spherical caps or rings (Goto et al., 1981; Yentekakis and Vayenas, 1987). All validations of existing and proposed models in this chapter are based on the realistic geometries obtained from the colorimetric experiments.

The estimation of catalyst effectiveness factors, defined as the ratio between the observed reaction rate in a pellet and the reaction rate in the absence of intraparticle mass transfer resistances, plays an important role in chemical reactor engineering and is governed by the solution to the reaction-diffusion equation within the catalyst:

$$\bigtriangledown^2 C - \phi^2 \times y(C) = 0 \tag{4.1}$$

where $\phi$ describes the ratio of reaction to diffusion and $y(C)$ is the kinetic expression in terms of the reagent concentration(s). The effectiveness factor can be evaluated by the integral of the reagent concentrations over the catalyst volume or the reagent fluxes over the catalyst's external area.

Exact analytical solutions for pellet efficiency factors are almost exclusively available for first- and zero-order reactions in pellets with well defined geometries[1] (Lee and Kim, 2006). Unique boundary conditions are also required, where the boundary condition at

[1]One-dimensional geometries for which analytical effectiveness factor derivations are available are those of an infinite slab, a sphere and an infinite cylinder.

the external surface is the same over the whole surface. Catalyst particles subject to trickle-flow generally do not confirm to these requirements:

- At least two reagents (a gas and a liquid) react in a trickle-bed reactor and the kinetic expression is probably not simply first order in one reagent. To simplify effectiveness factor derivations, the reaction in a trickle-bed reactor is usually classified as being either gas- or liquid-limited, i.e. the concentration of either the liquid or the gas reagent respectively is constant throughout the catalyst particle so that pseudo-first order kinetics can be assumed for the limiting reagent. A reaction is usually classified as gas- or liquid-limited based on $\gamma$, where

$$\gamma = \frac{\alpha D_B C_{B,bulk}}{D_A C_A^*} \tag{4.2}$$

  Throughout this chapter, $B$ refers to the liquid and $A$ to the gaseous reagent. A reaction is said to be gas-limited if $\gamma \gg 1$, and liquid-limited if $\gamma \ll 1$. Liquid-limited reactions are modelled differently from gas-limited reactions in trickle-beds.

- Boundary conditions for partially wetted particles are mixed, that is, the boundary condition for the wetted surface differs from that for the dry surface. Except for specific (theoretical) wetting and particle geometries, mixed boundary conditions will increase the dimensionality of Equation (4.1).

The chapter deals with the following questions surrounding pellet efficiency in trickle-bed reactors:

- What is the performance of existing models for liquid-limited and gas-limited reactions? Investigations that deal with this question already exist (Goto et al., 1981; Mills and Dudukovic, 1979) but not where true partial wetting geometries are used. In this chapter, the true wetting geometries shown in Figure 3.10 are used in the investigation.

- When can a reaction be classified as liquid- or gas limited, and is it possible to reconcile models for gas- and liquid-limited reactions in the case where both reagents play a role? For this purpose, the reaction $r_A = \alpha r_B = -\alpha k_r C_A C_B$ taking place in a partially wetted catalyst is investigated. A numerical study of this reaction was also performed by Yentekakis and Vayenas (1987), but no suggestions were made for an easy-to-use analytical expression.

- Many trickle-bed reactors make use of eggshell catalysts. Though it is rather easy to derive analytical expressions for a completely wetted eggshell catalyst with first-order reaction kinetics, the role of partial wetting may differ significantly for eggshell catalysts than for monodispersed catalysts. The effect of partial wetting on the performance of this type of catalyst is therefore also investigated.

The work is based on the numerical modelling of partially wetted monodispersed and eggshell catalyst spheres, using the finite element method (FEM) and true wetting geometries obtained from the work discussed in Chapter 3. FEM is used since it can easily handle complex geometries and is also suitable for higher order kinetic expressions (Mills et al., 1988; Ramachandran, 1991). All work is limited to isothermal conditions.

## 4.1 Numerical method

### 4.1.1 First-order reaction, $-r = k_r C$

Models for gas- and liquid-limited reactions in partially wetted catalysts assume a constant concentration of the non-limiting reagent and first-order kinetics for the limiting reagent so that the reaction can be written as $-r = k_r C$. In dimensionless form, the equation for steady-state diffusion combined with such a reaction within a catalyst sphere is given by

$$\nabla^2 c - \phi^2 c = 0 \tag{4.3}$$
$$c = \frac{C}{C_{bulk}};\ \phi = r_p \sqrt{\frac{k_r}{D}}$$

Hence, one wants to solve the following integral:

$$\int_V \left[\nabla^2 c - \phi^2 c\right] \cdot w \ dV = 0 \tag{4.4}$$

where $w$ is any one of all possible weighting functions, and $V$ is the body for which the diffusion-reaction equation will be solved. Making use of the product rule, Equation 4.4 can be written as:

$$\left[\int_V \nabla \cdot (w \nabla c) \ dV - \int_V \nabla w \nabla c \ dV\right] - \int_V \phi^2 c \cdot w \ dV = 0 \tag{4.5}$$

The boundary conditions can be accounted for by making use of the Gauss divergence theorem (analogous to a mass balance over the body):

$$\int_V \nabla \cdot f \ dV = \int_S f \cdot \overline{n} \ dA \tag{4.6}$$
$$\therefore \int_V \nabla (w \nabla c) \ dV = \int_S w \nabla c \cdot \overline{n} \ dA \tag{4.7}$$
$$\text{and } \nabla c \cdot \overline{n} = Bi\,(1 - c)\,; \text{ where } Bi = \frac{k_c r_p}{D} \tag{4.8}$$

And Equation (4.5) can be written as:

$$\int_S Bi(1-c)\cdot w\ dA - \int_V \bigtriangledown c \bigtriangledown w\ dV - \int_V \phi^2 c\cdot w\ dV = 0 \tag{4.9}$$

Equation (4.9) is valid for any body $V$ with external area $S$. In the finite element method, $V$ is divided into small elements $v$ with concentrations $\{c\}$ at each node point. The concentration at any point within the volume is approximated by an interpolation matrix, $[N]$.

$$\begin{aligned} c(x,y,z) &= [N]\{c\} \\ w(x,y,z) &= [N]\{w\} \\ &\text{and} \\ \bigtriangledown c(x,y,z) &= [B]\{c\} \\ \bigtriangledown w(x,y,z) &= [B]\{c\} \end{aligned} \tag{4.10}$$

where $[B] = \bigtriangledown[N]$ and $\{w\}$ is the value of $w$ at each node point. Note that $[N]$ and $[B]$ are functions of the element geometry only, and that $\{c\}$ is only defined for the node points. $[N]$ and $[B]$ are specific to each element and differ for the surface integral from that for the volume integrals. More information on the choice of element geometry and the contruction of $[N]$ and $[B]$ can be found in any textbook on finite element methods, for example Cook et al. (1989). For each element

$$\begin{aligned} &\int_s Bi(1-c)\cdot w\ dA - \int_v \bigtriangledown c \bigtriangledown w\ dV - \int_v \phi^2 c\cdot w\ dV \\ &\approx \{w\}^T \left[\int_s [N]^T Bi\ dA - \{c\}\int_s [N]^T[N] Bi\ dA \right. \\ &\left. -\{c\}\int_v [B]^T[B]\ dV - \{c\}\int_v \phi^2 [N]^T[N]\ dV\right] \end{aligned} \tag{4.11}$$

Equation (4.9) can be approximated by the sum of above integrals for all elements $v$ in the volume $V$:

$$\begin{aligned} &\sum_v^V \{w\}^T \left[\int_s Bi[N]^T\ dA - \{c\}\int_s Bi[N]^T[N]\ dA \right. \\ &\left. -\{c\}\int_v [B]^T[B]\ dV - \{c\}\int_v \phi^2 [N]^T[N]\ dV\right] = 0 \end{aligned} \tag{4.12}$$

The integrals for each specfic element are obtained according to a specified concentration variation within each element as a function of the nodal concentrations (e.g. linear or quadratic variation). Since Equation (4.12) should hold true for all possible weighting

functions $w$:

$$\sum_{v}^{V}\left[\left(\int_{v}[B]^{T}[B]\ dV\ +\ \int_{v}\phi^{2}[N]^{T}[N]\ dV+\int_{s}Bi[N]^{T}[N]\ dA\right)\{c\}\right]$$
$$=\sum_{v}^{V}Bi\int_{s}[N]^{T}\ dA \tag{4.13}$$

Which is of the form

$$\underbrace{[K]}_{n\times n}\times\underbrace{\{c\}}_{n\times 1}=\underbrace{[F]}_{n\times 1}$$

The stiffness matrix $[K]$ and vector $[F]$ are functions of the geometry and known constants only, so that the nodal concentrations $\{c\}$ can be solved for, solving a system of linear equations.

### 4.1.2 Reactions of the form $r_A = \alpha r_B = -\alpha k_r C_A C_B$

In dimensionless form, the reaction-diffusion equations for the reaction $r_A = \alpha r_B = -\alpha k_r C_A C_B$ in a spherical pellet are:

$$\begin{aligned}\bigtriangledown^2 a &- \phi_A^2 ab = 0\\ \bigtriangledown^2 b &- \phi_B^2 ab = 0\\ a &= \frac{C_A}{C_{A,\ bulk}};\ \phi_A = r_p\sqrt{\frac{\alpha k_r C_{B,\ bulk}}{D_A}}\\ b &= \frac{C_B}{C_{B,\ bulk}};\ \phi_B = r_p\sqrt{\frac{k_r C_{A,\ bulk}}{D_B}}\end{aligned} \tag{4.14}$$

Following the same route as Equations (4.4) to (4.13), the FEM equations for this reaction are:

$$\left[\sum_{V}\left(\int_{v}[B]^{T}[B]\ dV+\int_{s}Bi_A[N]^{T}[N]\ dA\right.\right.$$
$$\left.\left.+\ \int_{v}\phi_A^2[N]^{T}[N]\{b\}[N]\ dV\right)\right]\cdot\{a\}=\sum_{S}\int_{s}Bi_A[N]^{T}\ dA \tag{4.15}$$

$$\left[\sum_{V}\left(\int_{v}[B]^{T}[B]\ dV+\int_{s}Bi_B[N]^{T}[N]\ dA\right.\right.$$
$$\left.\left.+\ \int_{v}\phi_A^2[N]^{T}[N]\{a\}[N]\ dV\right)\right]\cdot\{b\}=\sum_{S}\int_{s}Bi_B[N]^{T}\ dA \tag{4.16}$$

$$\tag{4.17}$$

Since both equations contain the terms $\{a\}$ and $\{b\}$, the equations cannot be solved in the same fashion as Equation (4.13). The coupled system can be solved by defining the residuals $R_A$ and $R_B$ that should be equal to 0 for the correct concentration profiles:

$$\begin{aligned} R_A &= \left[\sum_V \left(\int_v [B]^T[B]\ dV + \int_s Bi_A[N]^T[N]\ dA \right.\right. \\ &+ \left.\left. \int_v \phi_A^2[N]^T[N]\{b\}[N]\ dV\right)\right] \cdot \{a\} - \sum_S \int_s Bi_A[N]^T\ dA \end{aligned} \tag{4.18}$$

$$\begin{aligned} R_B &= \left[\sum_V \left(\int_v [B]^T[B]\ dV + \int_s Bi_B[N]^T[N]\ dA \right.\right. \\ &+ \left.\left. \int_v \phi_A^2[N]^T[N]\{a\}[N]\ dV\right)\right] \cdot \{b\} - \sum_S \int_s Bi_B[N]^T\ dA \end{aligned} \tag{4.19}$$

The concentration profiles for which $R_A$ and $R_B$ are approximately zero were found by using the Newton-Rhapson iterative scheme for coupled non-linear systems:

$$\begin{bmatrix} \frac{\partial R_A}{\partial\{a\}} & \frac{\partial R_A}{\partial\{b\}} \\ \frac{\partial R_B}{\partial\{a\}} & \frac{\partial R_B}{\partial\{b\}} \end{bmatrix} \times \begin{Bmatrix} \Delta a \\ \Delta b \end{Bmatrix} = - \begin{Bmatrix} R_A \\ R_B \end{Bmatrix} \tag{4.20}$$

$$\left.\begin{Bmatrix} a \\ b \end{Bmatrix}\right|_{i+1} = \left.\begin{Bmatrix} a \\ b \end{Bmatrix}\right|_i + \left.\begin{Bmatrix} \Delta a \\ \Delta b \end{Bmatrix}\right|_i \tag{4.21}$$

This solution strategy requires the inversion of matrices of double the size of that for a first-order reaction when the same FEM grid is used, and is therefore more computationally intensive.

### 4.1.3 Meshing

A tetrahedral mesher for Matlab that was developed by Persson and Strang (2004) was used to generate 3-dimensional meshes of a sphere. In total, six different meshes were used for the investigation: Simulations of monodispersed and eggshell particles were performed with different meshes, since the shell had to be well-defined for the simulation of eggshells. For a grid size of $n$ nodes, the solution of Equation (4.13) requires the solution of an $n \times n$ system, whereas the iterative solution of Equations (4.18) to (4.20) requires the (iterative) solution of a $2n \times 2n$. Therefore, computational limitations required the meshes for the reaction $-r_A = \alpha k_r C_A C_B$ to be coarser than the corresponding meshes for first-order reactions. Meshes were created for both reactions, monodispersed particles; and eggshell particles with inner to outer shell diameter rations of $\rho = 0.9$ and $\rho = 0.5$. Cross-sections of the meshes for the monodispersed particles an eggshell particles with $\rho = 0.9$ are shown in Figure 4.1.

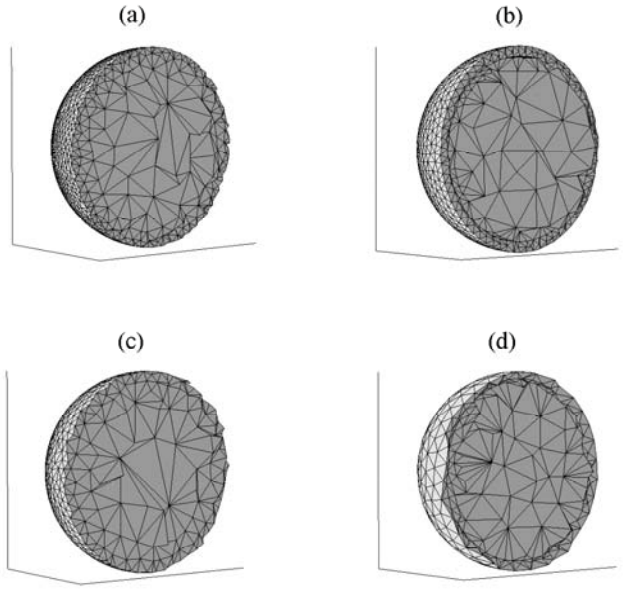


**Figure 4.1:** Finite element meshes for (a) a first order reaction in a monodispersed particle; (b) a first order reaction in an eggshell particle; (c) a reaction of the form $-r_A = k_r C_A C_B$ in a monodispersed particle; (d) a reaction of the form $-r_A = k_r C_A C_B$ in an eggshell particle.

Boundary conditions are based on the wetting geometries shown in Chapter 3, Figure 3.10: each surface triangle in the grid is assigned a Biot number based on its wetting condition (wet or dry). For the liquid reagent, $Bi_{B,d} = 0$ and for the gas reagent $Bi_{A,d} \gg Bi_{A,w}$. Note that the resolution at which the wetting geometry could be specified is a function of the mesh resolution. Quadratic interpolation matrices were used for the integration of the mesh elements. These were found to be more suited to the typical concentration profiles than linear interpolation.

### 4.1.4 FEM accuracy

The FEM solution for a first-order elementary reaction can be verified with the following analytical expressions for the concentration profile in the absence of external mass transfer

resistances:

For monodispersed catalyst:

$$c(\lambda) = \frac{\sinh(\phi \cdot \lambda)}{\sinh \phi} \tag{4.22}$$

For an eggshell catalyst:

$$c(\lambda) = \frac{A_1 e^{\phi \cdot \lambda} + A_2 e^{-\phi \cdot \lambda}}{\lambda} \qquad \rho \leq \lambda \leq 1 \tag{4.23}$$

$$c(\lambda) = c(\rho) \qquad \lambda \leq \rho$$

$$A_1 = \left( e^{\phi} + e^{\phi(1-2\rho)} \frac{\phi - \frac{1}{\rho}}{\phi + \frac{1}{\rho}} \right)^{-1}$$

$$A_2 = e^{\phi} - A_1 e^{2\phi}$$

Here, $c(\lambda)$ is the dimensionless radial concentration profile, and $\rho = r_s/r_p$ where $r_s$ is the inner dimension of the catalyst shell. Solutions are accurate and numerically stable for $\phi \leq 30$, as is shown in Figure 4.2.

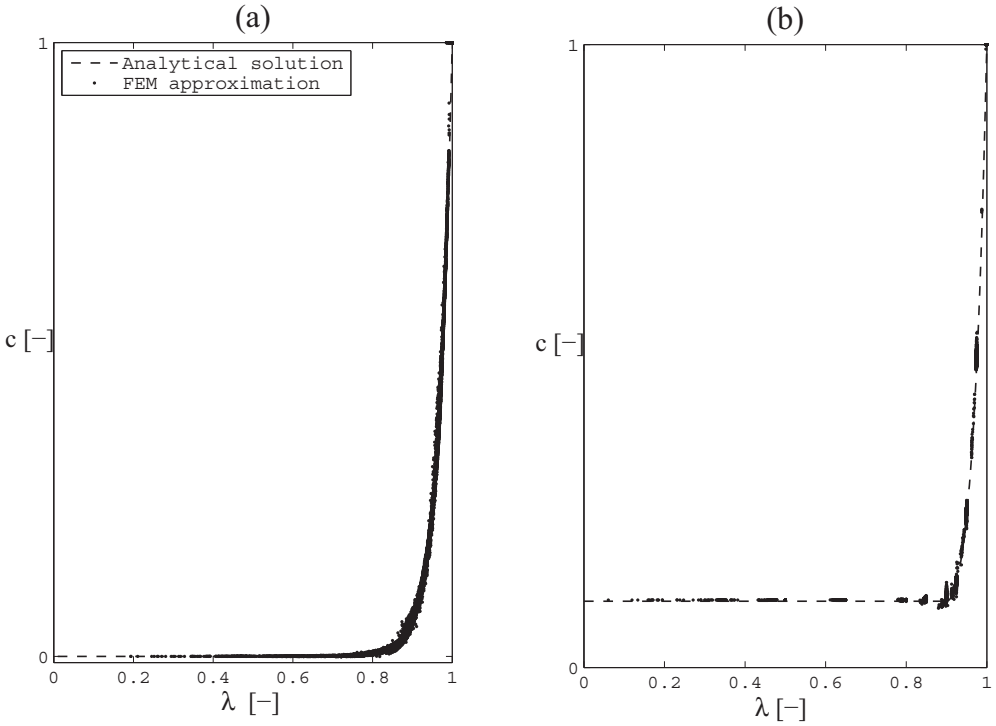


**Figure 4.2:** Numerical solutions for (a) a monodispersed catalyst and (b) an eggshell catalyst for $\phi = 30$ and no external mass transfer tested against the analytical solutions given in Equations (4.22).

For the reaction $-r_A = -\alpha r_B = \alpha k_r C_a C_b$ the FEM solutions can be verified as follows.

- For symmetric boundary conditions, $\phi_A \gg \phi_B$ and no external mass transfer resis-

tances, the concentration profile of reagent A should be given by Equations (4.22).

- For symmetric boundary conditions and any value of $\phi'_A$ and $\phi'_B$, the following relationship should hold true[2]:

$$b = \frac{a - 1 + \gamma'}{\gamma'} \qquad (4.24)$$
$$\gamma' = \left(\frac{\phi'_A}{\phi'_B}\right)^2$$

  Unlike $\phi_A$ and $\phi_B$, which are based on bulk concentrations, $\phi'_A$ and $\phi'_B$ are based on reagent surface concentrations. The same applies to $\gamma'$.

The derivation for this relationship is shown in Appendix A. Numerical and analytical concentration profiles are shown in Figure 4.3. Since the concentration profile is sharper for a higher Thiele modulus, increasingly smaller elements are required near the surface as the Thiele modulus increases. The meshes that were used are limited to a maximum Thiele modulus of 30, beyond which inaccuracies became unacceptably large. Note that the steepest concentration profiles are those shown in the figure, and not where $\phi_A = \phi_B = 30$ as one may intuitively expect.

## 4.2 Monodispersed particles

Preliminary results of the FEM simulations showed that the behaviour of partially wetted monodispersed catalysts differs significantly from that of eggshell catalysts. In this section, the behaviour of partially wetted monodispersed catalysts and different reaction expressions is described, based on FEM results.

### 4.2.1 Theory

To obtain an understanding of the behaviour of partially wetted monodispersed catalysts for different reaction cases, it is first neccesary to understand the relevant existing theories.

#### Geometry

For the theoretical particle geometries of a semi-infinite slab, a semi-infinite cylinder[3] and a sphere, a first-order reaction and a single boundary condition at the external surface,

[2]Note that for a reaction that is first order in A and in B, $\left(\frac{\phi_A}{\phi_B}\right)^2 = \frac{\alpha D_B C_{B,bulk}}{D_A C_A^*}$

[3]A semi-infinite slab has a finite thickness $L$ and an infinite height, and a semi-infinite cylinder has a finite radius $r_C$ and an infinite height.

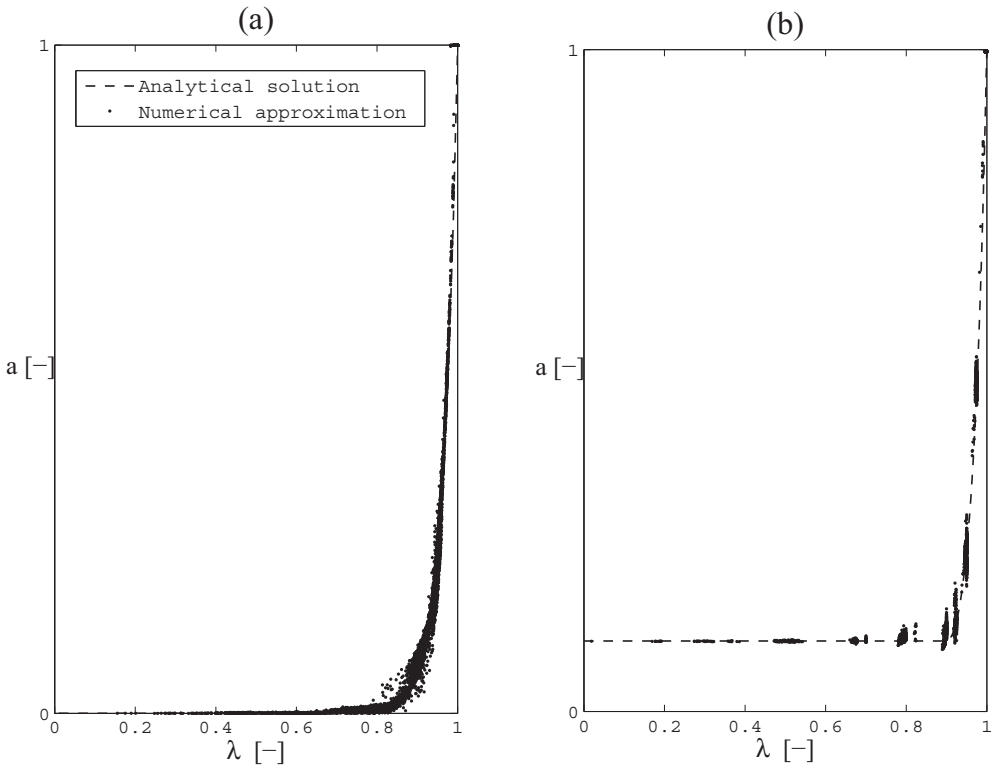


**Figure 4.3:** Numerical and analytical solutions for the reaction $r_A = \alpha r_B = -\alpha k_r C_A C_B$ for the case where $\phi_A \gg \phi_B = 30$. (a) Monodispersed particle, (b) eggshell particle with $\rho = 0.9$.

Equation (4.1) is one-dimensional; and exact analytical expressions for the pellet efficiency can derived:

$$\text{Semi-infinite slab: } \eta = \frac{\tanh \phi_G}{\phi_G} \quad \left(\phi_G = L\sqrt{\frac{k_r}{D}} = \frac{V_R}{S_x}\sqrt{\frac{k_r}{D}}\right) \tag{4.25}$$

$$\text{Semi-infinite cylinder: } \eta = \frac{2I_1(\phi_C)}{\phi_C I_0(\phi_C)} \quad \left(\phi_C = r_C\sqrt{\frac{k_r}{D}} = \frac{2V_p}{S_x}\sqrt{\frac{k_r}{D}}\right) \tag{4.26}$$

$$\text{Sphere: } \eta = \frac{3}{\phi^2}\left(\phi \coth \phi - 1\right) \quad \left(\phi = r_p\sqrt{\frac{k_r}{D}} = \frac{3V_p}{S_x}\sqrt{\frac{k_r}{D}}\right) \tag{4.27}$$

Aris (1957) showed that the efficiencies of all the above geometries have more or less the same functionality with the modulus of a slab, $\phi_G = L(k_r/D)^{1/2}$ (termed the generalised modulus), where $L$ is the ratio between the particle volume and external area. He therefore proposed to use Equation (4.25) to approximate pellet efficiency factors, regardless of the particle shape. The maximum error encountered when modelling a sphere as a slab, is approximately 10% at intermediate $\phi$. In the limits of $L \to 0$ and $L \to \infty$, efficiency factors for spheres, cylinders and slabs are exactly the same for the same $\phi_G$. The idea of a generalised modulus form the basis for modeling partially wetted particles under liquid-limited reaction conditions.

One-dimensional geometries are not necessarily limiting cases in terms of the modulus-efficiency relationship and there is no guarantee that this relationship will be close to that of a slab for all geometries. Burghardt and Kubaczka (1996) therefore suggested a different approach where not only the modulus, but also the modulus-efficiency relationship is determined by the shape of the particle. This work is based on the fact that the efficiency expressions for the three 1-D geometries can be written in terms of modified Bessel functions of the first kind[4]:

$$\eta = \frac{h+1}{\phi''}\frac{I_{(h+1)/2}(\phi'')}{I_{(h-1)/2}(\phi'')} \tag{4.28}$$

where $h = 0, 1$ and 2, for a slab, a cylinder and a sphere respectively. The modulus $\phi''$ is the modulus relevant to each geometry. Therefore, these authors propose the following expression which not only generalises the modulus but also the modulus-efficiency

[4]Modified Bessel functions are general solutions to the differential equation of diffusion and reaction in a semi-infinite cylinder. As for any second-order differential equation, two general solutions exist - in this case the modified Bessel functions of the first and second kind, $I_0(x)$ and $K_0(x)$

relationship for a given geometry:

$$\eta = \frac{h+1}{\phi_{GC}} \frac{I_{(h+1)/2}(\phi_{GC})}{I_{(h-1)/2}(\phi_{GC})}$$
$$h = \frac{S_p.R'}{V_p} - 1$$
$$\phi_{GC} = R' \sqrt{\frac{k_r}{D}} \tag{4.29}$$

where $R'$ is the maximum reagent penetration depth along the most favourable diffusion path. More information on how to calculate $R'$ for a given geometry can be found in the paper by these authors (Burghardt and Kubaczka, 1996). This method is commonly known as the generalised cylinder (GC) method. The GC model has never been used before in the modelling of partially wetted particles.

The expressions so far are for pellet efficiency factors and do not take external mass transfer resistances into account. To obtain an overall efficiency factor which takes external mass transfer resistances into account, one can make use of the following relationship:

$$\eta_0 = \eta \frac{C_s}{C_{bulk}} = \eta \left( 1 + \frac{(\phi_G)^2 \eta}{Bi''} \right)^{-1} \tag{4.30}$$
$$Bi'' = \frac{V_R k_c}{S_x D} \tag{4.31}$$

This relationship can be derived from the equality:

$$S_x k_c \left( C_{bulk} - C_s \right) = V_R \eta k_r C_s \tag{4.32}$$

### Modelling of partial wetting

Effectiveness factors for particles in trickle-bed reactors are complicated by the fact that the boundary conditions for Equation (4.1) are mixed: Due to incomplete wetting, two boundary conditions must be satisfied, one for the wetted and one for the dry surface. Even for the 1-D geometries of a sphere, a slab and a cylinder, the diffusion-reaction problem obtains extra dimensions[5].

For liquid-limited reactions, Dudukovic (1977) made use of the work of Aris (1957) to derive an expression for the catalyst efficiency of partially wetted particles for liquid-limited reactions, realising that only the wetted area can supply the reagent so that $S_x = S_p \cdot f$:

$$\eta = \frac{\tanh \phi_G}{\phi_G} \quad \text{where: } \phi_G = \frac{V_p}{f \cdot S_p} \sqrt{\frac{k_r}{D}} \tag{4.33}$$

The above equation suggests that partial wetting affects the effective geometry of a par-

[5]Exceptions are the geometries defined by Beaudry et al. (1987) and Valerius et al. (1996a)

ticle due to its effect on the external area available for reagent supply. It is important for the rest of this chapter to realise that if all shapes can be approximated for a slab with $L = V_R/S_x$ then it should also be possible to approximate all shapes with a sphere, so that Equation (4.33) becomes:

$$\eta = \frac{3f^2}{\phi^2}\left(\frac{\phi}{f}\coth\left(\frac{\phi}{f}\right) - 1\right) \quad \text{where: } \phi = \frac{3V_p}{S_p}\sqrt{\frac{k_r}{D}} \tag{4.34}$$

The overall efficiency that takes external mass transfer limitations into account can easily be modelled, making use of Equation (4.30), and taking into account that only the wetted area is available for external mass transfer:

$$\begin{aligned} \eta_0 &= \eta\frac{C_s}{C_{bulk}} = \eta\left(1 + \frac{(\phi_G)^2\eta}{Bi''}\right)^{-1} \\ &= \frac{\tanh\phi_G}{\phi_G\left(1 + \frac{\phi_G\tanh\phi_G}{Bi'_w f}\right)} \quad \text{Slab geometry} \end{aligned} \tag{4.35}$$

$$\text{or} \qquad \frac{3f^2\left(\frac{\phi}{f}\coth\frac{\phi}{f} - 1\right)}{\phi^2\left(1 + \frac{f\left(\frac{\phi}{f}\coth\frac{\phi}{f} - 1\right)}{Bi_w}\right)} \quad \text{Sphere geometry} \tag{4.36}$$

The above approach can not be followed for a gas-limited reaction, since the gas enters via both the wetted and the dry surface area. The most widely accepted model for a gas-limited reaction in a partially wetted catalyst was provided by Ramachandran and Smith (1979). The model is based on infinite slab geometry and the assumption that the reactant entering through the dry part and the wetted part of the slab can be treated separately and do not interact throughout the slab volume:

$$\eta_0 = \frac{f\cdot\tanh\phi_G}{\phi_G\left(1 + \frac{\phi_G\tanh\phi_G}{Bi'_w}\right)} + \frac{(1-f)\cdot\tanh\phi_G}{\phi_G\left(1 + \frac{\phi_G\tanh\phi_G}{Bi'_d}\right)} \tag{4.37}$$

When compared to Equation (4.30), it is clear that this expression is analagous to that of a slab where the entire surface is at a surface concentration $\overline{C_s}$, where $\overline{C_s} = f \times C_{s,w} + (1-f)\times C_{s,d}$. When using Equation (4.37), it is important to realise that this equation views gas-liquid-particle surface mass tranfer as one step, so that $Bi_w$ is a combined Biot number for gas-liquid and liquid-solid mass transfer. This can be done when the rate of liquid-solid and gas-liquid mass transfer is the same. For high conversions of the liquid reagent and negligible expense of the gas, this is a reasonable assumption. When the inlet condition (e.g. saturated liquid, or zero gas-side reagent in the liquid) is of importance[6], the differential description of the concentration profile of the gaseous reagent in the liquid

[6]For example at low conversions

that is necessary to evaluate the overall reaction rate $r$, analogous to equation (4.37), is:

$$\begin{aligned}\frac{dC_{bulk}}{dV_c} = k_{GL}a_{GL}\left(C* - C_{bulk}\right) - k_{LS}a_p f\left(C_{bulk} - C_{s,w}\right) \\ k_{LS}a_p\left(C_{bulk} - C_{s,w}\right) = \eta k_R C_{s,w} \\ -r = f\eta k_R C_{s,w} + \left(1-f\right)\eta k_R C^* \end{aligned} \tag{4.38}$$

Clearly, the modelling of gas-limited reactions is completely different from that of liquid-limited reactions: the limit of equation (4.37) where $Bi_d \rightarrow 0$ is only the same as the liquid-limited description of equation (4.35) at large moduli.

Valerius et al. (1996b) suggested a particle efficiency model which can take wetting efficiency into account and can be used for gas-limited *and* liquid-limited reactions. The model is based on a hollow cylinder geometry where the outer surface area represents the wetted area and the inner surface the dry area of a partially wetted pellet, and can therefore only be used for $f > 0.5$. This geometry is used in a later paper (Valerius et al., 1996a) to simplify the numerical calculations for intricate kinetic expressions by transforming a 3-D problem to a 2-D problem, rather than to obtain analytical expressions for pellet efficiency factors. Only the analytical expression for a liquid-limited reaction was reported and will be verified in this chapter.

### Kinetics

Exact explicit expressions of pellet efficiency factors only exist for simple kinetic expressions such as zero and first order kinetics (Lee and Kim, 2006). Large amounts of literature are therefore available, which present methods of approximating effectiveness factors for arbitrary kinetics. Probably the most important amongst these is that of Bischoff (1965), who suggested a general modulus for kinetics of any form. This modulus has more or less the same effect on pellet efficiency independent of the kinetic expression. To understand how the Bischoff modulus can be used, a short version of the derivation

of this modulus is now shown:

The diffusion-reaction equation in a slab is given by:

$$D\frac{d^2C}{dx^2} = r(C) \quad \left(C(0) = C_s; \quad \left.\frac{dC}{dx}\right|_{x=L} = 0\right) \tag{4.39}$$

$$\text{Let: } p = \frac{dC}{dx}, \text{ then: } \frac{d}{dx} = p \cdot \frac{d}{dC}$$

$$\therefore r(C) = D\frac{d^2C}{dx^2} = D \cdot p\frac{dp}{dC} = \frac{D}{2}\frac{d}{dC}\left(p^2\right) \tag{4.40}$$

Integrate from $p = 0$ (at $x = L$) to $p$:

$$\int_0^p d\left(p^2\right) = \frac{2}{D}\int_{C_L}^{C} r(\beta)d\beta$$

$$\therefore p^2 = \frac{2}{D}\int_{C_L}^{C} r(\beta)d\beta$$

$$\text{and} \quad \frac{dC}{dx} = p = -\sqrt{\frac{2}{D}}\left(\int_{C_L}^{C} r(\beta)d\beta\right)^{1/2} \tag{4.41}$$

The effectiveness factor can be evaluated using the flux of reagent into the slab:

$$\begin{aligned}\eta &= \frac{-S_pD \cdot \left.\frac{dC}{dx}\right|_{x=0}}{V_pr(C_s)} \\ &= \frac{S_p\sqrt{2D}\left(\int_{C_L}^{C_s} r(\beta)d\beta\right)^{1/2}}{V_pr(C_s)}\end{aligned} \tag{4.42}$$

It is well known that for simple order reactions in a slab, the pellet efficiency factor - Thiele modulus curve has the relationship $\eta = \phi_G^{-1}$ when $\phi_G \gg 1$. At such high Thiele moduli, $L$ or $r$ is very large and $C_L \to C_{eq}$, where $C_{eq}$ is the concentration where $r(C_{eq}) \to 0$. For example $C_{eq} = 0$ when a reaction is irreversible and involves only one reagent. To have the same behaviour for an arbitrary reaction at a large Bischoff modulus (large $L$ and/or fast reaction), this modulus can be defined as:

$$\phi_T'' = \left(\eta_{C_{eq}}\right)^{-1} = \frac{V_p \cdot r(C_s)}{S_p\sqrt{2D}}\left(\int_{C_{eq}}^{C_s} r(\beta)d\beta\right)^{-1/2} \tag{4.43}$$

In the original work, the diffusivity was also allowed to vary as a function of concentration, resulting in the following expression for the Bischoff modulus:

$$\phi_T'' = \frac{V_p \cdot r(C_s)}{S_p\sqrt{2}} \left( \int_{C_L}^{C_s} D(\beta) r(\beta) d\beta \right)^{-1/2} \tag{4.44}$$

Where the derivation of Bischoff (1965) was done for a slab (to be used with Equation 4.25), one can for the same reasons as discussed earlier, define a "spherical" Bischoff modulus that can be used with Equation (4.27):

$$\phi_T = \frac{3V_p \cdot r(C_s)}{S_p\sqrt{2D}} \left( \int_{C_{eq}}^{C_s} r(\beta) d\beta \right)^{-1/2} \tag{4.45}$$

### 4.2.2 Verification of existing models

Efficiency factors for partially wetted catalysts are only available for completely liquid-limited and completely gas-limited reactions where only one of the reagents plays a role. The accuracy of these models can now be evaluated with the FEM models for true wetting geometries. In this section, the Bischoff approximation for the reaction $-r_A = \alpha k_r C_A C_B$ is also derived and verified for fully wetted particles.

#### Liquid-limited reactions

Monodispersed particle efficiencies of all the photographed particles shown in Figure 3.10 were calculated for $0.1 \leq \phi \leq 30$ in the absence of external mass transfer resistances. Results are shown in Figure 4.4 as a function of the generalised modulus for partially wetted particles as suggested by Dudukovic (1977). It is clear from the figure that this approach yields rather good results, as can also be inspected by the parity plot in the top left corner.

It is proposed that, as for the generalised modulus approach, the GC method can be adapted to model the effect of partial wetting on liquid-limited reactions wetting by adjusting the "effective geometry":

$$\begin{aligned} \eta &= \frac{h+1}{\phi_{GC}} \frac{I_{(h+1)/2}(\phi_{GC})}{I_{(h-1)/2}(\phi_{GC})} \\ \phi_{GC} &= R' \sqrt{\frac{k_r}{D}} \\ R' &= r_p \text{ for a sphere} \\ h(f) &= 3f - 1 \end{aligned} \tag{4.46}$$

In this approach, not the characteristic length, but the efficiency-modulus relationship is influenced by partial wetting and it is therefore completely different from (4.33) where

the characteristic length is adjusted according to the fractional wetting.

The performance of this "modified GC model" is shown as a parity plot in Figure 4.4, and is even better than the traditional generalised modulus approach. The cylinder shell model of Valerius et al. (1996b) performs well, but is limited to $f > 0.5$. The treatment

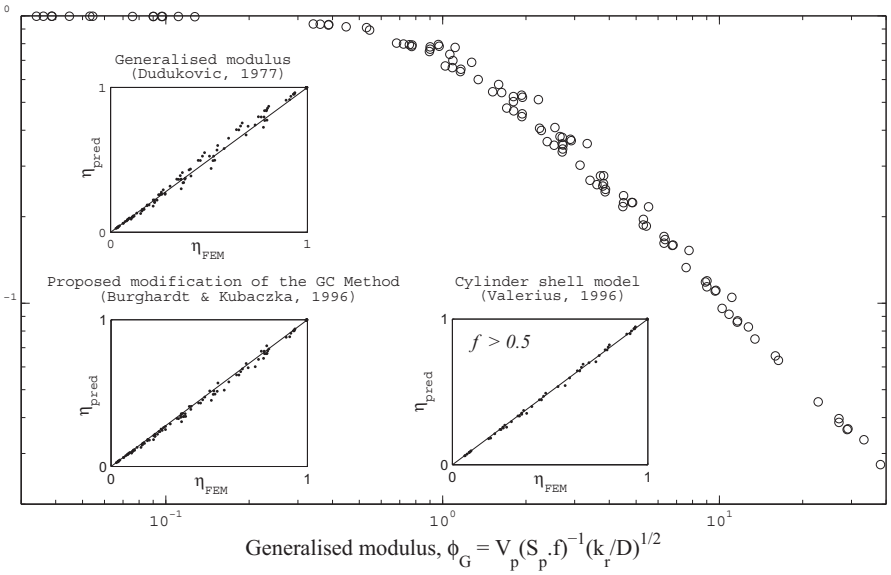


**Figure 4.4:** Particle efficiency versus generalised modulus for partially wetted particles and liquid-limited reaction conditions for real wetting geometries. The parity plots show the prediction performance for the discussed models for liquid-limited particle efficiency.

of external mass transfer for liquid-limited reactions is analytically correct and need not be verified.

### Gas-limited reactions

The most important model for the evaluation of partially wetted particle efficiency under gas-limited conditions is the "weighting method" of Ramachandran and Smith (1979), Equation (4.37). This weighting method should be accurate if the difference between dry and wet surface concentrations is small, so that unsymmetrical boundary conditions do not have a major influence on the concentration profiles in the slab (Ramachandran and Smith, 1979). Usually, $Bi_d$ is very high and it was therefore investigated for which values of $Bi_w$ the weighting method would still be accurate when external mass transfer limitations on the dry part of the catalyst were negligible. Results are shown as parity plots in Figure 4.5. Liquid-solid mass transfer Biot numbers are typically larger than 10 for trickle-bed reactor applications (see Figure 2.3) as is also the case for gas-liquid mass transfer (see database reported by Iliuta et al. (1999)). It can be concluded that equation (4.37) clearly yields accurate results for realistic values of $Bi_w$.

The only significant source of prediction error is the fact that slab geometry is used to model other pellet geometries (spherical in this work), as can be seen from the subplot in the bottom right corner. The equivalent of Equation (4.37) for a sphere is:

$$\eta_0 = \frac{3f\left(\phi\coth\phi - 1\right)}{\phi^2\left(1 + \frac{\phi\coth\phi - 1}{Bi_w}\right)} + \frac{3(1-f)\left(\phi\coth\phi - 1\right)}{\phi^2\left(1 + \frac{\phi\coth\phi - 1}{Bi_d}\right)} \tag{4.47}$$

Though the original derivation of Equation (4.37) by Ramachandran and Smith (1979) was only valid for the slab geometry defined in that work, Goto et al. (1981) have shown that one can also use Equation (4.47), as can also be seen from the FEM results.

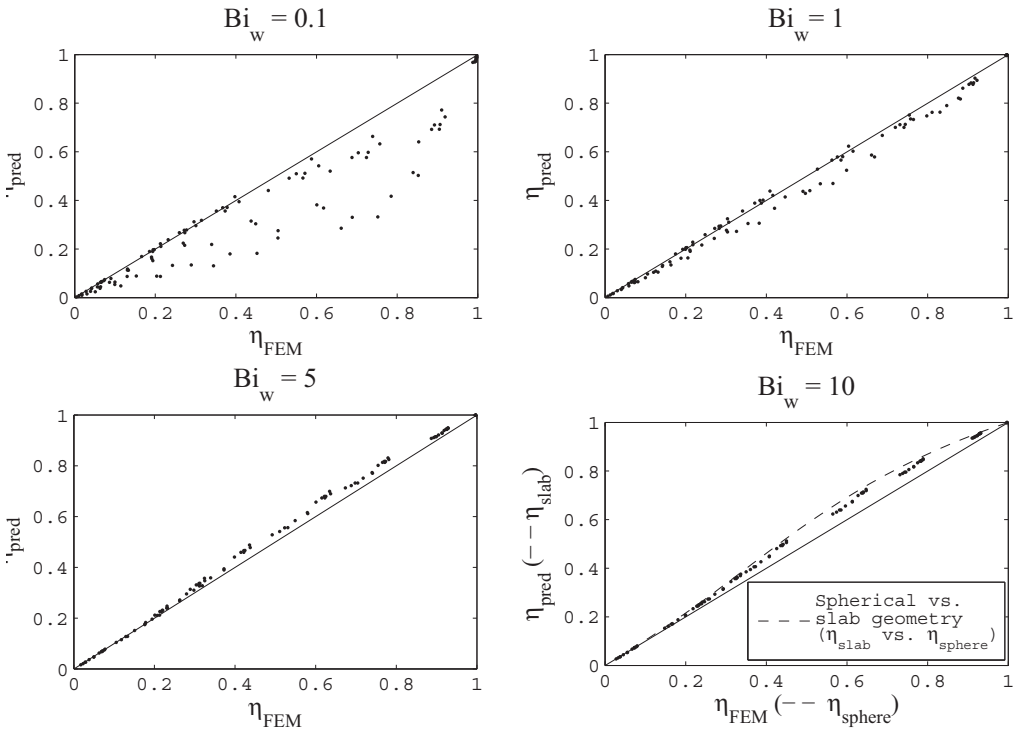


**Figure 4.5:** Parity plots of pellet efficiency factors as calculated with the weighting model vs. FEM results for different extents of mass transfer resistances over the wetted part of the catalyst if gas-solid mass transfer is negligible. In the last subplot, the parity between spherical and slab efficiency at the same generalised modulus is also shown.

### The Bischoff modulus

For a completely wetted particle, the Bischoff modulus[7] (based on surface concentrations) for the reaction $r_A = \alpha r_B = -\alpha k_r C_A C_B$ can be derived as follows, starting at the

[7]The work in this chapter makes use of the "spherical" modulus, Equation (4.45)

definition of the Bischoff modulus:

$$\phi_T = \frac{3V_p \cdot r(C_s)}{S_p\sqrt{2D}} \left( \int_{C_{eq}}^{C_s} r(\beta) d\beta \right)^{-1/2} \tag{4.48}$$

This definition allows for the integration of a reaction rate which is decribed in terms of one reagent only. If $\gamma > 1$, $C_{A,eq} = 0$ and $C_{B,eq}$ is unknown, so that $C_B$ should be written in terms of $C_A$. This can be done by using Equation (4.24), which relates the concentrations of A and B in the pellet:

$$\begin{aligned}
\phi_T &= \frac{3V_p \cdot r(C_{A,s}, C_{B,s})}{S_p\sqrt{2D_A}} \left( \int_0^{C_{A,s}} r(C_A) dC_A \right)^{-1/2} \\
&= \frac{r_p \cdot \alpha k_r C_{A,s} C_{B,s}}{\sqrt{2D_A}} \left( \int_0^1 \alpha k_r C_{A,s}^2 C_{B,s} a \left( \frac{a - 1 + \gamma'}{\gamma'} \right) da \right)^{-1/2} \\
&= \frac{r_p\sqrt{\alpha \cdot k_r C_{B,s}}}{\sqrt{2D_A}} \left( \int_0^1 \frac{a^2 - a + \gamma' a}{\gamma'} \right)^{-1/2} \\
&= \frac{\phi'_A}{\sqrt{2}} \left[ \left( \frac{a^3}{3\gamma'} - \frac{a^2}{2\gamma'} + \frac{1}{2} \right) \Big|_0^1 \right]^{-1/2} \\
&= \phi'_A \left( 1 - \frac{1}{3\gamma'} \right)^{-1/2}
\end{aligned} \tag{4.49}$$

when $\gamma' < 1$, $C_{B,eq} = 0$ and the above derivation should be performed in terms of $C_B$ to obtain:

$$\phi_T = \phi'_B \left( 1 - \frac{\gamma'}{3} \right)^{-1/2} \tag{4.50}$$

In this derivation $a$ and $b$ are dimensionless concentrations based on *surface* concentrations. Either equation (4.49) or (4.50) can be used when $\gamma' = 1$, since the equilibrium concentration of both reagents will then be equal to zero. Pellet effectiveness factors for completely wetted particles, $r_A = \alpha r_B = -\alpha k_r C_A C_B$ and negligible external mass transfer were calculated using FEM. These are shown as a function of the above derived Bischoff modulus in Figure 4.6. Clearly, the Bischoff modulus for this reaction can be used for a good approximation of pellet efficiency.

Equation (4.24), describing the relationship between $a$ and $b$ for complete wetting, is valid for *any* power law reaction $r_A = \alpha r_B = -k_r C_A^n C_B^m$, and one can write a general

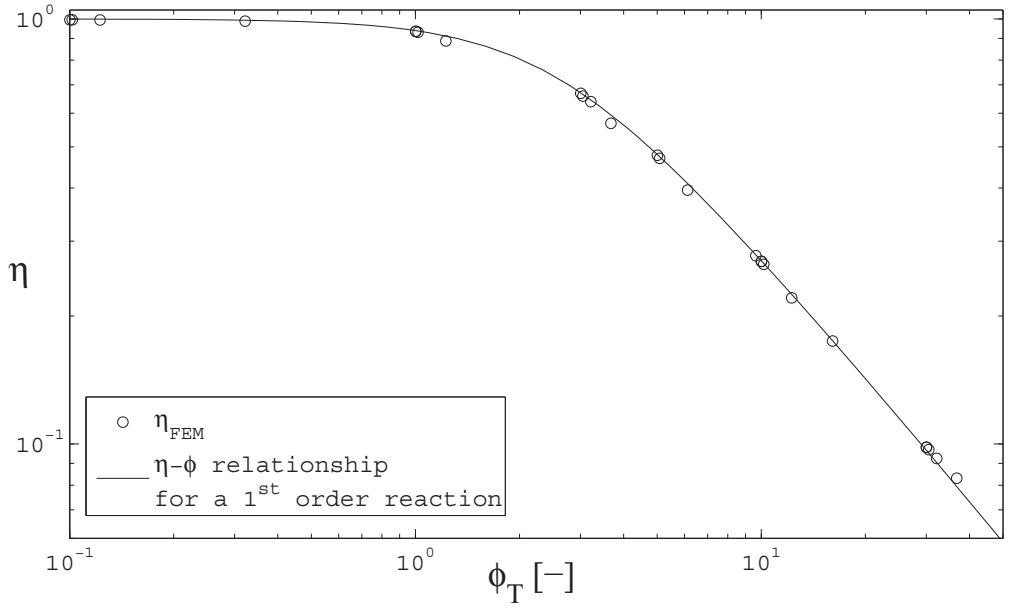


**Figure 4.6:** Pellet efficiency factors as a function of the Bischoff modulus for the reaction $r_A = \alpha r_B = -\alpha k_r C_A C_B$, fully wetted particles with no external mass transfer resistances. Also shown is the $\eta$-$\phi$ relationship for a first-order reaction in a sphere

expression for the Bischoff modulus for these types of reactions[8]:

$$\phi_T = \frac{\phi'_A}{\sqrt{2}} \left( \int_0^1 a^n \left( \frac{a-1+\gamma'}{\gamma'} \right)^m da \right)^{-1/2} \quad \gamma = \left( \frac{\phi'_A}{\phi'_B} \right)^2 > 1$$
$$\phi_T = \frac{\phi'_B}{\sqrt{2}} \left( \int_0^1 \left( \gamma' b + 1 - \gamma' \right)^n b^m db \right)^{-1/2} \quad \gamma = \left( \frac{\phi'_A}{\phi'_B} \right)^2 < 1 \tag{4.51}$$

Where:

$$\phi'_A = r_p \sqrt{\frac{\alpha k_r C_{A,s}^{n-1} C_{B,s}^m}{D_A}}; \quad \phi_B = r_p \sqrt{\frac{k_r C_{A,s}^n C_B^{m-1}}{D_B}} \tag{4.52}$$

The FEM investigation was performed for $n = 1$ and $m = 1$ only, as stated previously.

### 4.2.3 A unified model for $r_A = \alpha r_B = -\alpha k_r C_A C_B$

The previous section has shown that the existing models for liquid- and gas-limited reactions are satisfactory for true wetting geometries. These models are specific to either liquid- or gas-limited reactions but provide useful descriptions of the effect of partial wetting on the behaviour of the liquid and gaseous reagents, that can be summarised as follows:

- For liquid-limited reactions, the generalised modulus approach (Dudukovic, 1977)

[8]The dimensionless concentration term in the reaction expression does not play a role in the derivation of the relationship between $a$ and $b$, see Appendix A

can be recommended, giving acceptable predictions while being very simple to use. According to this approach, partial wetting affects the effective geometry (diffusion path length) of the limiting reagent when a reaction is liquid-limited. For a monodispersed catalyst pellet, the Thiele modulus of a partially wetted particle can be corrected for partial wetting by adjusting the effective geometry so that $\phi_{corr} = \phi/f$. Where in the previous discussion the Thiele modulus-efficiency relationship of a slab was used for any geometry, it is also possible to use that of a sphere. Overall pellet efficiency can be evaluated by taking external mass transfer resistances into account as is shown in Equation (4.35). Mathematically, the approach to liquid-limited reactions can be written as:

$$\eta_0 = \eta\left(\phi_B''/f\right) \times \frac{C_{B,s}}{C_{B,bulk}} \tag{4.53}$$

- Partial wetting affects the average external surface concentration of the limiting reagent when the reaction is gas-limited. Correcting overall pellet efficiency with the average external surface concentration weighted according to the fractional wetting, yield good results for realistic rates of external mass transfer. It is preferable to use the model of Ramachandran and Smith (1979) in conjunction with the Thiele modulus - pellet efficiency relationship specific to the particle geometry.

$$\eta_0 = \eta\left(\phi_A'\right) \times \frac{fC_{A,s}|_w + (1-f)C_{A,s}|_d}{C_{A,bulk}} \tag{4.54}$$

Combining the above approaches with the Bischoff modulus derived for the reaction $r_A = \alpha r_B = -\alpha k_r C_A C_B$, the following unified model for this reaction is suggested to

predict the efficiency of partially wetted particles over the whole $\gamma$-range:

$$\eta_0 = \frac{3\overline{C_{A,s}}C_{B,s}}{\phi_T^2 C_A^* C_{B,bulk}}\left(\phi_T \coth \phi_T - 1\right) \tag{4.55}$$

$$\phi_T = \phi'_A\left(1 - \frac{{\phi'_B}^2}{3{\phi'_A}^2}\right)^{-1/2} \quad \phi'_A \geq \phi'_B$$

$$\text{or } \phi_T = \phi'_B\left(1 - \frac{{\phi'_A}^2}{3{\phi'_B}^2}\right)^{-1/2} \quad \phi'_A < \phi'_B \tag{4.56}$$

$$\phi'_A = r_p\sqrt{\frac{k_r C_{B,s}}{D_A}}; \quad \phi'_B = \frac{r_p}{f}\sqrt{\frac{k_r \overline{C_{A,s}}}{D_B}} \tag{4.57}$$

$$\overline{C_{A,s}} = C_A^*\left[f\left(1 + \frac{{\phi'_A}^2\left(\phi_T \coth \phi_T - 1\right)}{\phi_T^2 Bi_{A,w}}\right)^{-1}\right.$$
$$\left. + \ (1-f)\left(1 + \frac{{\phi'_A}^2\left(\phi_T \coth \phi_T - 1\right)}{\phi_T^2 Bi_{A,d}}\right)^{-1}\right] \tag{4.58}$$

$$C_{B,s} = C_{B,bulk}\left(1 + \frac{{\phi'_B}^2 f\left(\phi_T \coth \phi_T - 1\right)}{\phi_T^2 Bi_{B,w}}\right)^{-1} \tag{4.59}$$

The model treats gas and liquid reagents according to the traditional approaches: the average surface concentration of the gas and the modulus for the liquid component are affected by fractional wetting according to the models of Ramachandran and Smith (1979) and Dudukovic (1977) respectively. The liquid external surface concentration is calculated according to Equation (4.30). The major discrepancy in this model is that it uses a Bischoff modulus that was derived for fully wetted particles, but the results are good for a wide $\gamma$-range, as is shown in Figure 4.7, especially when compared to predictions of the traditional liquid-limited and gas-limited models shown in Figure 4.8. As for Equation (4.37), the unified model makes uses an overall gas-liquid-solid Biot number, assuming equal rates of gas-liquid and liquid-solid mass transfer. If this does not apply, the wetted surface concentration of $A$ should be evaluated in a similar fashion as that shown in equation (4.38). The unified model is reported here in terms of spherical particles, but there is no reason why it cannot be applied to other shapes, since the principles of the model are not based on particle geometry.

## 4.3 Eggshell particles

The first, and probably most obvious, difference between monodispersed and eggshell catalyst spheres is that the latter tend to behave like a slab as the shell thickness decreases. This can best be seen from the definition of $h$ in the GC model: $h = 0$ for a slab, and

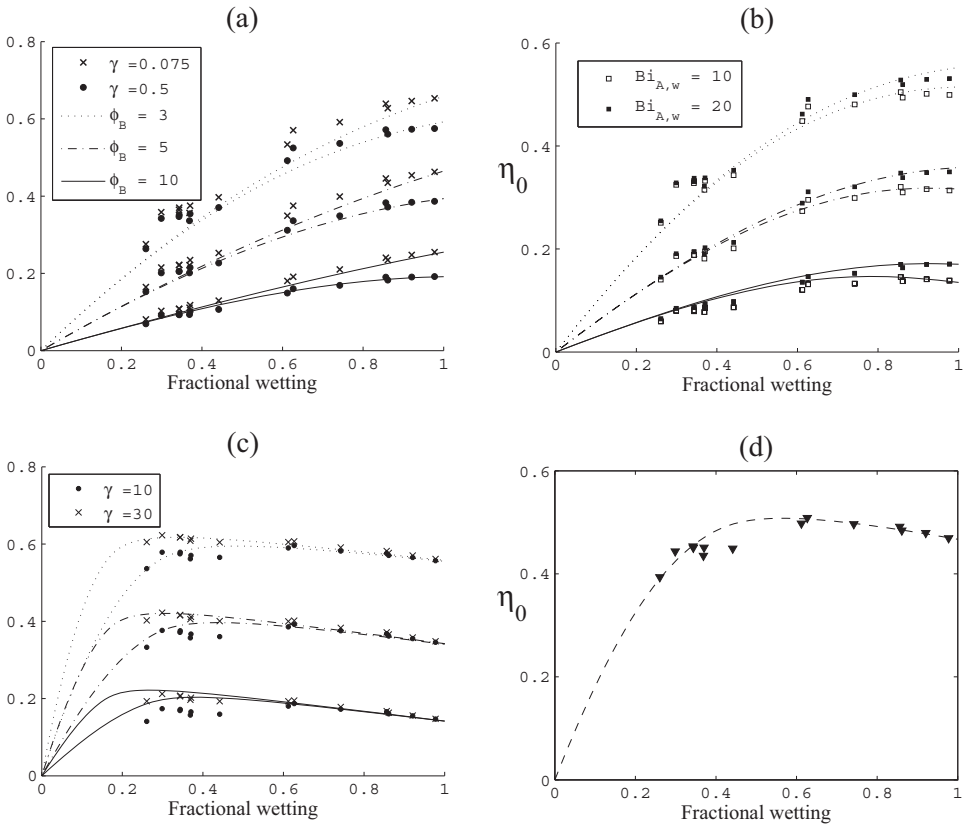


**Figure 4.7:** Performance of the unified model for the reaction $r_A = \alpha r_B = -\alpha k_r C_A C_B$. (a) Liquid-limited reaction, with some external mass transfer resistances for the gaseous reagent over the wetted surface ($Bi_{A,w} = 10$, $Bi_{A,d} \to \infty$, $Bi_{B,w} \to \infty$); (b) reaction that is not classified as either gas or liquid-limited with varying rates of external mass transfer for the gaseous reagent ($\gamma = 1$, $Bi_{A,d} \to \infty$, $Bi_{B,w} \to \infty$); (c) gas-limited reaction ($Bi_{A,w} = 10$, $Bi_{A,d} \to \infty$, $Bi_{B,w} \to \infty$); (d) arbitrarily chosen conditions ($\phi_A = 3$, $\gamma = 5$, $Bi_{A,w} = 5$, $Bi_{A,d} = 50$, $Bi_{B,w} = 10$). All Thiele moduli are as defined in the legend of subfigure (a).

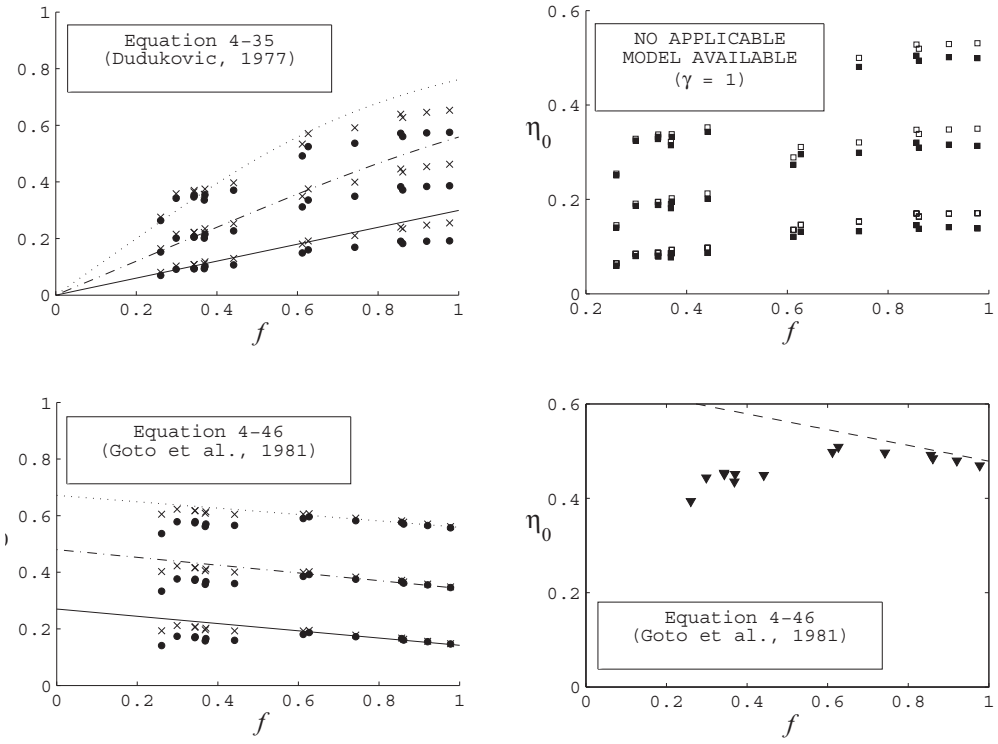


**Figure 4.8:** Predictions of the FEM data in Figure 4.7 by traditional models for liquid- and gas-limited reactions.

$h = 2$ for a sphere. For an eggshell sphere of inner to outer shell diameter ratio $\rho$:

$$\begin{aligned} h &= \frac{S_p}{V_p} R' - 1 \\ &= \frac{4\pi r_p^2}{4/3\pi r_p^3 \left(1-\rho^3\right)} \cdot r_p \left(1-\rho\right) - 1 \\ &= \frac{3\left(1-\rho\right)}{1-\rho^3} - 1 \end{aligned} \tag{4.60}$$

in the limit of $\rho \rightarrow 1$, $h \rightarrow 0$, which suggests slab geometry. Gas-limited reactions in partially wetted egshell particles clearly show "slab behaviour": for the investigated eggshell catalysts, Equation (4.37), which assumes slab geometry, works very well for $Bi_w \geq 5$ (within 5% accuracy for all simulation results). Another reason why gas-limited reactions within an eggshell catalyst can be predicted so well, is that the dry and wetted parts of the reaction zone are more segregated than in a monodispersed catalyst.

Liquid limititations are not predicted well by the traditional generalised modulus approach and incomplete wetting has a more detrimental effect than on monodispersed catalysts, as is shown in Figure 4.9. The reason why the generalised modulus approach performs so poorly for a partially wetted eggshell catalyst, is that a zone exists where diffusion without reaction takes place. The particle can therefore not be directly related

to a slab with diffusion and reaction throughout its volume. Due to symmetry, such zones will not exist in a fully wetted particle, so that the generalised modulus approach works well for eggshell catalysts with a high wetting efficiency.

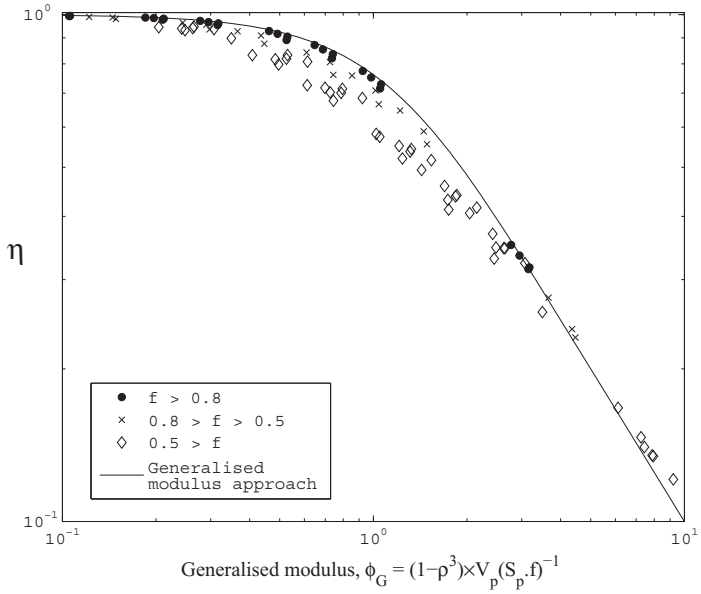


**Figure 4.9:** Particle efficiency versus generalised modulus for partially wetted particles and liquid-limited reaction conditions for real wetting geometries on a spherical eggshell catalyst ($\rho = 0.9$).

Similarly to the generalised modulus approach, it is difficult to define the characteristic length to use in the GC method (Equation (4.29, defined as the maximum distance for diffusion under reaction conditions). For a fully wetted particle this should be equal to $r_p\,(1-\rho)$, but for a fractionally wetted particle substantially more. To be consistent with the modified GC method proposed in section 4.2.2 (equation 4.46), the characteristic length for $\rho = 0$ should be equal to $r_p$, independent of the fractional wetting. It is possible to define a general expression for the characteristic length that meets these requirements:

$$R^{'} = r_p\,(1 - \rho \times g(f)) \tag{4.61}$$

The shape factor, $h$ is then given by:

$$h = \frac{S_x}{V_R} R^{'} - 1 = \frac{3f \times (1 - \rho \times g(f))}{1 - \rho^3} - 1 \tag{4.62}$$

where $g(f)$ should be equal to 1 for $f = 1$. Also, $R^{'}$ should increase and $g(f)$ should decrease as $f$ decreases, most likely in a non-linear function. Assuming a quadratic relationship between $g(f)$ and $f$, the following function was fitted onto FEM efficiency data for a liquid-limited reaction in eggshell catalysts with shell dimensions of $\rho = 0.9$

and $\rho = 0.5$:

$$g(f) = k_1\left(f^2 - 1\right) + k_2\left(f - 1\right) + 1 \tag{4.63}$$

Best-fit values for $k_1$ and $k_2$ are $-2$ and 4, respectively. Equations (4.61) to (4.63) simplify to Equations (4.46) for a monodispersed catalyst. The equations imply slab geometry for very thin eggshells ($h \to 0$ when $\rho \to 1$ and $f = 1$), which is also correct. The fitted parameter values for $g(f)$ suggest a limit of $R' = r_p(1 + \rho)$ when $f = 0$. Figure 4.10 shows the performance of the proposed partial wetting GC model for eggshell catalysts. Though empirical, the model performs well for $\rho = 0.9$, $\rho = 0.5$ and $\rho = 0$ (see figure 4.4 for the performance of the modified GC model when $\rho = 0$). No statement can be made about the model's performance when $\rho > 0.9$ or for shapes other than spheres[9]. External mass transfer can be accounted for in the normal fashion (Equation 4.30 or 4.32).

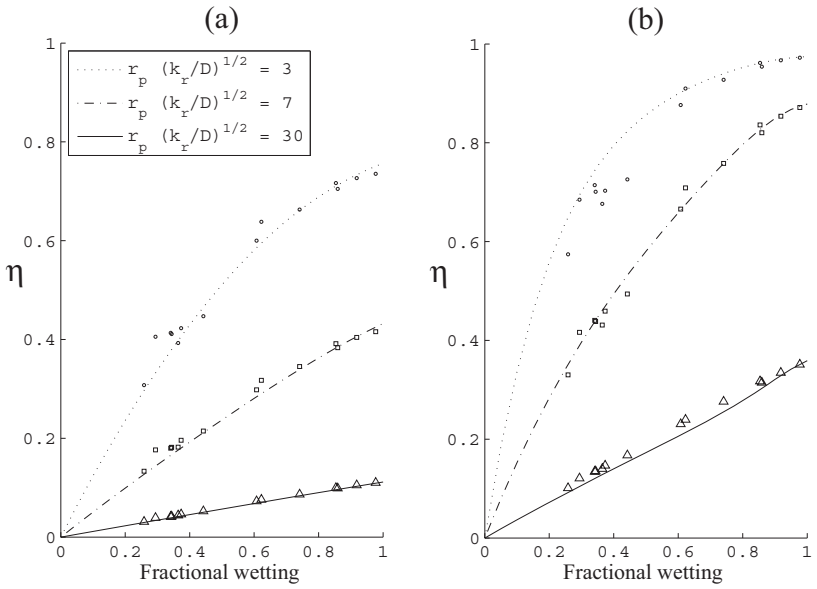


**Figure 4.10:** Proposed GC model for liquid-limited, partially wetted eggshell catalysts as compared with results from FEM simulations for different shell thicknesses: (a) $\rho = 0.5$ and (b) $\rho = 0.9$.

It is not possible to use the modified GC model together with the Bischoff modulus to obtain a unified model for eggshell catalysts, since the modulus-efficiency relationship varies with shape in the GC model. For this reason a generalied modulus-type description is needed for eggshell catalysts. Based on the limits of $R'$ in the GC model for egghell particles ($R' = (1 - \rho)$ for fully wetted particles, and $r_p\,(1 + \rho)$) and the generalised modulus for a fully wetted particle, the following correction of the generalised modulus

[9]An exception is for the case where $\rho = 0$. Here, it should be clear from the work of Burghardt and Kubaczka (1996) how to adjust Equation (4.46) for shapes other than spheres. The accuracy should be more or less the same as that shown in Figure 4.4

is suggested for eggshell particles:

$$\phi_G = \underbrace{\phi\frac{(1-\rho^3)}{3f}}_{\phi_G \text{ for partially wetted eggshell sphere}} \times \underbrace{[1+\rho(1-f)]}_{\text{correction factor}} \tag{4.64}$$

This modified generalised modulus for eggshell catalysts works rather well, especially for thin shells, as is shown in Figure 4.11. Though possibly somewhat less accurate than the modified GC model, this generalised eggshell modulus is far easier to use and can also be used in the unified model. To model eggshells with both liquid and gas reagent limitations, one should make use of slab geometry so that the unified model becomes:

$$\eta_0 = \frac{\overline{C_{A,s}}C_{B,s}}{\phi_T C_A^* C_{B,bulk}}\tanh\phi_T \tag{4.65}$$

$$\begin{aligned}
\phi_T &= \phi'_A\left(1-\frac{{\phi'_B}^2}{3{\phi'_A}^2}\right)^{-1/2} \quad \phi'_A \geq \phi'_B \\
\text{or } \phi_T &= \phi'_B\left(1-\frac{{\phi'_A}^2}{3{\phi'_B}^2}\right)^{-1/2} \quad \phi'_A < \phi'_B \\
\phi'_A &= \frac{r_p(1-\rho^3)}{3}\sqrt{\frac{k_r C_{B,s}}{D_A}} \\
\phi'_B &= \frac{r_p(1-\rho^3)(1+\rho-\rho\cdot f)}{3f}\sqrt{\frac{k_r\overline{C_{A,s}}}{D_B}}
\end{aligned} \tag{4.66}$$

$$\begin{aligned}
\overline{C_{A,s}} &= C_A^*\left[f\left(1+\frac{{\phi'_A}^2\tanh\phi_T}{\phi_T Bi'_{A,w}}\right)^{-1}\right. \\
&+ \left.(1-f)\left(1+\frac{{\phi'_A}^2\tanh\phi_T}{\phi_T Bi'_{A,d}}\right)^{-1}\right]
\end{aligned} \tag{4.67}$$

$$C_{B,s} = C_{B,bulk}\left(1+\frac{{\phi'_B}^2 f\tanh\phi_T}{\phi_T Bi_{B,w}}\right)^{-1} \tag{4.68}$$

Performance of the unified model for eggshell catalysts is shown in figure 4.12.

## 4.4 Summary

The wetting geometries obtained from the colorimetric work in Chapter 3 were used to investigate the effects of partial wetting on intraparticle diffusion, using FEM simulation. It was shown that existing models can predict the effectiveness factor of monodispersed catalyst particles satisfactorily for true wetting geometries for both liquid- and gas-limited reactions. These models are limited to first-order reactions, with a rate dependence only on either the gas or the liquid reagent. Adopting the traditional descriptions for partial

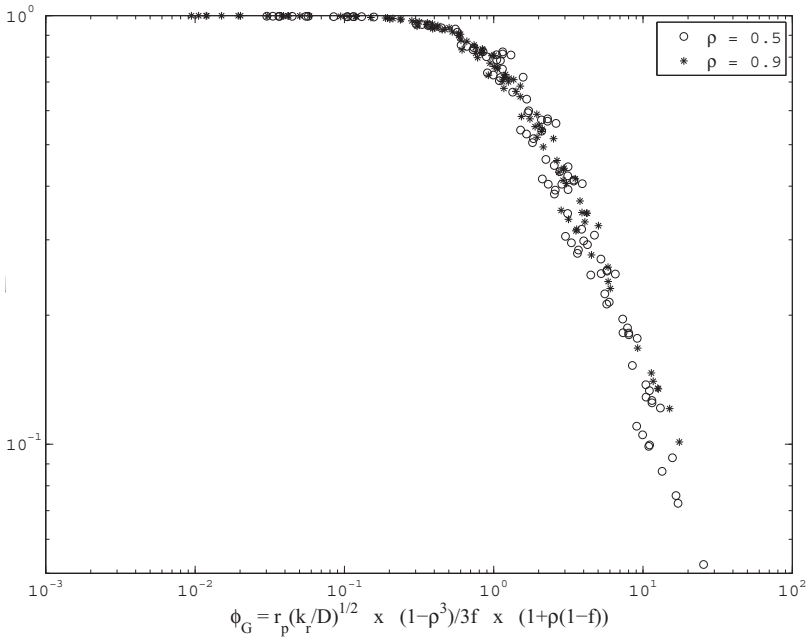


**Figure 4.11:** Pellet efficiency for partially wetted spherical eggshell catalysts as a function of the modified eggshell modulus (Equation 4.64)

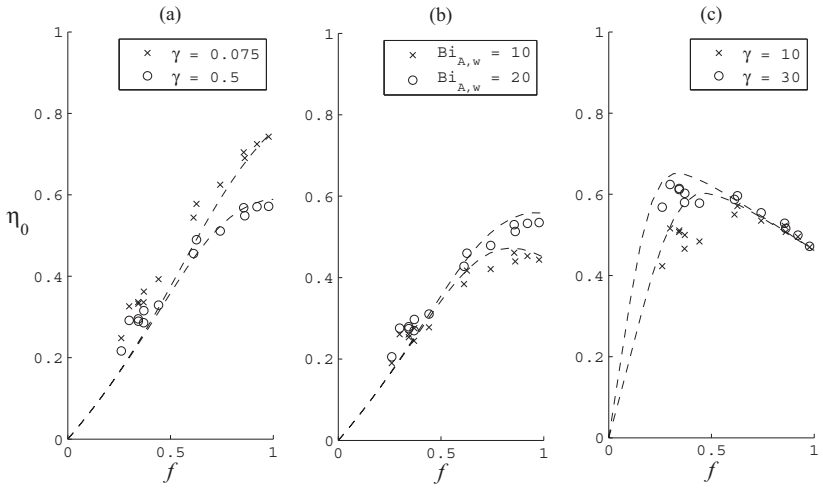


**Figure 4.12:** Overall efficiency factor for the reaction $-r_A = k_r C_A C_B$ in an eggshell catalyst where $\rho = 0.9$. (a) Liquid-limited reaction with some external mass transfer resistances for the gaseous reagent over the wetted surface ($Bi_{A,w} = 10$, $Bi_{A,d} \rightarrow \infty$ , $Bi_{B,w} \rightarrow \infty$); (b)reaction that is not classified as either gas- or liquid-limited with varying rates of external mass transfer for the gaseous reagent ($\gamma = 1$, $Bi_{A,d} \rightarrow \infty$, $Bi_{B,w} \rightarrow \infty$); (c) gas-limited reaction ($Bi_{A,w} = 10$, $Bi_{A,d} \rightarrow \infty$, $Bi_{B,w} \rightarrow \infty$). For all data, $\phi_i = 10$ where $i$ refers to the limiting reagent.

wetting effects on liquid- and gas-limited reactions, a unified model was developed for the reaction $r_A = -\alpha r_B = \alpha k_r C_A C_B$. This unified model can be used over the whole $\gamma$-range, so that a reaction need not be classified as either liquid- or gas-limited.

Eggshell catalysts have not previously been studied for trickle-bed reactor purposes, though these are quite common for hydrogenation purposes. Based on FEM results, models are suggested to estimate the effect of partial wetting on eggshell particles for any value of $\gamma$. It was shown that, in term of liquid-limitations, eggshell particles are more sensitive to partial wetting than monodispersed particles.

# Nomenclature

| | |
|---|---|
| $A_1$, $B_1$ | quantities defined in Equation (4-23), dimensionless |
| $a$ | dimensionless concentration of reagent $A$ |
| $a_p$ | ratio of catalyst surface area to catalyst volume in a reactor, $\mathrm{m}^{-1}$ |
| $a_{GL}$ | ratio of gas-liquid surface area to catalyst volume in a reactor, $\mathrm{m}^{-1}$ |
| $b$ | dimensionless concentration of reagent $B$ |
| $Bi$ | Biot number for a sphere, dimensionless |
| $Bi'$ | Biot number based on slab geometry, $Bi' = \frac{V_R k_c}{S_p D}$ |
| $Bi''$ | Biot number based on slab geometry and the external area available for mass transfer, $Bi' = \frac{V_R k_c}{S_x D}$ |
| $c$ | dimensionless concentration, $c = \frac{C}{C_{bulk}}$ |
| $C*$ | saturation concentration, $^{\mathrm{mol}}/_{\mathrm{m}^3}$ |
| $C_i$ | concentration of reagent $i$, $^{\mathrm{mol}}/_{\mathrm{m}^3}$ |
| $C_{eq}$ | concentration for which reaction rate is zero, $^{\mathrm{mol}}/_{\mathrm{m}^3}$ |
| $C_L$ | concentration in centre of slab, $^{\mathrm{mol}}/_{\mathrm{m}^3}$ |
| $D_i$ | effective diffusivity of reagent $i$, $^{\mathrm{m}^2}/_{\mathrm{s}}$ |
| $f$ | fractional wetting, dimensionless |
| $g(f)$ | fitted function to describe the $\eta$ - $f$ relationship for an eggshell particle based on the GC model |
| $h$ | shape factor for the GC model |
| $I_x(y)$ | modified Bessel function of the first kind, order $x$, evaluated at $y$ |
| $K_x(y)$ | modified Bessel function of the second kind, order $x$, evaluated at $y$ |
| $k_r$ | reaction rate constant, based on active catalyst volume, units dependent on rate expression |
| $k_R$ | first-order reaction rate constant, based on catalyst volume in reactor, $^{1}/_{\mathrm{s}}$ |
| $k_c$ | mass transfer coefficient for relevant mass transfer step, $^{\mathrm{m}}/_{\mathrm{s}}$ |
| $k_{GL}$ | gas-liquid mass transfer coefficient, $^{\mathrm{m}}/_{\mathrm{s}}$ |
| $k_{LS}$ | liquid-solid mass transfer coefficient, $^{\mathrm{m}}/_{\mathrm{s}}$ |
| $L$ | slab thickness, or $V_R/S_x$ |
| $\overline{n}$ | unit vector normal to external surface, dimensionless |
| $r_C$ | radius of semi-infinite cylinder |
| $r_p$ | radius of spherical particle, m |
| $r_i$ | rate of production of component $i$, $^{\mathrm{mol}}/_{\mathrm{s}}$ |
| $R'$ | characteristic diffusion length for the GC model, m |
| $R_i$ | residual for the estimation of dimensionless concentration $i$, dimensionless |
| $s$ | FEM surface triangle area, dimensionless |
| $S_p$ | external surface area of catalyst particle, $\mathrm{m}^2$ |
| $S_x$ | external surface area of catalyst particle over which mass transfer can take place, $\mathrm{m}^2$ |
| $v$ | FEM element volume, dimensionless |
| $V_c$ | volume of catalyst in a reactor, $\mathrm{m}^3$ |
| $V_p$ | volume of catalyst particle, $\mathrm{m}^3$ |
| $V_R$ | volume of catalyst particle in which reaction can take place. The same as $V_P$ for a monodispersed particle, but not for an eggshell particle |
| $w$ | arbitrary weighting function used in the derivation of FEM equations |
| $x$ | dimensionless position in a slab |
| $y(C)$ | concentration-dependent term in the kinetic description of reaction rate, units dependent on kinetic expression |

*Greek letters*

| | |
|---|---|
| $\alpha$ | stoichiometric coefficient, dimensionless |
| $\phi''$ | Thiele modulus relevant to specifiec geometry, dimensionless |
| $\phi_C$ | Thiele modulus for a cylinder, dimensionless |
| $\phi_G$ | generalised modulus, $L\sqrt{k_r/D}$ for a first-order reaction, dimensionless |
| $\phi_{GC}$ | modulus for the GC model, dimensionless |
| $\phi_i$ | Thiele modulus of component $i$ for a sphere. For a first-order reaction, $\phi = r_p\sqrt{\frac{k_r}{D}}$. Note that this definition is not adjusted for an eggshell catalyst. |
| $\phi_i'$ | same as $\phi_i$, but based on surface concentrations for higher-order reactions, dimensionless |
| $\phi_T''$ | Bischoff modulus for a slab |
| $\phi_T$ | Bischoff modulus for a (partially wetted) sphere |
| $\gamma$ | $(\alpha C_{B,bulk} D_B) \,/\, (C_A^* D_A)$, dimensionless |
| $\eta$ | pellet efficiency factor, dimensionless |
| $\eta_0$ | overall efficiency factor, dimensionless |
| $\lambda$ | dimensionless radial position in a spherical particle |
| $\lambda'$ | same as $\lambda$, but based on surface concentrations, dimensionless |
| $\rho$ | ratio of shell inner to outer diameter, dimensionless |

*Subscripts*

| | |
|---|---|
| $A$ | refers to reagent in the gas |
| $B$ | refers to non-volatile reagent |
| $bulk$ | refers to bulk liquid |
| $d$ | refers to dry external area |
| $w$ | refers to wetted external area |
| $s$ | refers to surface |

# CHAPTER 5

# LIQUID-SOLID CONTACTING IN A PILOT REACTOR

The literature review in Chapter 2 illustrates the importance of wetting efficiency measurements under reaction conditions relevant to typical industrial applications. All the reactor measurements of wetting efficiency are accompanied by some estimation of the kinetic expression of the catalysed reaction, and most are also dependent on a correlation-based estimation of external mass transfer. In this chapter, measurements of wetting efficiency and liquid-solid mass transfer coefficients are derived from reactor conversion data. Data include measurements for gas-liquid upflow, and different hydrodynamic states in trickle flow. Based on the theoretical insights from Chapter 4 regarding the behaviour of eggshell catalysts, typical conditions are identified for a reaction system where wetting efficiency and liquid-solid mass transfer effects can easily be recognised. These theoretical considerations are also useful for the identification of other possible reaction systems suitable for the proposed wetting efficiency measurement methods. A reaction study at such conditions in a high-pressure, 50 mm I.D. pilot reactor is then performed to obtain wetting efficiency and liquid-solid mass transfer coefficient measurements. As in Chapter 3, both boundaries of hydrodynamic multiplicity in pre-wetted beds are explored.

Approximations of the reported parameters are based on conversion data for two reactions: hydrogenation of linear octenes and hydrogenation of isooctenes (trimethylpentenes, or TMP). These reactions find their application in the Fischer-Tropsch refining industry (de Klerk, 2008): Fischer-Tropsch naphtha contains up to 85% olefins, and requires severe hydrogenation. This leads to a drastic decrease in the motor octane number (MON) of the treated process stream. The decrease in MON is highly dependent on the molecular structure of the hydrogenated olefin. As a rule, the hydrogenation of linear olefins leads to a more severe drop in the octane number than the hydrogenation of branched olefins. It

is therefore preferable to hydrogenate the branched olefins and retain the least-branched olefinic molecules.

## 5.1 Finding an applicable reaction system

### 5.1.1 Theoretical considerations

For a simple estimation of liquid-solid contacting effects, it is first necessary to identify conditions where reactor performance is linked in a simple way with wetting efficiency. From the previous chapter, the overall particle efficiency for a first-order liquid-limited reaction is given by the form[1]:

$$\eta_0 = \eta\left(1 + \frac{\phi_G^2}{Bi'.f}\eta\right)^{-1}$$
$$\text{where: } Bi' = \frac{V_R k_{LS}}{S_p D_{eff}} \quad \phi_G = \frac{V_R}{S_p}\sqrt{\frac{k_r}{D}_{eff}} \tag{5.1}$$

A linear dependence of $\eta_0$ on $f$ is ideal for the measurement of average wetting efficiency, since the PWD in the reactor will then not influence $\eta_0$. Theoretically, there are three possible cases where the overall reactor performance is linearly dependent on $f$ over the whole $f$-range:

1. $\frac{\phi_G^2}{Bi'}\eta \gg 1$ so that $\eta_0 = f\frac{Bi'}{\phi_G^2}$. In this case, the reaction rate is completely external mass transfer limited.

2. $\eta = k \cdot f$ so that $\eta_0 = k \cdot f\left(1 + \frac{\phi_G^2 k}{Bi'}\right)^{-1}$. Here, the reaction is internal diffusion limited, while external mass transfer limitations can also play a role. For an internal mass transfer limited system, $k \approx 1/\phi_G$.

A typical mass transfer study would employ case (1), using a very rapid reaction to measure mass transfer rates. It is, however, not possible to measure wetting efficiency and mass transfer independently when only case (1) is applicable to the system, even if it is possible to vary $\phi_G$ without changing the hydrodynamics of the reactor. For case (2), or a combination of case (1) and case (2), it is possible to distinguish between the effects of wetting efficiency and liquid-solid mass transfer by varying $\phi_G$ without changing hydrodynamic conditions in the reactor. Morita and Smith (1978) did this by repeating trickle-bed experiments (i.t.o hydrodynamic conditions) with catalysts of different activities. This requires reactor repacking, stable well-characterised catalysts and good hydrodynamic repeatability. An easier method is to perform two reactions of

[1]The previous chapter frequently deals with different particle shapes, and different forms of this equation are given. The equation shown here is valid for all shapes due to the definitions of $Bi'$ and $\phi_G$.

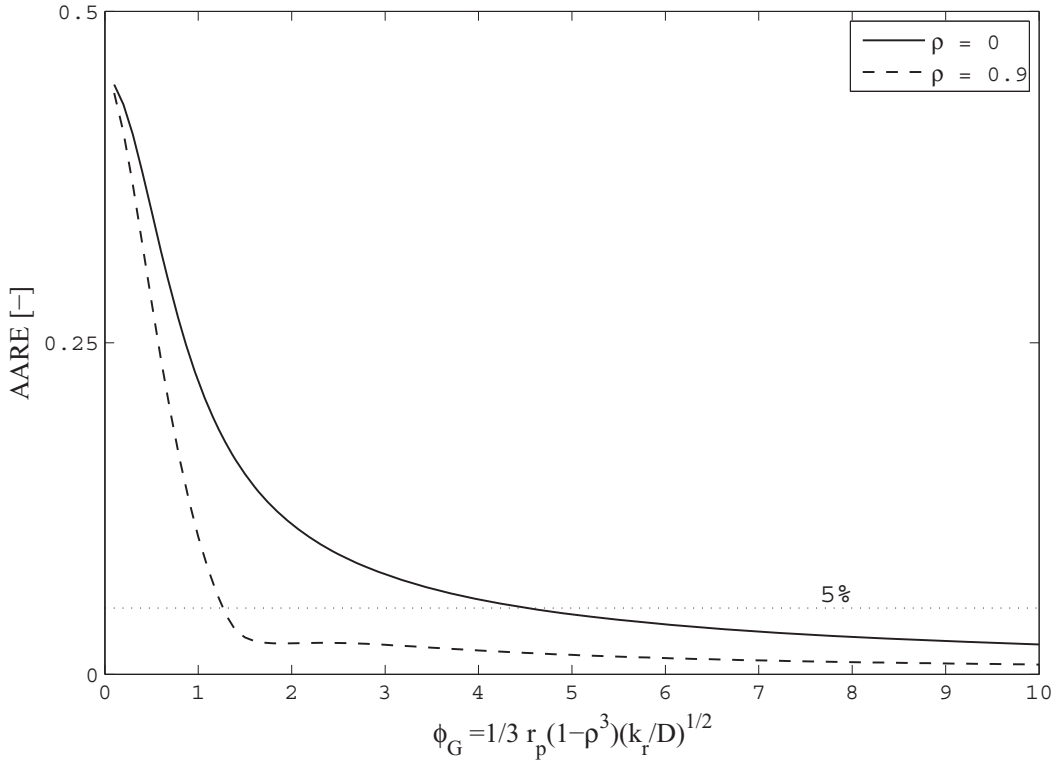


**Figure 5.1:** Absolute average relative errors obtained when approximating the relationship between $\eta$ and $f$ for a given $\phi_G$ as being linear over the whole $f$-range, as a function of $\phi_G$. Errors are calculated by comparing the modified GC model to the linear model $\eta = f \times \eta|_{f=1}$ and are reported for monodispersed and eggshell spherical particles.

different rates in parallel during the same experimental run, giving rise to measurements for two different moduli, $\phi_{G1} > \phi_{G2}$. This approach is followed in the experimental work presented in this chapter. Since $k_{LS}$ and therefore $Bi'$ is not dependent only on the hydrodynamic behaviour of the system, but also of molecular diffusivity of the reagents, care should be taken that both reagents have more or less the same diffusivity, so that $Bi'_1 = Bi'_2 = Bi'$. If this is not the case, it will still not be possible to decouple $Bi'_1$, $Bi'_2$ and $f$. This is dealt with in the next section. The faster reaction corresponding to $\phi_{G1}$ will be more affected by liquid solid mass transfer (in the limit corresponding to case 1) than the slower reaction ($\phi_{G2}$), where the effect of wetting efficiency on particle efficiency will be more prominent. This slower reaction therefore has to comply with case (2), and the particle efficiency should be linearly dependent on $f$. This is the first requirement on the system. Making use of the modified GC model developed in the Chapter 4 from FEM simulation, one can get an idea for which values of $\phi_G$ the particle efficiency will be linearly related to $f$. As shown in Figure 5.1, these values are $\phi_G > 1.5$ for eggshell particles with $\rho = 0.9$ (which are used in this study) and $\phi_G > 4.5$ for monodispersed spherical catalysts.

Where the first requirement stated in the beginning of this chapter is met as long as $\phi_{G2} > 1.5$, the second requirement, i.e. easy decoupling of $Bi'$ and $f$, requires the slow reaction ($\phi_{G2}$) to be slow enough to ensure that it is not completely limited by the resistance to external mass transfer. Say, for internal mass transfer effects to be discernible, overall rate of the slowest reaction should be at least 20% less than it would have been, had it been completely mass tranfser limited. Then:

$$\eta_0 \leq 0.8 f \frac{Bi'}{\phi_{G2}^2}$$

$$\eta \left(1 + \frac{\phi_{G2}^2}{Bi' f}\eta\right)^{-1} \leq 0.8 f \frac{Bi'}{\phi_{G2}^2}$$

$$\text{And:} \quad \eta \approx \frac{f}{\phi_{G2}}$$

$$\therefore \frac{f}{\phi_{G2}} \left(1 + \frac{\phi_{G2}}{Bi'}\right)^{-1} \leq 0.8 f \frac{Bi'}{\phi_{G2}^2}$$

$$\left(1 + \frac{\phi_{G2}}{Bi'}\right)^{-1} \leq 0.8 \frac{Bi'}{\phi_{G2}}$$

$$\therefore \phi_{G2} \leq 4Bi' \tag{5.2}$$

Where according to most correlations, this criterion is easily met for monodispersed particles ($Bi$ is typically larger than 10, see Chapters 2 and 4), it is much more stringent for eggshell particles. Remember that $Bi'$ is per definition proportional to the ratio of reaction volume to external surface area (see Equation 5.1). This is much less for an eggshell catalyst than for a monodispersed one. For example, if it can be safely assumed that for a monodispersed sphere $Bi = k_{LS} \times r_p / D_{eff} \geq 10$, then for an eggshell catalyst $Bi' \geq 10/3 \times (1 - \rho^3)$. Hence for the eggshell catalyst used in this investigation, it is required from equation (5.2) that $\phi_{G2} \leq 3.6$.

A summary of the approximate conditions to meet the first two requirements in the beginning of this chapter is given in Table 5.1, for monodispersed and eggshell catalysts ($\rho = 0.9$). It is clear that monodispersed particles are more suitable for the identification of wetting efficiency than eggshell catalysts. The other three requirements listed in the beginning of this chapter, and other hydrodynamic considerations such as dispersion and possible rate limitations imposed by the gaseous reagent, are dealt with in section 5.3.

**Table 5.1:** Approximate requirements for the reaction system.

| Monodispersed catalyst | Eggshell catalyst used in this study ($\rho = 0.9$) |
|---|---|
| Diffusivities of both liquid reagents in the solvent should be the same | Same as for monodispersed |
| First-order reactions | First-order reactions |
| $4.5 \leq \phi_{G2} \leq 13$ | $1.5 \leq \phi_{G2} \leq 3.6$ |
| $\phi_{G1} \gg \phi_{G2}$ | $\phi_{G1} \gg \phi_{G2}$ |

## 5.2 Reaction system characteristics

The trickle-bed reaction most often encountered in industry is hydrogenation, predominantly for hydrotreatment in the refining of crude oil (Gianetto and Specchia, 1992). Hydrotreatment is characterised by high conversions and low reagent concentrations. An exception to this rule is encountered in high temperature Fischer-Tropsch refineries: HTFT naphtha contains up to 85% olefins, which need to be decreased to $< 18\%$ (de Klerk, 2008). This corresponds to a rather low conversion of approximately 0.8 and since not all of the olefins need to be hydrogenated, it was suggested that some way should be found to selectively hydrogenate the branched olefins rather than linear olefins in the feed stream, to maximise the octane number of the refined naphtha. This study focuses on reactor hydrodynamics and therefore does not further elaborate on this rather interesting problem (due to molecular structure, linear olefins are by nature more rapidly hydrogenated than branched olefins). Nevertheless, a similar reaction system has been selected for the trickle-bed study, mainly because of the large difference in the hydrogenation rates of branched and linear olefins and the fast rate of the hydrogenation of linear olefins in the naphtha boiling range.

The model reactions of this process have been chosen as (i) the hydrogenation of linear octenes, and (ii) the hydrogenation of isooctenes. According to the Wilke-Chang equation, this reaction system meets the requirement of equal diffusivities for both reagents, since the molar masses and densities are equal. Mixtures of all isomers of these reagents are used, so that these are in fact more than two reactions that yield only two paraffinic products. It should therefore be ensured that all reactions leading to the same product can be modelled as one reaction. Also, both reactions should be first-order, for easy modelling of the effect of wetting efficiency on internal diffusion.

The reaction mixture contains roughly 1% linear octene isomers and 2% isooctene isomers in a $C_{14}$-$C_{20}$ paraffin solvent. Concentrations had to be this low for the trickle-bed reactor to run isothermally while useful conversions can be measured. Physical properties of the reaction mixture are listed in Table 5.2.

**Table 5.2:** Liquid reaction mixture properties.

| Property | Estimated value | Estimation method |
|---|---|---|
| Viscosity | 1.71 mPa.s | van Velzen et al. (1972)<br>Kendall (1917) |
| Surface tension | 27 $^{mN}/_{m}$ | Sugden (1924) |
| Density | 765 $^{kg}/_{m^3}$ | Measured |
| Reagent molecular diffusivity in solvent | | Wilke and Chang (1955) |
| Linear octenes | $1.13 \times 10^{-9}$ $^{m^2}/_{s}$ | |
| Isooctenes | $1.13 \times 10^{-9}$ $^{m^2}/_{s}$ | |
| Average molar mass | $\sim$230 $^{kg}/_{kmol}$ | Estimated from GC analysis |

A 0.3% $Pd/Al_2O_3$ spherical eggshell catalyst with a diameter of 3 mm was used to catalyse the reactions. The catalyst was supplied by Heraeus, and is marketed as a hydrogenation catalyst. Particle density is $\pm$ 1100 $^{kg}/_{m^3}$. Shell thickness was determined with a microscope at 0.3 mm.

To characterise the kinetic sytem, batch experiments were performed in a 450 ml Parr autoclave reactor with the temperature controlled ($\pm$ 1 °C) at 60 °C, measuring conversion versus time. The catalyst was crushed to approach intrinsic kinetics. Liquid reagent starting concentrations were the same as in the packed-bed experiments. Before sampling, the sampling line was purged twice with the liquid in the reactor. After completion of the experiment, the total volume of sampled or purged liquid was less than 5% of the total reactor volume. Concentration versus time profiles obtained from sampling of the liquid at different time intervals are shown in figure 5.2. At a given pressure, both reactions are first-order with respect to the liquid reagent. It is clear from the figure that reaction rates are affected by $H_2$ partial pressure. Packed-bed conversion data will therefore be treated using a first-order rate expression, with a pseudo rate constant that is a function of the $H_2$ partial pressure. This approach is only valid if the liquid in the packed bed is saturated with $H_2$ throughout the bed. Care should therefore be taken with separate reactor experiments that this is indeed the case.

At 60 bar and 60°C, the reactions comply with the requirements listed in section 5.1.1. At this pressure and temperature, the first-order rate constant for isooctene hydrogenation is $k_{r2} \approx 0.3\ s^{-1}$, based on the catalyst shell volume. This corresponds to a particle modulus[2] of $\phi_{G2} \approx 2.6$. The rate of hydrogenation of the linear octenes is not very important, as long as it is much faster than that of the isooctenes, which is clearly the case ($k_{r1} \approx 6s^{-1}$, $\phi_{G1} \approx 12$).

The figure also confirms that all linear octene isomers can be viewed as one reagent: since almost pure 1-octene was used as reagent, the linear octene isomer composition changed during the experiment, which clearly did not affect the rate of octane production.

[2]To approximate the generalised modulus, an approximation of the effective diffusivity is necessary. The approximation is based on a particle porosity of 0.8, a tortuosity of $\sqrt{2}$, and a constriction factor of 0.8. See Levenspiel (2006).

The same applies to the isooctene reaction mixture.

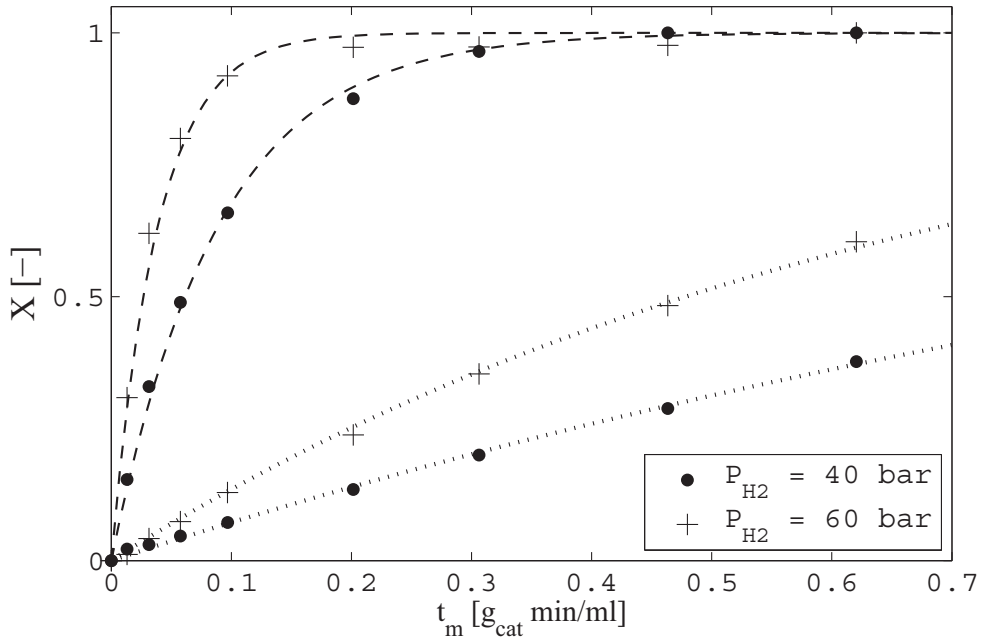


**Figure 5.2:** Reaction kinetics for grinded catalyst. Dotted lines are first order fits in term of liquid reagent concentrations.

It may seem peculiar that only two kinetic experiments are presented. Proper kinetic experiments typically require a variation of feed concentration, pressure, degree of grinding, stirring speed, etc. Some of these were included, but in the view of the objectives of this study, they are not necessary and even undesirable, since it will be attempted to measure wetting efficiency without an excessive kinetic decription. Batch experiments were only performed to find a region where Table 5.1 is applicable. External and even internal mass transfer limitations may have influenced rate measurements of the linear octene hydrogenation and the reaction may be faster than estimated, but this is not important in view of the requirements listed in Table 5.1. What is more important is the rate isooctene hydrogenation. It can be said that external mass transfer resistances did not influence the rate of this reaction, since a rate constant of more than 20 times higher was measured in the same experiment. Also, even for this reaction, the requirements for $\phi_{G2}$ allow for some error in the estimation of $k_{r2}$. The constraint of $1.5 \leq \phi_{G2} \leq 3.6$ translates to $0.1 \leq k_{r2} \leq 0.5\text{s}^{-1}$. It can be said with reasonable certainty that this is indeed the case.

## 5.3 Pilot studies

### 5.3.1 Experimental

#### Trickle-bed reactor setup

A schematic of the experimental setup is shown in Figure 5.3. The setup is designed to provide for gas-liquid upflow, gas-liquid downflow and countercurrent flow. The liquid reaction mixture, containing $\sim 1\%$ linear octene isomers and $\sim 2\%$ isooctene isomers, is pumped with a Bran & Luebbe H2-31 diaphragm metering pump capable of delivering $70\,\ell/\text{min}$ at 80 bar. The liquid feed is preheated to the reaction temperature before entering a 50 mm I.D., 1000 mm length reactor. The reactor walls are temperature controlled using three external heaters with wall thermocouples. Eight internal thermocouples are used as illustrated in Figure 5.4 to measure internal temperatures and verify isothermal operation. A Rosemount model 3051CD differential pressure transmitter is used for pressure-drop measurements to check for flow stability. A distributor with a drip point density of $11000\,\text{m}^{-2}$ is situated at the top of the reactor to ensure good liquid and gas distribution for trickle flow runs. If the liquid and gas enter through the bottom of the reactor (during upflow runs), these are distributed only by a retaining sieve plate and the packing itself.

Nitrogen and hydrogen can be fed to the reactor, the flow rates being controlled by 0-30 $\ell/\text{min}$ Brookes mass flow controllers. The maximum operating pressure of the system is 80 bar. A water-cooled heat exchanger is installed in the product line to cool down the product to approximately 30°C. Pressure is regulated with a back pressure regulator and monitored with pressure indicators and transducers at strategic points in the system. Samples are taken in a sampling bomb with a diptube for gas-liquid separation. Based on the high boiling points of the liquid components, it can be assumed that evaporation and the entrainment of liquid product in the gas will not significantly affect the product composition at 30°C. The product stream can either be recycled to the feed tank or routed to the product tank.

#### Experimental conditions and procedure

For each experimental run, the olefins in the liquid feed were hydrogenated over a packed bed with the catalyst described in section 5.2, diluted with inert $\gamma-Al_2O_3$ supports[3] of the same shape. All experiments were performed for five different liquid flow rates, corresponding to superficial velocities of 1.8, 2.6, 3.6, 4.5 and 7.5 $\text{mm}/\text{s}$; and three different flow configurations, namely upflow, Levec pre-wetted trickle flow and extensively pre-wetted trickle flow. The start-up procedure for each type of flow configuration is as follows:

[3]From batch experiments, it was found that the supports catalyse double-bond isomerisation. Since all double-bond isomers can be viewed as one reagent, the supports can be still be regarded as inert.

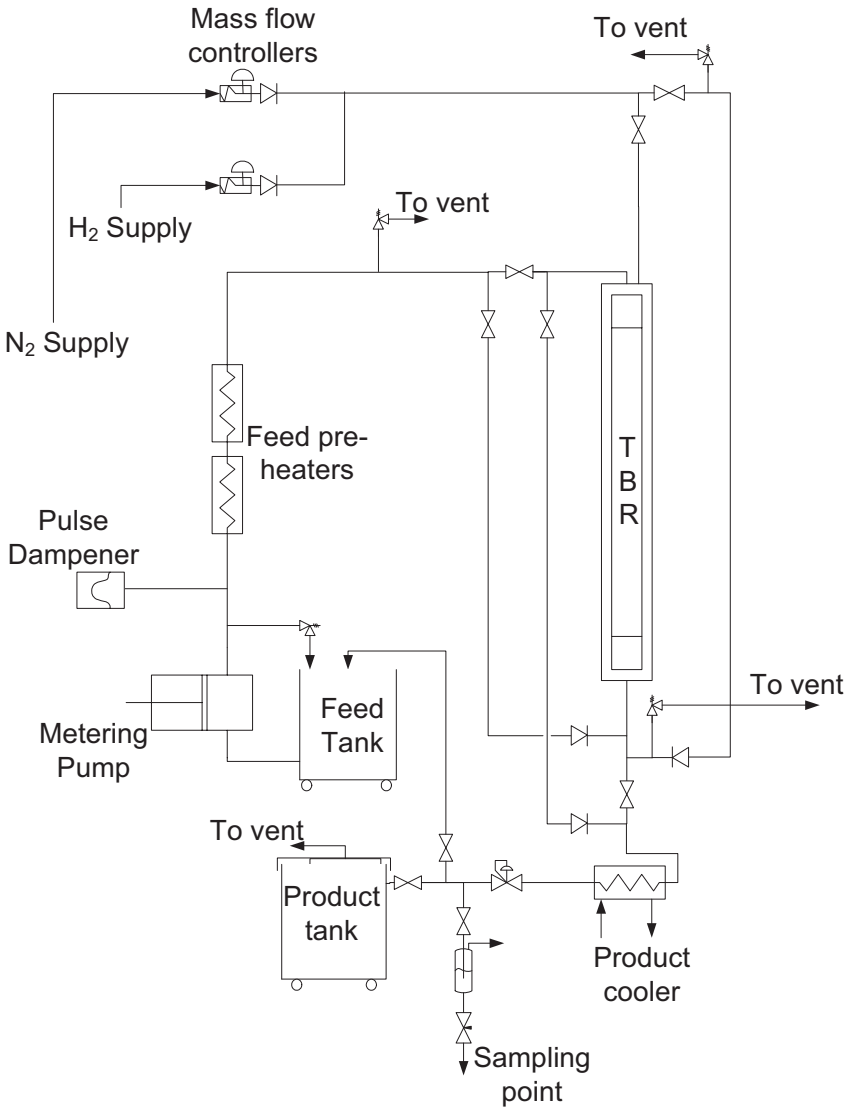


**Figure 5.3:** Schematic of the trickle-bed facility.

- *Upflow.* The liquid flow is set to the required rate by adjusting the pump stroke length and pump motor speed, and is fed to the bottom of the reactor, exiting at the top. Temperature control setpoints for the liquid feed preheaters and reactor heaters are set to the required temperatures. Nitrogen gas flow is introduced and the liquid is recycled to the feed tank until flow and temperature steady state are reached. Once steady state has been achieved, the product stream is rerouted to the product tank, nitrogen flow is shut off and hydrogen is introduced to the reactor. The feed tank is stirred, to ensure that the composition of the feed entering the reactor stays constant.

- *Levec pre-wetted trickle flow.* After the bed is flooded by feeding liquid in upflow,

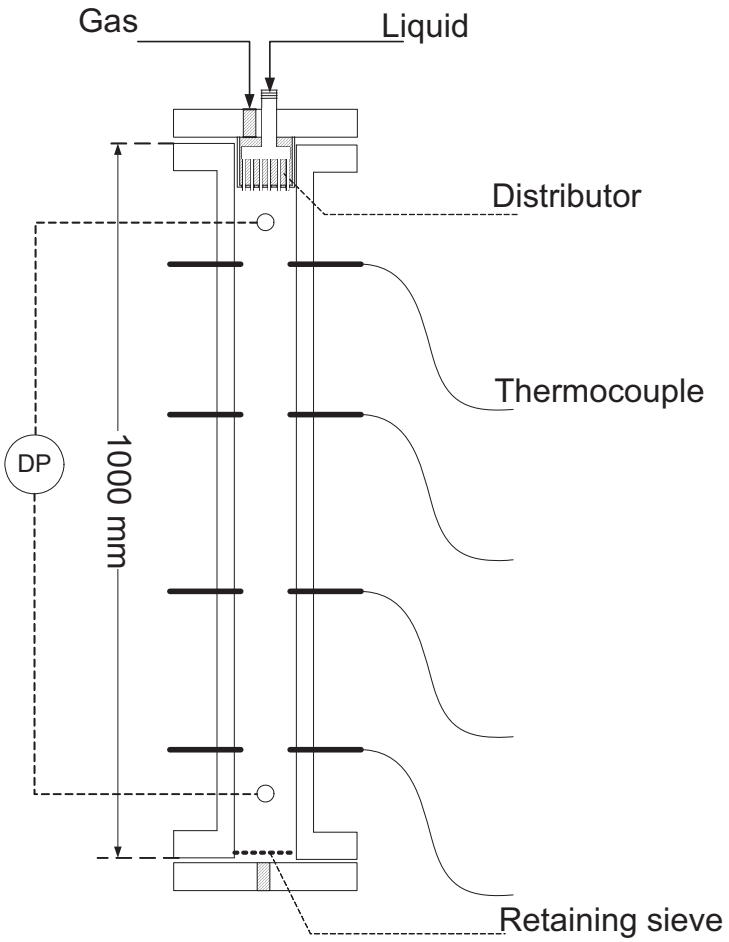


**Figure 5.4:** Reactor detail.

the liquid in the reactor is purged with nitrogen at atmospheric pressure, until no liquid can be detected in the reactor exit stream. The reactor is then pressurised with nitrogen to the required pressure, after which liquid is introduced to the top of the reactor at the required flow rate. It is ensured that the reactor pressure stays constant during the introduction of the liquid. The rest of the start-up procedure is the same as for upflow.

- *Extensively pre-wetted trickle flow.* The reactor is flooded by feeding liquid at the required rate to the bottom of the reactor under recycle conditions, until no gas can be detected in the reactor exit stream. The liquid feed configuration is then changed from upflow to downflow, and nitrogen is introduced to the reactor. The rest of the start-up procedure is the same as for upflow. This pre-wetting procedure will in most cases result in operating on the upper boundary of the multiplicity envelope (Loudon et al., 2006). Note that the pre-wetting procedure here differs from the procedure for extensive pre-wetting in Chapter 3. According to van der Merwe (2008), both pre-wetting procedures have the same hydrodynamic behaviour.

The above start-up procedures require a measure for steady state before nitrogen can be replaced by hydrogen. Steady state was verified by thermocouple readings, pressure drop and flow rate measurements: Once temperature and pressure-drop steady state is reached, the liquid flow rate in the product stream is repeatedly measured with a graduated cylinder and a stopwatch. If the product liquid flow rate stays constant, it is assumed that liquid holdup in the reactor stays constant and therefore that hydrodynamic stability has been reached. This takes between 10 and 20 system residence times, depending on the flow rate and configuration.

While switching over from nitrogen to hydrogen, the flow in the reactor can be disturbed. It is therefore important to choose the nitrogen and hydrogen flow rates in such a way that the disturbance is minimised. It was found that starting up with a volumetric nitrogen flow rate of roughly 60% that of the required hydrogen flow rate led to the smallest disturbances in terms of pressure drop and temperature. This is somewhat higher than is suggested by Ergun's equation for a minimum in pressure drop disturbance (25%-50% at the employed flow rates), since disturbance in bed temperature should also be kept as low as possible. For each experiment, at least 50% stoichiometric excess of hydrogen is fed to the reactor. With the highest conversions reported in this paper, this translates to at least 4.5 times the amount that has reacted. Experimental liquid and gas linear velocities through the reactor are shown in Figure 5.5. It is clear from the figure that all downflow experiments were performed in the trickle flow regime where incomplete wetting occurs. All experiments were performed at 60°C and 50 bar.

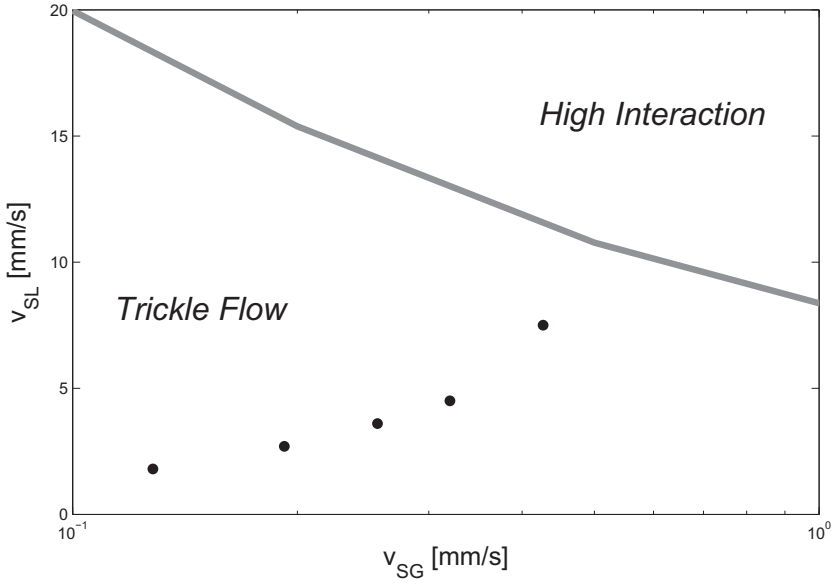


**Figure 5.5:** Flow map of experimental flow conditions. Adapted from Larachi et al. (1999). Hydrodynamic simulator available at http://www.gch.ulaval.ca/bgrandjean, accessed 22 May 2009

Two product samples were taken for each specific flow rate and configuration. The first sample was taken 10 reactor residence times (based on void volume) after achieving steady state under reaction conditions; and the second one 3-5 residence times later. The second sample serves to verify steady state conditions in the reactor.

Samples were analysed with an Agilent Technologies 6890 gas chromatograph (GC) fitted with a flame ionisation detector (FID). Elutriation was established on a 50 m-long Pona column with a 0.2 mm inner diameter and a 0.5 mm film thickness, using $N_2$ as carrier gas at a flow rate of 25 $^{ml}/_{min}$. A split ratio of 100:1 was used. The initial column temperature was 40°C, where it was held for 5 minutes. Then the temperature was ramped for 15 minutes at 4°C/min to obtain a good separation of the $C_8$ reagents, after which the temperature was increased to 300°C at 25°C/min.

Both the catalyst and support were supplied by Hereaus. A 630 mm bed of 70 g catalyst diluted with inert $\gamma$-$Al_2O_3$ supports was packed between two layers of 140 mm of inert supports at the entrance of and exit to the reactor. For a conversion of $X \leq 0.6$, the dispersion criterion of Sie and Krishna (1998) suggest a minimum reactor length of 550 mm for dispersion to be negligible in all modes of operation if the reaction is first-order. Bed porosity was 0.4 for all experiments.

### Gas mass transfer resistances

To be able to adopt first-order kinetics by neglecting any influences that hydrogen may have on the reaction rate, it should first of all be ensured that the liquid entering the bed is saturated with hydrogen, independent of the liquid flow rate and flow configuration. For all experiments, 140 mm of inert supports were used to provide for hydrogen saturation before entering the bed. That this amount of support was indeed enough to ensure saturation was verified experimentally: two experimental runs were performed, one with an undiluted (70 g) catalyst bed situated 140 mm from the top reactor inlet and another with the bed situated close to the bottom of the reactor (the depth of the bed was 715 mm - 775 mm). The available area for gas-liquid mass transfer before entering the catalyst bed was far more in the former than in the latter case for gas-liquid upflow, and vice versa for trickle flow. The results for linear octene hydrogenations in these beds are shown in Figure 5.6. Since these two runs agree satisfactorily for all experimental conditions, it can be assumed that the liquid is saturated with the gas before entering the bed. Both experiments were repeated with good repeatability.

To ensure that any resistances to gas mass transfer within the catalyst bed are negligible, the hydrogenation of a 1% linear octenes and 2% isooctenes feed was compared with the hydrogenation of 0.5% linear octenes and 0.5% isooctenes. If gas mass transfer resistances play a role, the conversions for the lower concentration feed will be the highest. The results are shown in Figure 5.7. Close agreement between the results confirms that

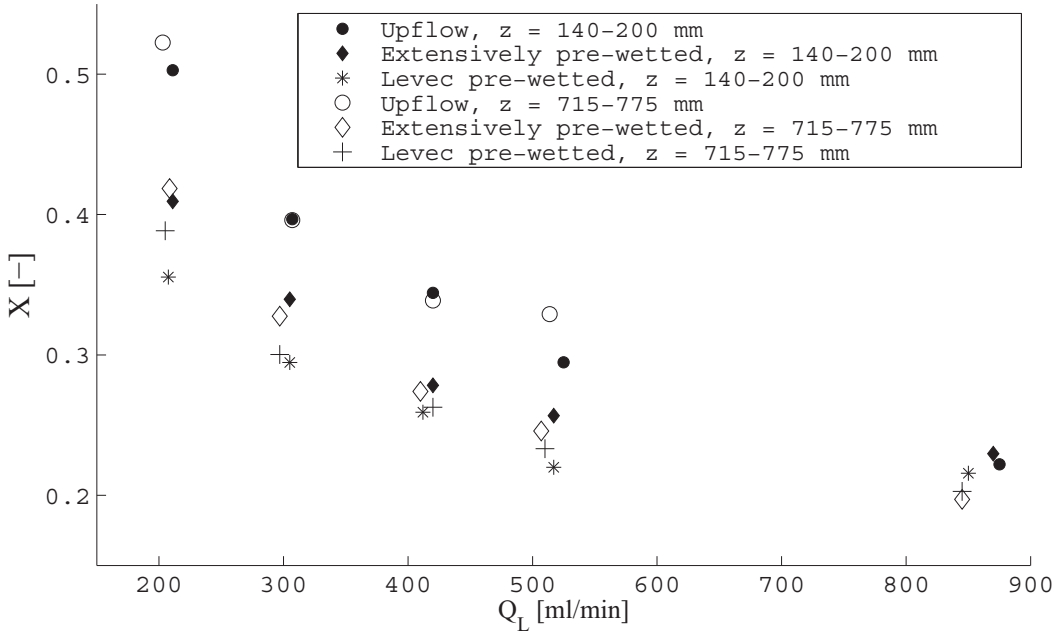


**Figure 5.6:** Test for saturation of liquid with hydrogen before entering the catalyst bed. The quantity $z$ refers to the position of the bed as measured from the top.

hydrogen mass transfer can be ignored. The results also confirm the first-order behaviour of the reactions in terms of the liquid reagents.

### 5.3.2 Results and discussion

#### Conversion data

Typical conversion data for an experimental run are shown in Figure 5.8. In the rest of the discussion, an "experimental run" refers to two conversion datapoints for both reactions at five different liquid flow rates for all three different modes of operation. All the datapoints from an experimental run were generated consecutively (in no specific order) without interruption. Conversion data for the two different reactions are of course generated in parallel. In total, nine experimental runs were performed, each consisting of a total of 60 conversion measurements (30 product samples containing linear and isooctenes for 15 different flow conditions).

At all the liquid flow rates and for both reactions, conversion decreases in the order upflow- extensively pre-wetted trickle flow - Levec pre-wetted trickle flow at the same liquid flow rate. Although both reactions are known to be first-order in terms of the olefin concentration, none of the data shows good first-order behaviour for the fastest reaction, and conversion rates increase with liquid flow rate. For the slower reaction, the upflow conversion data approximates first order behaviour.

These observations are clear indicators that external liquid-solid mass transfer affects

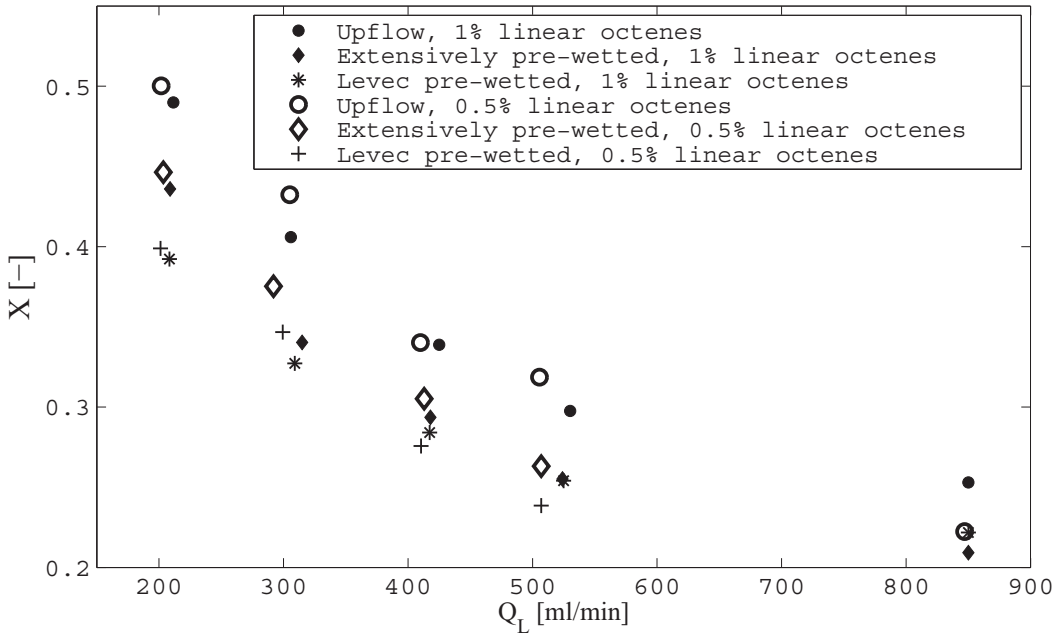


**Figure 5.7:** Conversion of linear octenes for feed concentrations of 0.5% and 1% linear octenes. The feed also contained 0.5% and 2% isooctenes, respectively

the reaction system: rates are slower at lower liquid velocities, and reaction inhibition is more pronounced for the fast reaction than for the slow reaction. Where upflow conversion data for the slow reaction approximate first-order behaviour, significant deviations still persist in trickle flow at low liquid flow rates. This can be due to even slower mass transfer rates in this mode of operation or incomplete wetting, or a combination of both. Since both reaction are known to be first order in terms of the non-volatile reagents, it is assumed that all deviations from first order behaviour can be ascribed to hydrodynamic effects, and the reactor design equation for both reactions can be written as:

$$\begin{aligned} -\ln(1-X) &= \frac{k_T.V_{cat}}{Q_L} \\ \text{Where} \quad V_{cat} &= m_{cat}/\rho_{cat} \end{aligned} \tag{5.3}$$

where $k_T$ is a function of the hydrodynamic properties of the system and can be affected by the rate of liquid-solid mass transfer, or the wetting efficiency, or both. Since both external mass transfer and particle efficiency are linearly affected by the wetting efficiency,

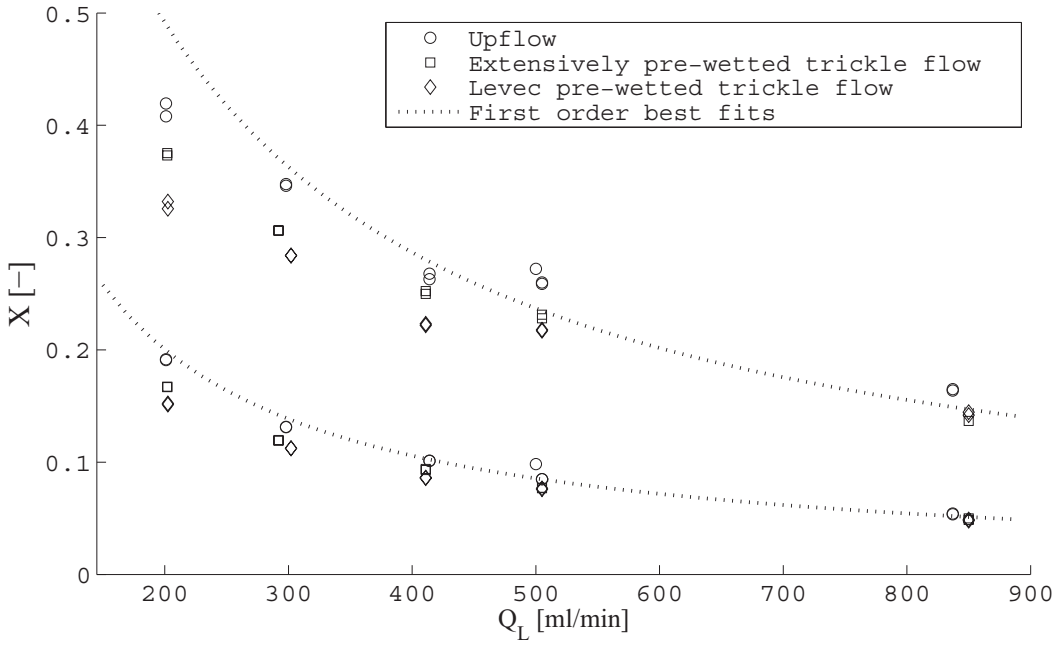


**Figure 5.8:** Typical conversion versus flow rate dataset for an experimental run.

$k_T$ can be written as:

$$\begin{aligned} k_T &= \frac{(f.k_R).k_{LS}(a.f)}{(f.k_R)+k_{LS}(a.f)} \\ &= f\frac{k_R k_{LS} a}{k_R + k_{LS} a} \\ \text{Where} \quad a &= 6/d_p \\ k_R &= k_r \frac{V_R}{V_p}\,\eta|_{f=1} \end{aligned} \tag{5.4}$$

Equation (5.4) will be used in the treatment of conversion data. Note that for the rest of the discussion, $k_T$ is specific to each conversion datapoint.

Although the characteristics of Figure 5.8 were highly repeatable for most of the experimental runs, only a few experimental runs were quantitatively repeatable. An example of how the conversion data varied from one experimental run to another is shown in Figure 5.9. The large scatter is attributed to differences in catalyst activity. Two types of activity variations are possible: one where the catalyst activity varied within a run, and another where the catalyst was stable during a run, but at a different activity than during other experimental runs. Data from the former type of activity variation can not be used, whereas data from the latter type can still be useful if treated correctly. For the selection of useful conversion data, it is first of all necessary to discard all data from experimental runs during which the catalyst deactivated. Deactivation of the catalyst while performing an experimental run might influence the interpretation

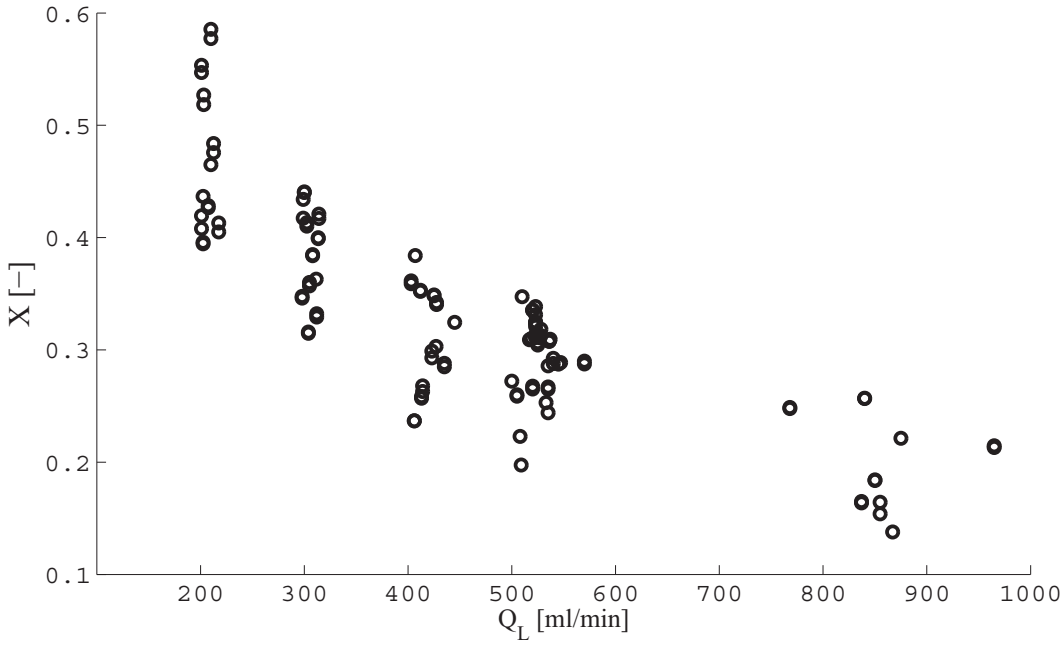


**Figure 5.9:** Unrefined upflow conversion data for the hydrogenation of linear octenes.

of hydrodynamics. For an indication of catalyst stability during an experimental run, the following catalyst activity indicator (CAI) was defined, which can be calculated from conversion data without any knowledge of the reaction rate constants (using the equation on the right):

$$\text{CAI} = \frac{k_{R1}.k_{R2}}{k_{R1} - k_{R2}} = \left.\frac{k_{T1}k_{T2}}{k_{T1} - k_{T2}}\right|_{\text{upflow}} \tag{5.5}$$

The derivation of above Equation is shown in Section 5.3.3 (Equations 5.7 and 5.8), where it is used for the estimation of wetting efficiency. For complete wetting in the upflow mode, the CAI should be independent of liquid flow rate under liquid-limited conditions, and is directly related to the catalyst activity. All experimental runs during which the CAI decreased notably, were discarded. An example of how the CAI is used is shown in Figure 5.10.

Because of catalyst deactivation, data from four of the nine experimental runs had to be discarded. Most of the discarded datasets were from experiments where a new catalyst bed was packed. Although all of the retained datasets were generated with stable catalyst, the stable catalyst activity varied from one experimental run to another, as seen in Figure 5.11. It is therefore important to develop methods for the estimation of liquid-solid contacting which are insensitive to the specific catalyst activity.

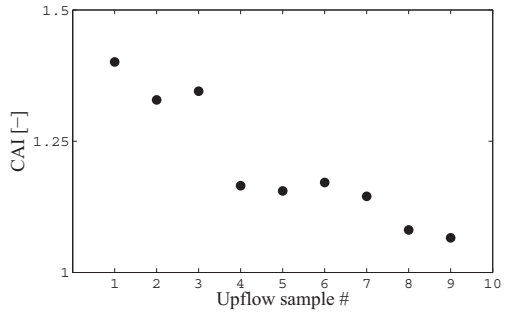


(a) An example of an experimental run for which the CAI indicates a drop in catalyst activity. All data generated during this run were discarded.

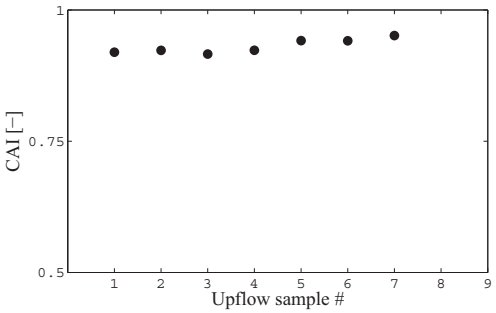


(b) An example of an experimental run with stable catalyst. The dataset generated during this experimental run can be used.

**Figure 5.10:** Catalyst stability checks

### 5.3.3 Wetting efficiency

Consider two first-order reactions with effective kinetic rate constants $k_{R1}$ and $k_{R2}$ occurring in a trickle bed reactor as modelled in Equation (5.4). From the effective rate constants $k_{T1}$ and $k_{T2}$ obtained from conversion data, the liquid mass transfer coefficient can be calculated twice for known reaction rate constants and wetting efficiency:

$$k_{LS}a = \frac{k_{T1}k_{R1}}{f.k_{R1} - k_{T1}} = \frac{k_{T2}k_{R2}}{f.k_{R2} - k_{T2}} \tag{5.6}$$

Note that Equation (5.6) is only valid if both reactions take place under the same hydrodynamic conditions, and refers to the treatment of one specific conversion datapoint in terms of liquid flow rate and catalyst activity. The relationship also relies on the assumption that the molecular diffusivity of both reagents is the same, which was established as holding true.

By rearranging Equation (5.6), it is possible to calculate wetting efficiency at a specific hydrodynamic state (mode of operation and liquid flow rate) if $k_{R1}$ and $k_{R2}$ are known.

$$f = \underbrace{\frac{k_{R1} - k_{R2}}{k_{R1}k_{R2}}}_{A} \cdot \underbrace{\frac{k_{T1}k_{T2}}{k_{T1} - k_{T2}}}_{B} \tag{5.7}$$

For constant catalyst activity, part (B) of Equation (5.7) is directly proportional to wetting efficiency and should be constant during upflow operation if the assumption of complete wetting in upflow operation holds true, so that:

$$\frac{k_{R1} - k_{R2}}{k_{R1}k_{R2}} = \left.\frac{k_{T1} - k_{T2}}{k_{T1}k_{T2}}\right|_{upflow} \tag{5.8}$$

Compare Equation (5.8) to the definition of the CAI in Equation (5.5). Since the CAI did

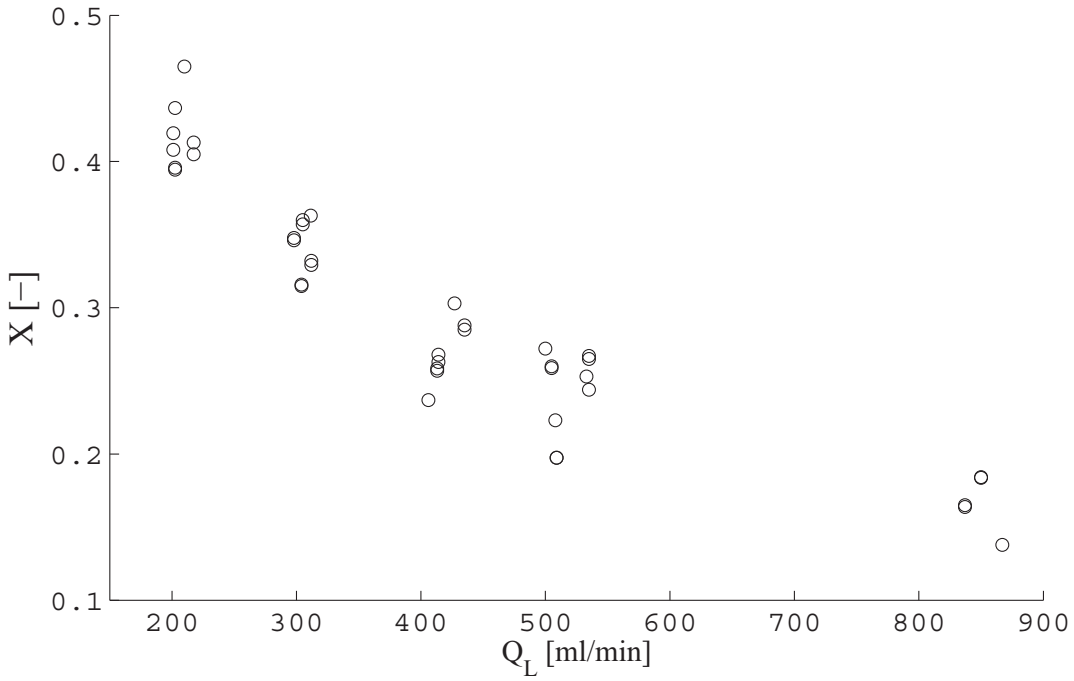


**Figure 5.11:** Upflow linear octene conversion data from experimental runs with stable catalyst

not show any correlation with liquid flow rate and was constant as long as the catalyst activity remained constant, complete wetting in upflow operation can be assumed. Wetting efficiencies in trickle-flow operation can therefore be calculated if conversion data is available for upflow operation at the same catalyst activity.

$$f_{TBR} = \left.\frac{k_{T1}k_{T2}}{k_{T1}-k_{T2}}\right|_{TBR} \left.\frac{k_{T1}-k_{T2}}{k_{T1}k_{T2}}\right|_{upflow} \tag{5.9}$$

Note that for the calculation of wetting efficiency, no knowledge of the kinetic rate constants $k_{R1}$ and $k_{R2}$ is required, and it is possible to calculate wetting efficiency from the raw conversion data as long as upflow conversion data is available at the same catalyst activity, i.e. the catalyst was stable during an experimental run. Note that it is not necessary to have upflow data available at all liquid flow rates: only one upflow conversion datapoint for both reactions is needed to calculate the quatinity defined in equation (5.8), as long as the catalyst was stable during an experimental run.

All measured wetting efficiencies as calculated with Equation (5.9) are shown in Figure 5.12. For easy comparison of Levec- and extensively pre-wetted trickle flow, averaged wetting efficiencies are shown in Figure 5.13. As expected from Chapter 3, hydrodynamic multiplicity is the most severe (about 10-15% variation) at low liquid velocities, where liquid flow in Levec pre-wetted beds tends to channel. The wetting efficiency correlation suggested by Julcour-Lebique et al. (2009) is shown by a dotted line. This correlation was developed from an extensive set of wetting efficiency data which were exclusively

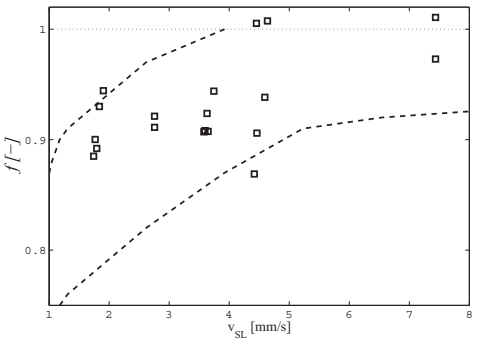


(a) Wetting efficiency measurements for extensively pre-wetted trickle flow.

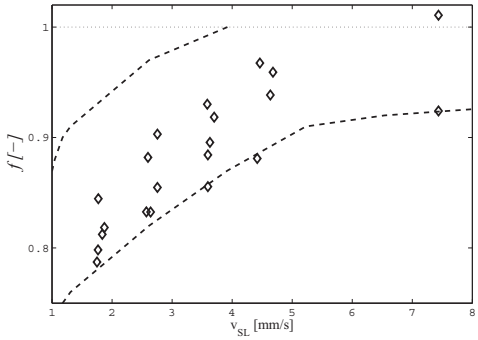


(b) Wetting efficiency measurements for Levec pre-wetted trickle flow.

**Figure 5.12:** Measured wetting efficiencies as a function of liquid superficial velocity. Dotted lines indicate the estimations of wetting efficiencies by Satterfield (1975)

measured by a colorimetric method. It is reassuring that the results from this technique compare so well with the pilot reactor measurements[4]. Quantitatively, the results from Chapter 3 differ significantly from the current results. The most obvious difference between the two systems that were used is the difference in surface tension of the liquid (2.5 times more for water than for the current reaction mixture). Surface tension was suggested to be the reason for differences in reactive wetting efficiency measurements by Leung et al. (1987) and Morita and Smith (1978). Still, the correlation shown here cannot explain the differences in measured wetting efficiencies, though some colorimetric data by the same authors do coincide with the measurements in Chapter 3 (Baussaron et al., 2007).

### 5.3.4 Liquid-solid mass transfer

Based on the fact that differences in catalyst activity affected conversion rates of the linear octenes, it can be concluded that even this (fast) reaction is not completely limited by the rate external liquid-solid mass transfer. Contrary to the estimation of wetting efficiency, approximations of effective kinetic rate constants $k_{R1}$ and $k_{R2}$ are therefore needed to estimate mass transfer rates from conversion data. However, liquid-solid mass transfer coefficients should be independent of the reaction rates and be a function of liquid flow rate only, provided that all liquid and bed properties are constant and the effect of gas flow is negligible. For all experiments, the gas flow rate was very low, as can be seen in Figure 5.5. Most liquid-soled mass transfer correlations have the following functional relationship with the liquid flow rate:

$$k_{LS}a = k_0 Q^{k_1} \tag{5.10}$$

[4]Liquid-solid mass transfer measurements, for example, seem to be sensitive to the measurement method.

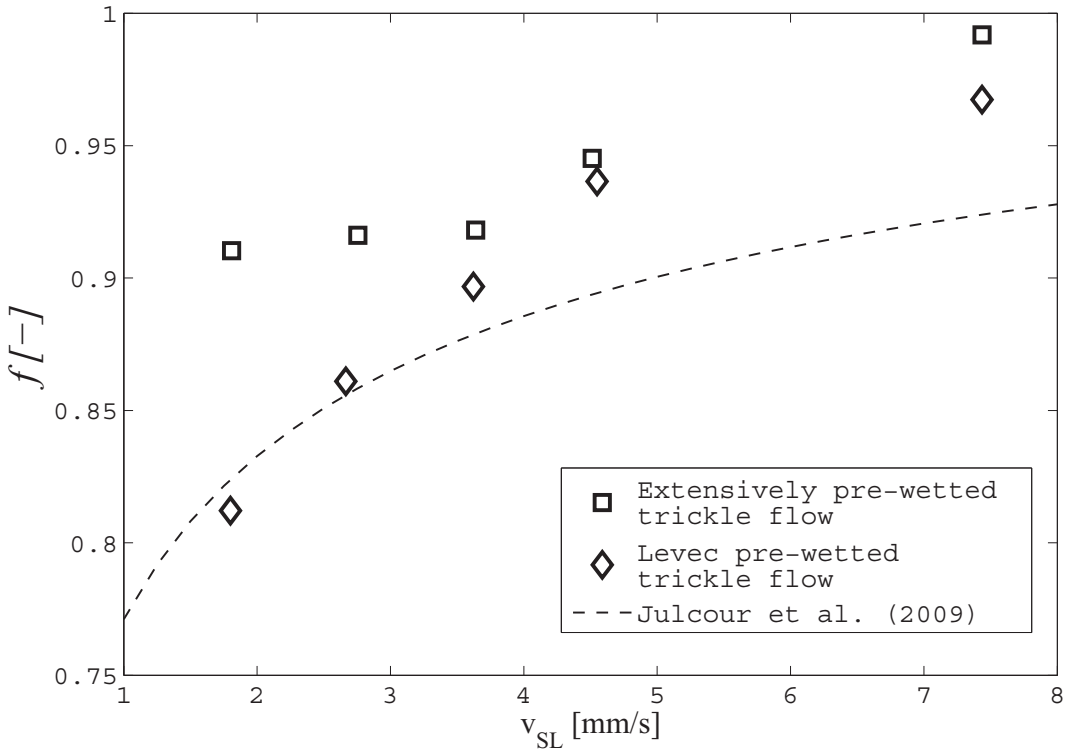


**Figure 5.13:** Averaged wetting efficiency for trickle flow operation as a function of liquid superficial velocity.

Based on this relationship, the apparent rate constant at a specific liquid flow rate in upflow operation will, according to Equation (5.4), be equal to:

$$k_{Tx,ij} = \frac{k_{Rx,i} k_0 Q_j^{k_1}}{k_{Rx,i} + k_0 Q_j^{k_1}} \tag{5.11}$$

Where $x$ = 1 for linear octene hydrogenation
$x$ = 2 for isooctene hydrogenation
$i$ refers to a specific experimental run
$j$ refers to the liquid flow rate

The coefficiencts $k_0$ and $k_1$ should be independent of the reaction rates, and the following function was minimised in order to obtain approximations of *(a)* kinetic rate constants for both reactions $x$ and all experimental datasets $i$, and *(b)* liquid-solid mass transfer for upflow operation as a function of liquid flow rate:

$$F = \sum_{xij} \left| X_{xij} + \exp\left( \frac{k_{Rx,i} k_0 Q_j^{k_1 - 1} . V_{cat}}{k_{Rx,i} + k_0 Q_j^{k_1}} \right) - 1 \right| \tag{5.12}$$

The minimisation of this function is an iterative procedure, where $k_{R,xi}$ is fitted onto conversion dataset $i$ specific to reaction $x$ with set values for $k_0$ and $k_1$ (1 parameter fitted to 10 datapoints), and $k_0$ and $k_1$ are fitted to all conversion datasets with $k_{R,xi}$ set for each dataset/reaction (2 parameters fitted to 100 datapoints). Figure 5.14 shows the datafits obtained with this procedure. The estimated values for $k_{R1}$ and $k_{R2}$ (based on catalyst volume), vary between 0.11 and 0.05, and 0.015 and 0.01 $s^{-1}$ respectively. These correspond to $1.2 \leq \eta \cdot k_{r1} \leq 0.55$ and $0.11 \leq \eta \cdot k_{r1} \leq 0.17$. For the isooctene hydrogenation, these values agree well with the batch experiments, since $\eta \approx 1/\phi_G$. The estimated higher limit of linear octene hydrogenation is much higher than the batch experiments suggest (the results from batch experiments correspond to the lower limit). Accurate estimations of very high kinetic rates for the determination of liquid-solid mass transfer are not too important, since the reaction will become more and more limited by external mass transfer rates.

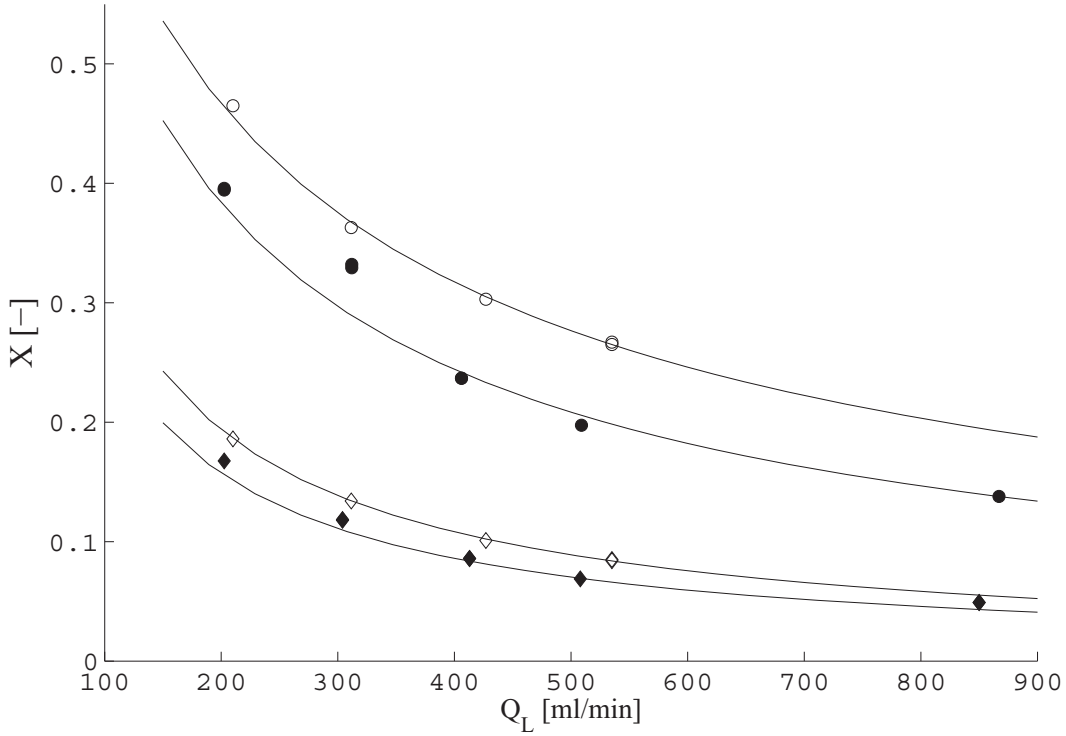


**Figure 5.14:** Fits of upflow conversion data obtained from minimising equation (5.12). The highest and lowest catalyst activity cases are shown.

Now that estimations of the effective kinetic rate constants are available, mass transfer coefficients can be calculated for all flow rates and operating modes by substituting Equation (5.7) into Equation (5.6):

$$k_{LS}a = \frac{k_{T1} - k_{T2}}{k_{T2}/k_{R2} - k_{T1}/k_{R1}} \tag{5.13}$$

With the wetting efficiency results from the previous section, it is also possible to calculate mass transfer coefficients directly with equation (5.6). Equation (5.13) is preferred, so that mass transfer rates can be calculated without making use of the wetting efficiency results. Liquid-solid mass transfer coefficients calculated with Equation (5.13) are independent of the wetting efficiency and an indication of the specific rate of mass transfer at any specific point in the bed. Most liquid-solid mass transfer studies in trickle-beds are based on either a dissolution (Sylvester and Pitayagulsarn, 1975; Dharwarkar and Sylvester, 1977; Specchia et al., 1978; Lakota and Levec, 1990) or an electrochemical method (Hirose et al., 1976; Chou et al., 1979; Sims et al., 1993; Latifi et al., 1997; Trivizadakis and Karabelas, 2006). These experimental methods lead to mass transfer coefficient measurements which include wetting efficiencies, i.e. usually $k_{LS} \times f$ is measured. To calculate $k_{LS} \times f$, one can once again use Equations (5.6) and (5.7) to find the following relationship:

$$k_{LS}a.f = \frac{k_{R1} - k_{R2}}{k_{R1}/k_{T1} - k_{R2}/k_{T2}} \tag{5.14}$$

For upflow where $f = 1$, Equation (5.13) and (5.14) should yield the same results, which can be used as a test whether the estimated reaction rate constants and the assumption that $f = 1$ in upflow operation are reasonable. That this is indeed the case is shown in Figure 5.15, which is a parity plot of upflow mass transfer rates calculated via equation (5.13) and via equation (5.14). Average wetting efficiency-based ($k_{LS}f$, Equation 5.14) and specific ($k_{LS}$, Equation 5.13) liquid-solid mass transfer coefficients for trickle-bed operation are shown in Figure 5.16. Overall, hydrodynamic multiplicity gave rise to about 10 - 20% variation in $k_{LS}f$. The correlations of Dharwarkar and Sylvester (1977) and Latifi et al. (1997) are also shown. The former was developed from a large database, while the latter is recommended by Dudukovic et al. (2002) for trickle-bed design purposes and was developed from electrochemical-based data. However, many correlations, especially those developed from dissolution data, predict liquid-solid mass transfer coefficients as much as ten times smaller than reported in the figure.

The multiplicity behaviour of liquid-solid mass transfer in trickle beds has previously been explained as a combined liquid holdup - wetting efficiency effect **?**: At a specific superficial liquid velocity, a low liquid holdup should enhance mass transfer due to higher interstitial liquid velocities. On the other hand, low wetting efficiencies should be detrimental for mass transfer. That liquid holdup (interstitial velocity) and wetting efficiency (area for mass transfer) are not the only hydrodynamic properties that influence mass transfer rates, is clear from the inset in Figure 5.16. Though the specific mass transfer coefficients in this subfigure are not affected by wetting efficiency, a marked difference between Levec and extensively pre-wetted beds still persists. The differences cannot be explained in terms of interstitial velocity, since the liquid holdup in a Levec pre-wetted bed is generally lower than in an extensively pre-wetted bed, resulting in higher inter-

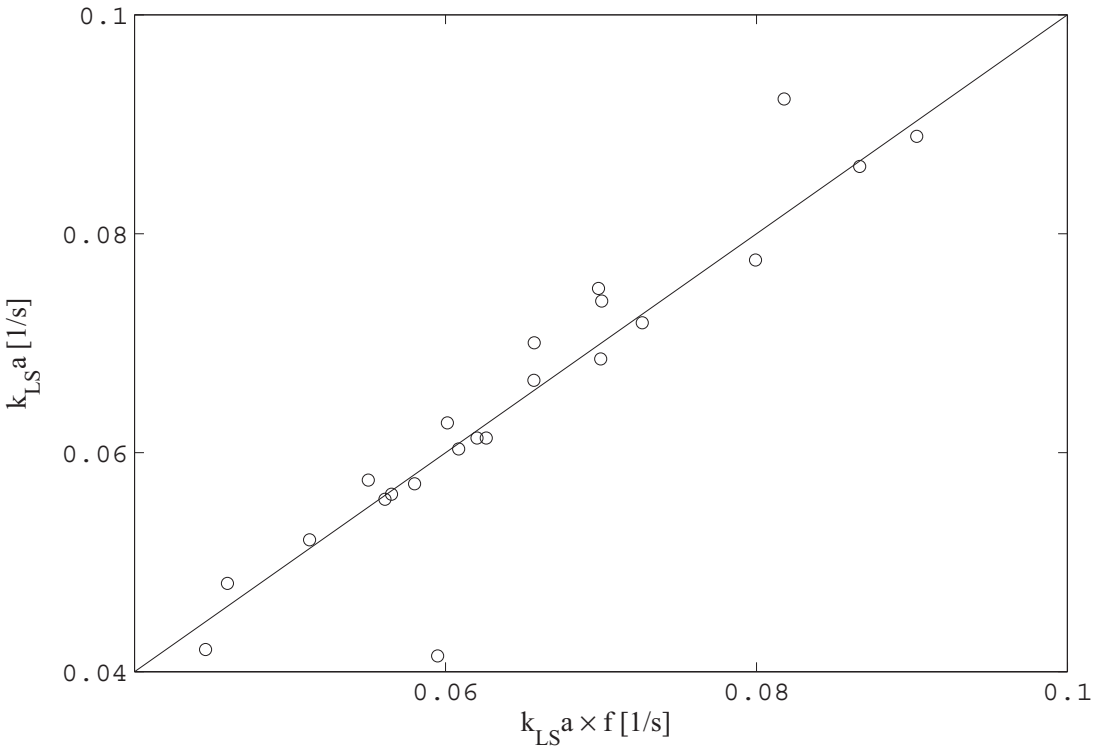


**Figure 5.15:** Parity plot for $k_{LS}a.f$ and $k_{LS}a$ for upflow operation. Good agreement confirms reasonability of estimated values for $k_{R1}$ and $k_{R2}$, and that $f_{upflow} = 1$.

stitial liquid velocities. Still, the mass transfer coefficients are lower and the observed multiplicity behaviour of liquid-solid mass transfer is therefore related to the differences in flow structure. Several studies of trickle-flow hydrdynamic muliplicity have been reported where these differences were observed (Kan and Greenfield, 1979; Lutran et al., 1991; Ravindra et al., 1997a; van der Merwe et al., 2007). The findings are also in accordance to the findings in Chapter 3.

Lastly, liquid-solid mass transfer in trickle-flow operation is compared to mass transfer in upflow operation in Figure 5.17. Liquid-solid mass transfer coefficients for upflow operation are 12 to 30% higher than for trickle-flow operation at the same superficial liquid velocity, confirming that some flow characteristics in the trickle flow regime are detrimental to the overall liquid-solid mass transfer rates.

## 5.4 Conclusions

By using a simple first-order reaction model for two reactions occurring in parallel, wetting efficiency could be measured in a pilot trickle-bed reactor without the need for a proper kinetic description of the reactions. Measurements were based on conversion data for linear and isooctene hydrogenation. On the basis of theoretical considerations, some general criteria could be given for a reaction system to be suitable for wetting

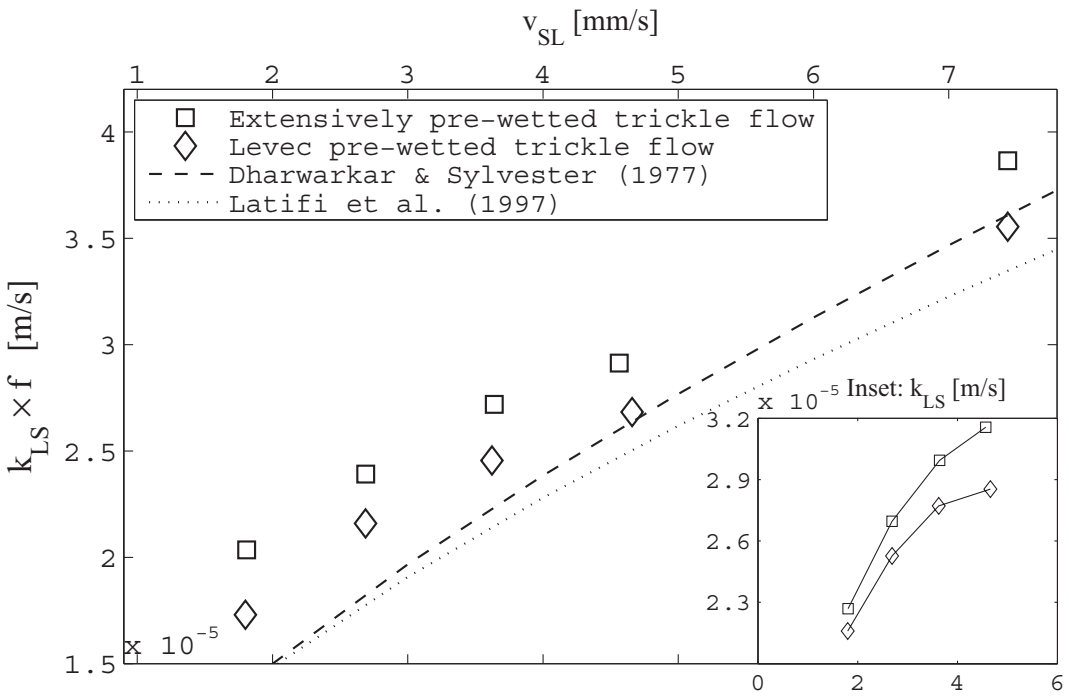


**Figure 5.16:** Averaged wetting efficiency-based liquid-solid mass transfer coefficients for trickle flow operation. Inset: Specific mass transfer coefficients.

efficiency measurements. With estimations of reaction rates, it was also possible to measure specific liquid-solid mass transfer coefficients, independently of the wetting efficiency measurements. The multiplicity behaviour of liquid-solid mass transfer coefficients suggests that different flow patterns exist that determine the characteristics of liquid-solid mass transfer in trickle flow, and that liquid-solid mass transfer cannot be simply related to interstitial liquid velocity. The multiplicity envelope shows up to 10% variation in wetting efficiency and 10% - 20% variation in mass transfer rates, both being higher for extensively pre-wetted beds. The results compare well with the colorimetric study in Chapter 3, the results of which also suggest different types of flow for Levec and extensively pre-wetted beds. Under liquid-limited conditions, upflow operation outperforms trickle flow operation at the same liquid flow rate, partly because of complete wetting, but also because of higher specific liquid-solid mass transfer coefficients.

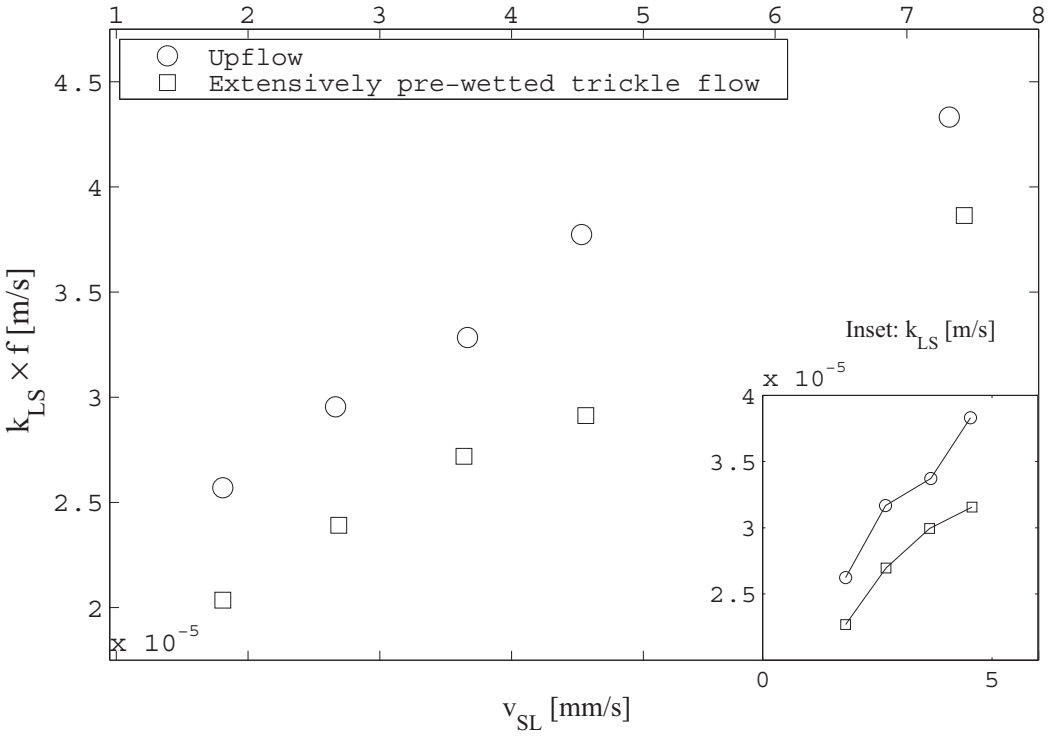


**Figure 5.17:** Comparison of liquid-solid mass transfer in trickle-flow and upflow operation. Inset: Specific mass transfer coefficents.

# Nomenclature

| | |
|---|---|
| $a$ | area per volume of catalyst particle, $^1/_{\mathrm{m}}$ |
| $Bi$ | Biot number for a sphere, $Bi' = \frac{k_{LS} r_p}{D_{eff}}$ |
| $Bi'$ | modified Biot number, $Bi' = \frac{k_{LS} V_R}{S_P D_{eff}}$ |
| $D_{eff}$ | liquid reagent effective diffusivity, $^{\mathrm{m}^2}/_{\mathrm{s}}$ |
| $D$ | molecular diffusivity, $^{\mathrm{m}^2}/_{\mathrm{s}}$ |
| $d_p$ | catalyst pellet diameter, m |
| $f$ | wetting efficiency, dimensionless |
| $k_0$ | fitting constant for approximation of upflow external liquid-solid mass transfer |
| $k_r$ | first-order reaction rate constant based on shell volume, $\mathrm{s}^{-1}$ |
| $k_R$ | first-order reaction rate constant based on catalyst volume, $\mathrm{s}^{-1}$ |
| $k_T$ | apparent first order reaction rate constant based on catalyst volume, $\mathrm{s}^{-1}$ |
| $k_{LS}$ | liquid-solid mass transfer coefficient, $^{\mathrm{m}}/_{\mathrm{s}}$ |
| $m_{cat}$ | mass of catalyst particles in reactor, kg |
| $Q_L$ | liquid volumetric flow rate, $^{\mathrm{m}^3}/_{\mathrm{s}}$ ($^{\mathrm{ml}}/_{\mathrm{min}}$ in figures) |
| $S_P$ | pellet external area, $\mathrm{m}^2$ |
| $V_{cat}$ | volume of catalyst in reactor, $\mathrm{m}^3$ |
| $V_R$ | catalyst shell volume for an egghell catalyst, $\mathrm{m}^3$ |
| $v_{Si}$ | superficial velocity of i-phase $v_{Si} = \frac{Q_i}{A_c}$, $^{\mathrm{m}}/_{\mathrm{s}}$ |
| $X$ | conversion, dimensionless |
| $z$ | depth in reactor measured from top inlet, mm |

*Greek letters*

| | |
|---|---|
| $\phi_G$ | Generalised (Aris) modulus, $\phi_G = \frac{V_R}{S_p}\sqrt{\frac{k_r}{D_{eff}}}$ |
| $\eta$ | pellet efficiency factor, dimensionless |
| $\eta_0$ | overall efficiency factor, dimensionless |
| $\rho_{cat}$ | catalyst particle density, $^{\mathrm{kg}}/_{\mathrm{m}^3}$ |

*Subscripts*

| | |
|---|---|
| 1 | refers to faster reaction |
| 2 | refers to slower reaction |
| i | refers to specific experimental run with stable catalyst |
| j | refers to specific flow rate |
| x | refers to specific reaction, either 1 or 2 |

# CHAPTER 6

# CLOSING REMARKS

Wetting efficiency and liquid-solid mass transfer effects in trickle-bed reactors were studied at three different levels. Fractional wetting in a TBR was characterized on a bed and particle scale in a non-reactive $N_2$-water experimental study, making use of colorimetry. The study illustrates multiplicity effects in terms of flow morphology and subsequently wetting efficiency, using particle-scale wetting distributions. These results correspond well with another study on wetting efficiency and liquid-solid mass transfer, performed in a high-pressure pilot trickle-bed reactor. Here, it was also found that pre-wetting had a major effect on partial wetting, while liquid-solid mass transfer results suggest different types of flow for the two boundaries of hydrodynamic multiplicity in pre-wetted trickle-bed reactors.

Liquid-solid contacting was also investigated at a particle-scale level. The wetting geometries obtained from the colorimetric study were used to investigate the effects of partial wetting on intraparticle diffusion, using FEM simulation. With FEM simulations, it is possible to study intraparticle diffusion and reaction using the fundamental description of this process. Using realistic geometries for partial wetting, realistic data could be generated regarding wetting efficiency and intraparticle diffusion. These data were used for simplified theoretical decriptions of liquid-solid contacting effects on a particle-scale level, which aided in the experimental planning of a reactive method for the measurement of wetting efficiency.

An important reason to study liquid-solid contacting from different angles, was to link hydrodynamic observations and theory to gain a sense of what to expect from a reactor under trickle-flow conditions. Though integrated to some degree and corresponding well with each other, the overall study leaves much scope for further investigation into how liquid flow morphology influences transfer processes in a trickle-bed reactor. For example, only the simple case of strong internal diffusion limitations under liquid-limited

conditions was considered in a reactor study, while many of the ideas from the study of intraparticle diffusion and reaction were left unexplored. A typical continuation of the reactor study would be to explore reactor behaviour over a large $\gamma$-range. For this reason, a preliminary study was performed under gas-limited conditions. Though some agreement was found with the work in the body of this report, unexpected behaviour was also found. For example, the liquid-solid mass transfer results from the liquid-limited study did not correspond to observed rates in the reactor or even with existing liquid-solid and gas-liquid mass transfer correlations. The study was not presented in the main body of this thesis, since it consists of limited data which would not suffice for a clear understanding of the reactor, but is reported in Appendix B. Though the work presented in this thesis elucidates liquid-solid contacting effects in gas-liquid packed bed reactors to some extent, this study is yet another indication that there is still room for improvement in the understanding of these reactors.

More specific contributions of this work include the following:

- Presentation of the distribution of particle wetting of a packed bed under different conditions in the multplicity envelope of trickle flow. This may help explain multiplicity behaviour of trickle-bed reactors.

- An easy-to-use model which can be used to model simultaneous rate-limiting behaviour of both volatile and non-volatile reagents in a trickle-bed reactor.

- A description for partial wetting effects on eggshell catalysts and the illustration that these differ from monodispersed catalysts.

- The development and implication of a wetting efficiency measurement method without the need of kinetic descriptions or estimations of external mass transfer.

- Estimation of wetting efficiency and liquid-solid mass transfer multiplicity behaviour under high-pressure reaction conditions relevant to industry.

# BIBLIOGRAPHY

M. H. Al-Dahhan and M. P. Dudukovic (1995). Catalyst wetting efficiency in Trickle-bed reactors at high pressure. *Chemical Engineering Science*, 50:2377.

R. Aris (1957). On shape factors for irregular particles-1. The steady state problem. Diffusion and reaction. *Chemical Engineering Science*, 6:262.

M. Banchero, L. Manna, S. Sicardi, J. Boelhouwer, M. Urseanu, and G. Kwant (2004). Conversion rate and mass transfer limitation in trickle bed reactors in the presence of a fast reaction. *Chemical Engineering Science*, 59:5411.

L. Baussaron, C. Julcour-Lebigue, A. Wilhelm, C. Boyer, and H. Delmas (2007). Partial Wetting in Trickle Bed Reactors: Measurement Techniques and Global Wetting Efficiency. *Industrial & Engineering Chemistry Research*, 46:8397.

E. G. Beaudry, M. P. Dudukovic, and P. L. Mills (1987). Trickle-bed Reactors: Liquid diffusional effects in a gas-limited reaction. *AIChE Journal*, 33:1435.

K. B. Bischoff (1965). Effectiveness factors for general reaction rate forms. *AIChE Journal*, 11:351.

J. G. Boelhouwer, H. W. Piepers, and A. A. H. Drinkenburg (2002). Nature and characteristics of pulsing flow in trickle-bed reactors. *Chemical Engineering Science*, 57:4865.

A. Burghardt, G. Bartelmus, M. Jaroszynski, and A. Kolodziej (1995). Hydrodynamics and mass transfer in a three-phase fixed-bed reactor with cocurrent gas-liquid downflow. *The Chemical Engineering Journal*, 58:83.

A. Burghardt and A. Kubaczka (1996). Generalization of the effectiveness factor for any shape of a catalyst pellet. *Chemical Engineering and Processing*, 35:65.

R. V. Chaudhari, R. Jaganathan, S. P. Mathew, C. Julcour, and H. Delmas (2002). Hydrogenation of 1,5,9-cyclododecatriene in fixed-bed reactors: Down- vs. upflow Modes. *AIChE Journal*, 48:110.

T. S. Chou, F. L. Worley, and D. Luss (1979). Local particle-liquid Mass Transfer Fluctuations in mixed-phase Cocurrent Downflow through a Fixed Bed in the Pulsing Regime. *Industrial & Engineering Chemistry Fundamentals*, 18:279.

G. Christensen, S. G. McGovern, and G. Sudaresan (1986). Cocurrent downflow of air and water in a two-dimensional packed column. *AIChE Journal*, 32:1677.

A. J. Colombo, G. Baldi, and S. Sicardi (1976). Solid-liquid contacting effectiveness in trickle-bed reactors. *Chemical Engineering Science*, 31:1101.

R. D. Cook, D. S. Malkus, and M. E. Plesha (1989). *Concepts and Applications of Finite Element Analysis*. Wiley, New York, 3rd ed., international ed edition.

A. de Klerk (2008). Hydroprocessing peculiarities of Fischer-Tropsch syncrude. *Catalysis Today*, 130:439.

A. Dharwarkar and N. Sylvester (1977). Liquid-solid mass transfer in trickle beds. *AIChE Journal*, 23:377.

M. P. Dudukovic (1977). Catalyst effectiveness factor and contacting efficiency in trickle-bed reactors. *AIChE Journal*, 23:940.

M. P. Dudukovic, F. Larachi, and P. L. Mills (2002). Multiphase catalystic reactors: A perspective on current knowledge and future trends. *Catalysis Reviews*, 44:123.

L. J. Florusse, C. J. Peters, J. C. Pamies, L. F. Vega, and H. Meijer (2003). Solubility of Hydrogen in Heavy n-Alkanes: Experiments and SAFT Modeling. *AIChE Journal*, 49:3260.

S. Fukushima and K. Kusaka (1977). Interfacial area and boundary of hydrodynamic flow regions in packed columns with cocurrent downflow. *Journal of Chemical Engineering Japan*, 10:461.

A. Gianetto and V. Specchia (1992). Trickle-bed reactors: State of art and perspectives. *Chemical Engineering Science*, 47:3197.

D. Gonzalez-Mendizabal, M. E. Aguilera, and F. Pironti (1998). Solid-liquid mass transfer and wetting factors in trickle bed reactors: effect of the type of solid phase and the presence of chemical reaction. *Chemical Engineering Communication*, 169:35.

S. Goto, A. Lakota, and J. Levec (1981). Effectiveness factors of nth order kinetics in trickle-bed reactors. *Chemical Engineering Science*, 36:157.

S. Goto, J. Levec, and J. M. Smith (1975). Mass transfer in packed beds with two-phase flow. *Industrial Engineering Process Design and Development*, 14:473.

S. Goto and K. Mabuchi (1984). Oxidation of ethanol in gas-liquid cocurrent upflow and downflow reactors. *Canadian Journal of Chemical Engineering*, 62:865.

P. R. Gunjal and V. V. Ranade (2007). Modeling of laboratory and commercial scale hydro-processing reactors using CFD. *Chemical Engineering Science*, 62:5512.

M. Hartman and R. W. Couglin (1972). Oxidation of SO2 in a trickle-bed reactor packed with carbon. *Chemical Engineering Science*, 27:867.

H. C. Henry and J. B. Gilbert (1973). Scale Up of Pilot Plant Data for Catalytic Hydroprocessing. *Industrial Engineering Chemistry Process Design and Development*, 12:328.

M. Herskowitz, R. G. Carbonell, and J. M. Smith (1979). Effectiveness factors and Mass Transfer in Trickle-bed reactors. *AIChE Journal*, 25:272.

M. Herskowitz and S. Mosseri (1983). Global rates of reaction in trickle-bed reactors: effects of gas and liquid flow rates. *Industrial & Engineering Chemistry Fundamentals*, 22:4.

W. Highfill and M. Al-Dahhan (2001). Liquid-Solid Mass Transfer Coefficient in High Pressure Trickle Bed Reactors. *Chemical Engineering Research and Design*, 79:631.

T. Hirose, Y. Mori, and Y. Sato (1976). Liquid to particle mass transfer in fixed bed reactor with cocurrent gas-liquid downflow. *Journal of Chemical Engineering of Japan*, 9:220.

I. Iliuta and F. Larachi (1999). The generalized slit model: Pressure gradient, liquid holdup & wetting efficiency in gas-liquid trickle flow. *Chemical Engineering Science*, 54:5039.

I. Iliuta, F. Larachi, B. Grandjean, and G. Wild (1999). Gas liquid interfacial mass transfer in trickle-bed reactors: state of the art correlations. *Chemical Engineering Science*, 54:5633.

C. Julcour-Lebigue, L. Baussaron, H. Delmas, and A. Wilhelm (2007). Theoretical analysis of tracer method for the measurement of wetting efficiency. *Chemical Engineering Science*, 62:5374.

C. Julcour-Lebique, F. Augier, H. Maffre, A. Wilhelm, and H. Delmas (2009). Measurements and modeling of wetting efficiency in trickle-bed reactors: liquid viscosity and bed packing effects. *Submitted to Industrial Engineering Chemistry Research, manuscript ID: ie-2009-002443.*

K. M. Kan and P. F. Greenfield (1978). Multiple hydrodynamics states in cocurrent two-phase downflow through packed beds. *Industrial Engineering Chenistry Process Design and Development*, 17:482.

K. M. Kan and P. F. Greenfield (1979). Pressure Drop and Holdup in Two-Phase Cocurrent Trickle Flows through Beds of Small Packings. *Industrial Engineering Chemistry Process Design and Development*, 18:740.

J. Kendall (1917). The viscosity of liquids. II. The viscosity-composition curve for ideal liquid mixtures. *Journal of the American Chemical Society*, 39:1787.

M. R. Khadilkar, P. L. Mills, and M. P. Dudukovic (1999). Trickle-bed reactor models for systems with a volatile liquid phase. *Chemical Engineering Science*, 54:2421.

M. R. Khadilkar, Y. X. Wu, M. H. Al-Dahhan, and M. P. Dudukovic (1996). Comparison of trickle-bed and upflow reactor performance at high pressure: Model predictions and experimental observations. *Chemical Engineering Science*, 51:2139.

V. A. Kirillov and I. V. Koptyug (2005). Critical Phenomena in Trickle-Bed Reactors. *Industrial & Engineering Chemistry Research*, 44:9727.

J. Klassen and R. S. Kirk (1955). Kinetics of the liquid-phase oxidation of ethanol. *AIChE Journal*, 1:488.

Z. V. Kuzeljevic, W. van der Merwe, M. H. Al-Dahhan, M. P. Dudukovic, and W. Nicol (2008). Effect of Operating Pressure on the Extent of Hysteresis in a Trickle Bed Reactor. *Industrial & Engineering Chemistry Research*, 47:7593.

A. Lakota and J. Levec (1990). Solid-liquid mass transfer in packed beds with concurrent downward two-phase flow. *AIChe Journal*, 36:1444.

K. Lappalainen, V. Alopaeus, M. Manninen, and J. Aittamaa (2008). Improved Hydrodynamic Model for Wetting Efficiency, Pressure Drop, and Liquid Holdup in Trickle-Bed Reactors. *Industrial & Engineering Chemistry Research*, 47:8436.

F. Larachi (2005). Catalytic wet oxidation: micro- meso- macro- methodology from catalyst synthesis to reactor design. *Topics in Catalysis*, 33:109.

F. Larachi, L. Belfares, and B. P. A. Grandjean (2001). Prediction of liquid-solid contacting efficiency in trickle flow reactors. *Int. Comm. Heat Mass Transfer*, 28:595.

F. Larachi, I. Iliuta, M. Chen, and B. P. A. Grandjean (1999). Onset of pulsing in trickle beds: Evaluation of current tools and state-of-the-art correlation. *Canadian Journal of Chemical Engineering*, 77:751.

M. A. Latifi, A. Laurent, and A. Storck (1988). Liquidsolid mass transfer in a packed bed with downward cocurrent gasliquid flow: An organic liquid phase with high Schmidt number. *The Chemical Engineering Journal*, 38:47.

M. A. Latifi, A. Naderifar, and N. Midoux (1997). Experimental investigation of the liquid/solid mass transfer at the wall of a trickle-bed reactor: influence of Schmidt number. *Chemical Engineering Science*, 52:4005.

C. L. Lazzaroni, H. R. Kesselman, and H. S. Figoli (1988). Colorimetric evaluation of efficiency of liquid-solid contacting in trickle-bed reactors. *Industrial Engineering Chemistry*, 27:1132.

J. Lee and D. H. Kim (2006). An approximation method for the effectiveness factor in porous catalysts. *Chemical Engineering Science*, 61:5127.

P. C. Leung, F. Recasens, and J. M. Smith (1987). Hydration of isobutene in a Trickle-bed Reactor: Wetting Efficiency and Mass Transfer. *AIChe Journal*, 33:996.

J. Levec and J. Smith (1976). Oxidation of acetic acid solutions in a trickle bed reactor. *AIChE Journal*, 22:159.

O. Levenspiel (2006). *Elements of chemical reaction engineering*, chapter 12, 815. Prentice Hall, Boston, fourth edition.

J. J. Llano, R. Rosal, H. Sastre, and F. V. Diez (1997). Determination of Wetting Efficiency in Trickle-Bed Reactors by a Reaction Method. *Industrial Engineering Chemistry Research*, 36:2616.

D. Loudon, W. van der Merwe, and W. Nicol (2006). Multiple hydrodynamic states in trickle flow: Quantifying the extent of pressure drop, liquid holdup and gas-liquid mass transfer variation. *Chemical Engineering Science*, 61:7551.

P. G. Lutran, K. M. Ng, and E. P. Delikat (1991). Liquid distribution in trickle-beds. An experimental study using computer-assisted tomography. *Industrial Engineering Chemistry Research*, 30:1270.

A. L. Marquez, C. Nguyen, S. Poncin, G. Wild, and N. Midoux (1994). A novel hydrazine oxidation technique for the determination ofkLa in gasliquid and gasliquidsolid reactors. *Chemical Engineering Science*, 49:5667.

A. Mata and J. M. Smith (1981). Transport processes in multiphase reaction systems. *AIChE Symposium Series*, 29–35.

D. E. Mears (1971). The role of axial dispersion in trickle-flow laboratory reactions. *Chemical Engineering Science*, 26:1361.

D. E. Mears (1974). The role of liquid holdup and effective wetting in the performance of trickle-bed reactors. *Adv. Chem. Ser.*, 218–220.

P. L. Mills and M. P. Dudukovic (1979). A Dual-series solution for the effectiveness factor of partially wetted catalysts in trickle-bed reactors. *Industrial Engineering Chemisrty Fundamentals*, 18:139.

P. L. Mills and M. P. Dudukovic (1981). Evaluation of liquid-solid contacting in trickle-beds by tracer methods. *AIChE Journal*, 27:893.

P. L. Mills, S. Lai, M. P. Dudukovic, and P. A. Ramachandran (1988). A numerical study of approximation methods for solution of linear and nonlinear diffusion-reaction equations with discontinuous boundary conditions. *Computers & Chemical Engineering*, 12:37.

A. K. Mogalicherla, G. Sharma, and D. Kunzru (2009). Estimation of Wetting Efficiency in Trickle-Bed Reactors for Nonlinear Kinetics. *Industrial & Engineering Chemistry Research*, 48:1443.

S. Morita and J. M. Smith (1978). Mass Transfer and contacting efficiency in a Trickle-bed reactor. *Industrial Engineering Chemistry Fundamentals*, 17:113.

K. Onda, H. Takeuchi, and Y. Kayama (1967). Effect of packing materials on wetted surface area. *K. Kagaku Kogaku*, 31:126.

P. Persson and G. Strang (2004). A Simple Mesh Generator in MATLAB. *SIAM Review*, 46:329.

F. Pironti, D. Mizrahi, A. Acosta, and D. Gonzalez-Mendizabal (1999). Liquid-solid wetting factor in trickle-bed reactors: its determination by a physical method. *Chemical Engineering Science*, 54:3793.

S. S. Puranik and V. Vogelpohl (1974). Effective interfacial area irrigated packed columns. *Chemical Engineering Science*, 29:501.

P. A. Ramachandran (1991). Boundary integral element method for linear diffusionreaction problems with discontinuous boundary conditions. *The Chemical Engineering Journal*, 47:169.

P. A. Ramachandran, M. P. Dudukovic, and P. L. Mills (1986). A new model for assessment of external liquid-solid contacting in trickle-bed reactors from tracer response measurements. *Chemical Engineering Science*, 41:855.

P. A. Ramachandran and J. M. Smith (1979). Effectiveness factors in Trickle-bed Reactors. *AIChe Journal*, 25:538.

P. V. Ravindra, D. P. Rao, and M. S. Rao (1997a). Liquid Flow texture in trickle-bed reactors: An experimental study. *Industrial Engineering Chemistry Research*, 36:5133.

P. V. Ravindra, D. P. Rao, and M. S. Rao (1997b). A Model for the Oxidation of Sulfur Dioxide in a trickle-bed Reactor. *Industrial & Engineering Chemistry Research*, 36:5125.

C. M. Ruecker and A. Ackgerman (1987). Determination at wetting efficiencies for a trickle-bed reactor at high temperature and pressure. *Industrial Engineering Chemistry Research*, 26:164.

C. N. Satterfield (1975). Trickle-bed reactors. *AIChe Journal*, 21:209.

C. N. Satterfield, A. A. Pellossof, and T. K. Sherwood (1969). Mass transfer limitations in a trickle-bed reactor. *AIChE Journal*, 15:226.

T. G. Schwartz, E. Wegwe, and M. P. Dudukovic (1976). A new tracer method for determination of liquid-solid contacting effectiveness in trickle-bed reactors. *AIChE Journal*, 22:894.

A. J. Sederman and L. F. Gladden (2001). Magnetic resonance imaging as a quantitative probe of gas-liquid distribution and wetting efficiency in trickle-bed reactors. *Chemical Engineering Science*, 56:2615.

W. Sedriks and C. N. Kenney (1972). Partial wetting in trickle-bed reactors: the reduction of crotonaldehyde over a palladium catalyst. *Chemical Engineering Science*, 28:559.

S. Sie and R. Krishna (1998). Process development and scale up: III. Scale-up and scale-down of trickle bed processes. *Reviews in Chemical Engineering*, 14:203.

W. B. Sims, F. G. Schulz, and D. Luss (1993). Solid-liquid mass transfer to hollow pellets in a trickle bed. *Industrial & Engineering Chemistry Research*, 32:1895.

V. Specchia, G. Baldi, and A. Gianetto (1978). Solid-liquid mass transfer in cocurrent two-phase flow through packed beds. *Industrial Engineering Chemistry Design and Development*, 17:362.

S. Sugden (1924). A relation between surface tension, density, and chemical composition. *Journal of the Chemical Society Transactions*, 125:1177.

N. Sylvester and P. Pitayagulsarn (1975). Mass transfer for two-phase cocurrent downflow in a packed bed. *Industrial Engineering Chemistry Process Design and Development*, 14:421.

M. Trivizadakis and A. Karabelas (2006). A study of local liquid/solid mass transfer in packed beds under trickling and induced pulsing flow. *Chemical Engineering Science*, 61:7684.

G. Valerius, X. Zhu, and H. Hofmann (1996a). Modelling of a trickle-bed reactor I. Extended definitions and new approximations. *Chemical Engineering and Processing*, 35:1.

G. Valerius, X. Zhu, H. Hofmann, D. Arntz, and T. Haas (1996b). Modelling of a trickle-bed reactor II. The hydrogenation of 3-hydroxypropanal to 1,3-propanediol. *Chemical Engineering and Processing*, 11–19.

W. van der Merwe (2008). *Trickle flow hydrodynamic multiplicity*. Ph.D. thesis, University of Pretoria.

W. van der Merwe and W. Nicol (2005). Characterization of Multiple Flow Morphologies within the Trickle Flow Regime. *Industrial Engineering Chemistry Research*, ASAP Article.

W. van der Merwe and W. Nicol (2009). Trickle flow hydrodynamic multiplicity: Experimental observations and pore-scale capillary mechanism. *Chemical Engineering Science*, 64:1267.

W. van der Merwe, W. Nicol, and M. Al-Dahhan (2008). Effect of hydrodynamic multiplicity on trickle bed reactor performance. *AIChE Journal*, 54:249.

W. van der Merwe, W. Nicol, and F. de Beer (2007). Trickle flow distribution and stability by X-ray radiography. *Chemical Engineering Journal*, 132:47.

A. van Houwelingen, C. Sandrock, and W. Nicol (2006). Particle Wetting Distribution in Trickle-Bed Reactors. *AIChE Journal*, 52:3532.

A. van Houwelingen, W. van der Merwe, and W. Nicol (2007). Extension of liquid-limited trickle-bed reactor modelling to incorporate channelling effects. *Chemical Engineering Science*, 62:5543.

D. van Velzen, R. Cardozo, and H. Langenkamp (1972). A liquid viscosity-temperature-chemical constitution relation for organic compounds. Industrial Engineering Chemistry Fundamentals. *Industrial Engineering Chemistry Fundamentals*, 11:20.

C. Wilke and P. Chang (1955). Correlation of diffusion coefficients in dilute solutions. *AIChE Journal*, 1:264.

Y. Wu, M. A. Al-Dahhan, M. R. Khadilkar, and M. P. Dudukovic (1996). Evaluation of trickle-bed reactor models for a liquid limited reaction. *Chemical Engineering Science*, 51:2721.

I. V. Yentekakis and C. G. Vayenas (1987). Effectiveness factors for reactions between volatile and non-volatile components in partially wetted catalysts. *Chemical Engineering Science*, 42:1323.

S. P. Zimmerman and K. M. Ng (1986). Liquid distribution in Trickling flow trickle-bed reactors. *Chemical Engineering Science*, 41:861.

# APPENDIX A

## DERIVATION OF EQUATION 4-24

This appendix uses the same notation as Chapter 4. For a sphere with symmetrical boundary conditions, the diffusion-reaction equations for an elementary A + B → C reaction are:

$$\frac{d^2a}{d\rho^2}+\frac{2}{\rho}\frac{da}{d\rho}-\frac{k_r r_p^2 C_{B,bulk}}{D_A}a\cdot b=0$$

$$\frac{d^2b}{d\rho^2}+\frac{2}{\rho}\frac{db}{d\rho}-\frac{k_r r_p^2 C_{A,bulk}}{D_B}a\cdot b=0$$

$$\text{If } \gamma=\frac{\phi_A^2}{\phi_B^2}$$

$$\frac{d^2a}{d\rho^2}+\frac{2}{\rho}\frac{da}{d\rho}-\gamma\phi_B^2 a\cdot b=0$$

$$\frac{d^2b}{d\rho^2}+\frac{2}{\rho}\frac{db}{d\rho}-\phi_B^2 a\cdot b=0$$

$$\therefore \frac{d^2a}{d\rho^2}+\frac{2}{\rho}\frac{da}{d\rho}=\gamma\left(\frac{d^2b}{d\rho^2}+\frac{2}{\rho}\frac{db}{d\rho}\right) \tag{A.1}$$

$$\text{And } \frac{d^2}{d\rho^2}(\gamma\cdot b-a)=\frac{2}{\rho}\frac{d}{d\rho}(a-\gamma\cdot b)$$

$$\text{Let } \Theta=a-\gamma\cdot b$$

$$\text{Then: } \frac{d^2\Theta}{d\rho^2}+\frac{2}{\rho}\frac{d\Theta}{d\rho}=0 \tag{A.2}$$

$$\begin{aligned}
\text{Let } y &= \Theta\rho \\
\text{It can be shown that: } \frac{d^2y}{d\rho} &= 0 \\
\therefore y(\rho) &= k_1\rho + k_2 \\
\Theta(\rho) &= k_1 + \frac{k_2}{\rho}
\end{aligned} \tag{A.3}$$

$$\begin{aligned}
\text{Since } \Theta \text{ is finite at } \rho = 0\text{:} \\
\Theta(\rho) &= k_1 \\
\text{At } \rho = 1,\ a = 1 \text{ and } b = 1\text{:} \\
\therefore k_1 &= 1 - \gamma \\
\therefore a - \gamma b &= 1 - \gamma \\
\text{And } b &= \frac{a - 1 + \gamma}{\gamma}
\end{aligned} \tag{A.4}$$

The same relationship can be derived for an infinite slab.

# APPENDIX B

# HYDROGENATION OF LINEAR OCTENE UNDER GAS-LIMITED CONDITIONS

Many trickle-bed reactor studies under gas-limited conditions are reported in the literature. In terms of wetting efficiency, many of these are based on the additive procedure as shown in Chapter 2. In Chapter 4, it is shown that, especially for eggshell catalysts, gas-limited reactions may be subject to limitations of the liquid reagent even when a reaction is generally considered as gas-limited. A preliminary study on the hydrogenation of linear octenes under gas-limited conditions is reported here.

**Reaction system and operating conditions.** The experimental procedure followed is exactly the same as that described in Chapter 5, except for the reaction system and operating conditions. In order to operate under gas-limited conditions, reactor operating pressures were kept low. For all liquid flow rates, a gas feed mixture of 85% $N_2$ and 15% $H_2$ was fed to the reactor, operating at a pressure of 6 bar and a temperature of 60 °C. At these conditions, the liquid reagent can still be regarded as non-volatile. Relevant propertie other than those reported in Chapter 5 are listed in Table B.1. The total gas flow rate was 10 $^{nL}/_{min}$ for all liquid flow rates, corresponding to a superficial gas velocity $v_{SG}$ =17 $^{mm}/_{s}$. The liquid feed contained 8%(v/v) linear octenes and no isooctenes. Under these conditions, $\gamma \approx 40$.

The reactor was packed with 110 g catalyst, corresponding to a bed height of approximately 9 cm, between two layers of inert support. Startup and operation were exactly the same as in the previous chapter. Experiments were conducted for $v_{SL}$ = 1.9, 2.7, 3.8 and 4.7 $^{mm}/_{s}$. Only two repeat runs were performed.

**Table B.1:** Hydrogen property estimations

| Property | Estimated value | Estimation method |
|---|---|---|
| Saturated $H_2$ concentration in solvent | $3.25\ ^{mol}/_{m^3}$ | Florusse et al. (2003) |
| Hydrogen molecular diffusivity in solvent | $4.5 \times 10^{-9}\ ^{m^2}/_{s}$ | Wilke-Chang |

**Experimental results.** Overall reaction rates are reported in Figure B.1. Since all conversions were less than 10%, the reactor was regarded as a differential reactor. Reaction rates are unexpectedly high, and upflow reaction rates can not be explained with the liquid-solid mass transfer results from Chapter 5, and especially not if considered that overall hydrogen-to-catalyst surface mass transfer is also affected by gas-liquid mass transfer. Therefore, it was not possible to use upflow rate data as a basis for the treatment of trickle-flow data, as was done in Chapter 5, and only the general trends will be discussed. The trends reported in Figure B.1 also seem counterintuitive to some extent.

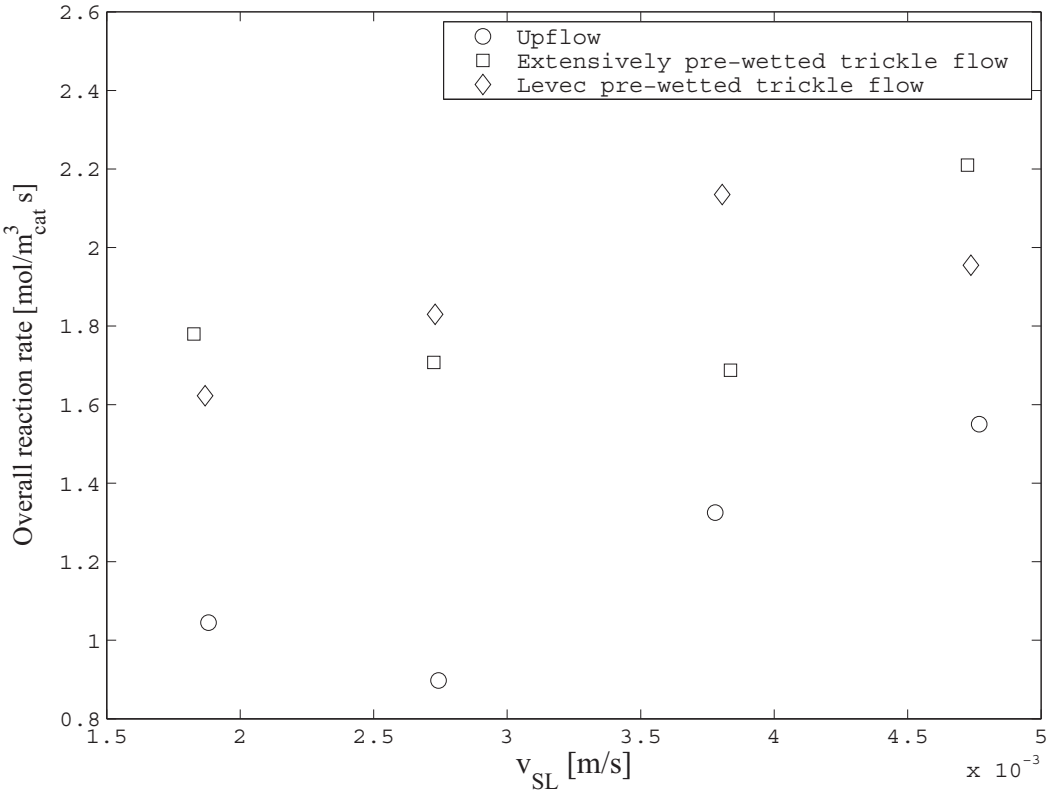


**Figure B.1:** Overall reaction rates of linear octene hydrogenation under gas-limited conditions.

As expected, downflow outperforms upflow, but any other enhancement effects due to partial wetting seem to be low, or even non-existent. The reaction rates for Levec and extensively pre-wetted flow are more or less the same and reaction rate does not increase (notably) with a decrease in liquid flow rate as is reported for so many of the reactor

studies discussed in the literature review[1]. A possible explanation might be the combination of liquid-limited effects in eggshell particles and the distribution of particle wetting due to flow morphology. Figure B.2 shows a rough approximation of overall trickle-bed efficiency (based on particle wetting distribution) for the best and least wetted cases in the colorimetric study as a function of $\phi_A$ when $\gamma = 40$, using the unified model for eggshell particles. Biot numbers are roughly based on liquid-solid mass transfer results from Chapter 5: experimental $k_{LS}$-values for octene at the relevant flow rate and pre-wetting conditions were adapted for hydrogen and then halved to allow for gas-liquid mass transfer resistance. It is clear from the figure that it is definitely possible that Levec pre-wetted beds do not outperform extensively pre-wetted beds, or even exhibit lower overall rates of reaction.

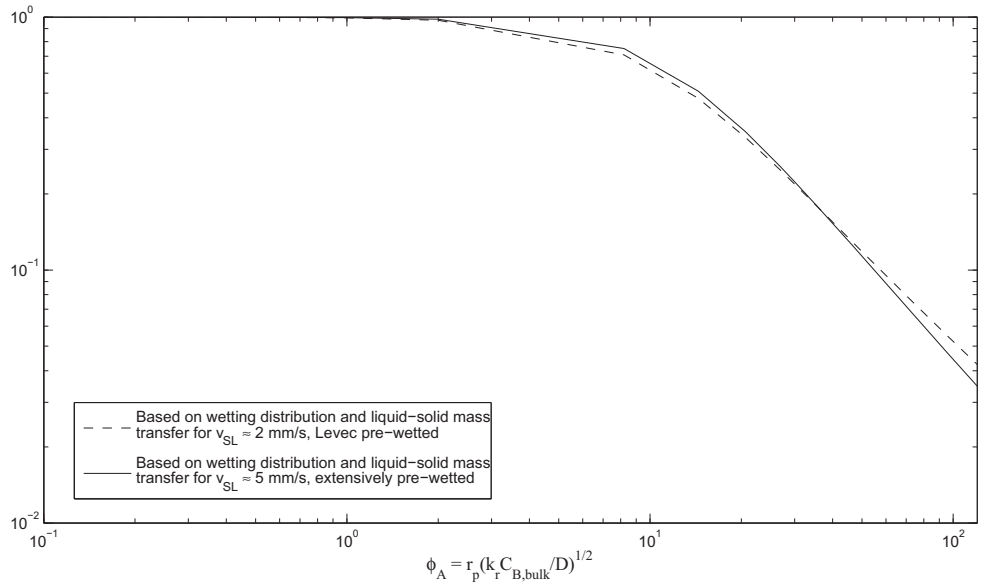


**Figure B.2:** Approximations of overall efficiency at boundaries of the colorimetric and liquid-limited reactor investigations for the current system, as a function of the Thiele modulus of the gaseous reagent.

[1]Extensively pre-wetted results agree to some extent with the study of Mata and Smith (1981)